AD NUMBER

ADB100944

NEW LIMITATION CHANGE

TO

Approved for public release, distribution unlimited

FROM

Distribution authorized to U.S. Gov't. agencies only; Test and Evaluation; JAN 1986. Other requests shall be referred to US Air Force Wright Aeronautical Laboratory, Attn: POTX, Wright-Patterson AFB, OH 45433.

AUTHORITY

AFWAL ltr 13 Jul 1987

AD B100 944

AUTHORITY:
BRWAL ltr 13 July 87

AFWAL-TR-85-2103
Volume I

LABYRINTH SEAL ANALYSIS

Volume I - Development of a Navier-Stokes Analysis for Labyrinth Seals

January 1986
Final Report for June 1980 - March 1985

R. C. Buggeln
H. McDonald
Scientific Research Associates, Inc.
P.O. Box 498
Glastonbury, CT 06033

AERO PROPULSION LABORATORY
AIR FORCE WRIGHT AERONAUTICAL LABORATORIES
AIR FORCE SYSTEMS COMMAND
WRIGHT PATTERSON AIR FORCE BASE, OH 45433

NOTICE

When Government drawings, specifications, or other data are used for any purpose other than in connection with a definitely related Government procurement operation, the United States Government thereby incurs no responsibility nor any obligation whatsoever; and the fact that the government may have formulated, furnished, or in any way supplied the said drawings, specifications, or other data, is not to be regarded by implication or otherwise as in any manner licensing the holder or any other person or corporation, or conveying any rights or permission to manufacture, use, or sell any patented invention that may in any way be related thereto.

GARY F. WILLMES, 2 Lt, USAF
Compressor Research Group

WALKER H. MITCHELL
Chief, Technology Branch

FOR THE COMMANDER

H. I. BUSH
Director
Turbine Engine Division

If your address has changed, if you wish to be removed from our mailing list, or if the addressee is no longer employed by your organization please notivy AFWAL/POTX, Wright-Patterson AFB OH 45433- 6563 to help maintain a current mailing list.

Copies of this report should not be returned unless return is required by security consdierations, contractual obligations, or notice on a specific document.

UNCLASSIFIED
SECURITY CLASSIFICATION OF THIS PAGE

AD-B100944L

REPORT DOCUMENTATION PAGE

1a REPORT SECURITY CLASSIFICATION: Unclassified	1b RESTRICTIVE MARKINGS: N/A
2a. SECURITY CLASSIFICATION AUTHORITY	3 DISTRIBUTION / AVAILABILITY OF REPORT: Distribution limited to U.S. Government agencies only; ~~critical technology~~, July 1985. Other requests for this document must be referred to AFWAL/POTX, Wright-Patterson AFB, OH 45433
2b. DECLASSIFICATION / DOWNGRADING SCHEDULE: N/A	
4. PERFORMING ORGANIZATION REPORT NUMBER(S): 310001F	5. MONITORING ORGANIZATION REPORT NUMBER(S): AFWAL-TR-85-2103, Vol I
6a NAME OF PERFORMING ORGANIZATION: Scientific Research Associates, Inc. / 6b. OFFICE SYMBOL (If applicable):	7a. NAME OF MONITORING ORGANIZATION: Aero Propulsion Laboratory (AFWAL/POTX), Air Force Wright Aeronautical Laboratories
6c. ADDRESS (City, State, and ZIP Code): P.O. Box 498, Glastonbury, CT 06033	7b. ADDRESS (City, State, and ZIP Code): Wright Patterson AFB, OH 45433
8a. NAME OF FUNDING / SPONSORING ORGANIZATION: Aero Propulsion Laboratory, Air Force Wright Aeronautical / 8b OFFICE SYMBOL (If applicable): AFWAL/POTX	9 PROCUREMENT INSTRUMENT IDENTIFICATION NUMBER: F33615-80-C-2014
8c. ADDRESS (City, State, and ZIP Code): Wright Patterson Air Force Base, OH 45433	10. SOURCE OF FUNDING NUMBERS: PROGRAM ELEMENT NO: 62203F; PROJECT NO: 3066; TASK NO: 10; WORK UNIT ACCESSION NO: 18

11 TITLE (Include Security Classification)
Labyrinth Seal Analysis Volume I - Development of a Navier-Stokes Analysis for Labyrinth Seals (Unclassified)

12 PERSONAL AUTHOR(S)
R.C. Buggeln and H. McDonald

13a TYPE OF REPORT	13b TIME COVERED	14 DATE OF REPORT (Year, Month, Day)	15 PAGE COUNT
Final	FROM 6/80 TO 3/85	January 1986	97

16 SUPPLEMENTARY NOTATION Vol IV
Volume II contain computer software; therefore distribution is limited in accordance with AFR 300-6. Non-DOD requests must include the statement of terms and Conditions

17 COSATI CODES		
FIELD	GROUP	SUB-GROUP
21	05	
20	04	

18 SUBJECT TERMS (Continue on reverse if necessary and identify by block number)
Labyrinth Seals, Navier-Stokes Equations; Computational Fluid Mechanics; Alternating Direction Implicit

19 ABSTRACT (Continue on reverse if necessary and identify by block number)
A technique has been developed to solve the Navier-Stokes equations for the flow in labyrinth seals. The technique utilizes a linearized block implicit-alternating direction implicit procedure to efficiently solve the unsteady governing equations to a steady state with appropriate boundary conditions and initial conditions. The resulting code was used to calculate the flow in a wide variety of labyrinth seal geometries under various flow conditions. Comparison with available experimental data indicates that the code will be a valuable tool in analytically evaluating the performance of existing and future labyrinth seals.

20 DISTRIBUTION / AVAILABILITY OF ABSTRACT: ☐ UNCLASSIFIED/UNLIMITED ☒ SAME AS RPT ☐ DTIC USERS	21 ABSTRACT SECURITY CLASSIFICATION: Unclassified
22a NAME OF RESPONSIBLE INDIVIDUAL: Topham, Keith C., 1LT, USAF	22b TELEPHONE (Include Area Code): (513) 255-6720 / 22c OFFICE SYMBOL: AFWAL/POTX

DD FORM 1473, 84 MAR — 83 APR edition may be used until exhausted; All other editions are obsolete

SECURITY CLASSIFICATION OF THIS PAGE

FOREWORD

This final report describes technical work accomplished during the Labyrinth Seal Analysis program conducted under Contract F33615-80-C-2014. The work described was performed during the period ~~15~~ June 1980 to ~~30~~ MARCH ~~April~~ 1985. This contract with Allison Gas Turbine Division of General Motors Corporation was sponsored by the Air Force Wright Aeronautical Laboratories Aeropropulsion Laboratory, United States Air Force, Wright Patterson AFB, Ohio, with Mr. Charles W. Elrod (AWAFL/POTX) as Project Engineer. Technical coordination was provided by 1st Lt. Keith C. Topham.

The technical effort reported in this volume was performed by personnel of Scientific Research Associates, Inc., Glastonbury, Connecticut. The empirical data used to evaluate the results of the Analysis Model development were provided by Allison Gas Turbine Division.

This report was submitted in four volumes in May 1985. Volume I summarizes the development of the labyrinth seal Analysis Model. Volume II presents the user's manual for the Analysis Model computer code. Volume III contains the experimental results and summarizes the Design Model based on these empirical data. Volume IV presents the user's manual for the Design Model computer code.

Publication of this report does not constitute Air Force approval of the findings or conclusions presented. It is published only for the exchange and stimulation of ideas.

TABLE OF CONTENTS

LIST OF FIGURES

LIST OF FIGURES (Continued)

LIST OF TABLES

1.0 INTRODUCTION

The present trend of aircraft gas turbine design has been characterized by significant increases in cycle pressure ratio and turbine inlet temperatures required to provide higher thermal and propulsive efficiencies. Also, increased interest in engine performance and fuel economy has created additional emphasis for improving the efficiency of gas turbine engines. These trends accentuate the need for improvements in sealing technology and the development of advanced design and analysis capabilities to reduce gas path seal leakage, maintain costly vent leakage to a minimum, provide better control over sophisticated cooling circuits, and prevent high levels of seal leakage into critical aerodynamic locations in the turbine gas path which can result in considerable penalty from thermal and momentum losses.

Current and advanced gas turbine engine requirements that impact labyrinth seal design and performance include a broad engine power operating range which usually results in a wide range of seal clearances. Normally, seals are designed to run as tight a clearance as possible at the maximum mission time condition. In setting the design clearance, consideration is given to transient differential growth, maneuver deflections, mechanical and thermal growths, eccentricity, and manufacturing tolerances. However, with variable geometry engines and multiple role applications the engine seals will not always operate at the design clearance nor provide minimum leakage across the operating spectrum. Improved seal design and analysis capabilities must be developed to address this problem.

Gas turbines require a variety of labyrinth seal designs. The seal configuration selected for a given application is based on the purpose of the seal and satisfying design criteria that includes the following considerations: axial envelope available, axial travel, clearance range, potential wear, system sensitivity to seal clearances, cooling flow requirements, sensitivity to damage in handling, assembly requirements, and pressure ratio.

Labyrinth seals are used throughout a gas turbine engine, including: compressor and turbine airfoil end seals, bearing compartment seals, and flow system seals to minimize or control flow. The purposes of these seals are not always the same. Labyrinth seals used in the flow path are intended to minimize end leakage. Bearing compartment seals are intended to keep the oil in the bearing compartment and to minimize the amount of air leakage and heat addition to the oil. Thrust balance labyrinth seals are located radially to provide a desired off-setting axial load component to reduce bearing loads to the design level. Other flow system network seals have several functions including: controlling leakage flows either to a minimum or to a level to satisfy disc pumping and thus prevent hot gas recirculation in a cavity, controlling cavity pressures to reduce axial bearing loads, or preventing excessive leakage.

The variety of locations, functions, and operating conditions imposed on labyrinth seals in a gas turbine engine requires a design and analysis capability that takes advantage of the numerous seal geometries available and accurately predicts the seal performance. Labyrinth seal geometries include straight-through seals, step seals, and a variety of advanced complex geometry designs. The seal knives may be vertical or slanted, the knives may be placed on a rotating or stationary surface. Seal lands may be smooth and solid, honeycomb, roughened surface solid, striated, or abradable (porous or non-porous). Other seal geometry variables include knife edge thickness and sharpness, clearance, knife pitch, cavity depth and shape, number of knives, step height, knife location on the step, and knife angle. Aerodynamic parameters that must be considered in seal design include rotational speed, pressure ratio, temperature, and Reynolds number.

If a labyrinth seal design is to be successful for the application intended, an accurate seal design and analysis model is necessary. The design and analysis capabilities available today rely heavily on empirical relationships which severely limit the application range. Available analytical formulations were originated many years ago and do not take advantage of modern flow field calcuation techniques such as the advances offered by solution algorithms for the Navier-Stokes equations. Available seal design and analysis models are severely restricted relative to analyzing new and advanced seal designs. Also, many of the geometric and aerodynamic parameters in a lab seal have interfacing effects which make it

difficult to accurately assess individual parameter effects from test data. Therefore, to examine the numerous individual and combinations of seal geometric and aerodynamic parameters experimentally would be time consuming and very expensive. In addition, empirically derived models do not provide the capability to assess new configurations nor do they provide the design engineer with guidance on how to improve the efficiency of the seal beyond what information has been determined experimentally.

Therefore, a critical need exists for labyrinth seal design and analysis calculation models that provide the seal design specialist with the analytical tools to calculate, study, understand and evaluate the details of the labyrinth seal internal flow field and to assess subtle geometric changes relative to improving the seal efficiency. Final tuning and verification of the resulting configuration would still be accomplished on a seal test rig.

Originally, the design of a conventional straight-through labyrinth seal was usually a compromise between the number of seal knives and a knife pitch that was large enough to reduce the kinetic energy carryover to a minimum. However, numerous investigators have identified a significant number of additional performance influence parameters. Today, the qualified seal designer recognizes there are a large number of geometric and aerodynamic parameters that influence the performance level of a labyrinth seal. These parameters, for a conventional straight-through seal, include:

- Clearance
- Pitch
- Number of knives
- Knife tip thickness
- Rotational speed
- Cavity volume
- Knife sharpness
- Pressure ratio
- Knife angle
- Land surface (smooth, honeycomb, striated, etc.)
- Knife height
- Reynolds number
- Eccentricity

To the above list several additional parameters can be added when a step seal is considered. These additional parameters include:

- Step height
- Step configuration
- Distance from seal knife to step face
- Flow direction

It should be noted that the seal performance influence parameters listed above do not operate independently. The inherent design of a labyrinth seal causes the individual geometric and aerodyamic influence parameters to have overlapping or interfacing effects. For example, the effect of seal clearance on leakage is significantly different depending on the knife pitch and number of knives. Therefore, a very large matrix of identified parameter combinations exists which determine labyrinth seal performance.

There are numerous types and applications of labyrinth seals in a gas turbine. The labyrinth seal may be a straight-through, slanted straight, a back-to-back or fir tree arrangement, stepped, or slanted stepped. Flow may be "up" or "down" the step. The seal lands may be solid-smooth, roughened, abradable (porous or non-porous), or honeycomb.

The flow fields in the various types of labyrinth seals used in a gas turbine have similar complexities but differ significantly between a conventional straight-through and stepped seal (see Fig. 1). The stepped seal has a mechanism, the vertical step face, to spoil the through flow. The straight seal has a core of through-flow (referred to as kinetic energy carry-over) that results in higher seal leakage rates compared to a stepped seal. Therefore, the step seal provides additional parameters for the design engineer to consider.

The number of tests and amount of hardware, time, and cost to develop all labyrinth seal performance empirically are prohibitive. In addition, any new labyrinth seal design concepts would have to be tested to determine their performance. If one additional geometric or aerodynamic variable that had not been experimentally evaluated before is introduced or varied, then not only must this new parameter be evaluated, but each geometric and aerodynamic parameter interface must also be evaluated to determine combination effects. Therefore, it is desirable to supplement the empirical approach and consider analytical techniques to assist in the design and analysis of labyrinth seals. However, the labyrinth seal flow field must be classified as one of the most complex and challenging for a theoretical analysis. The flow field is turbulent, separated, compressible, viscous, has one wall rotating, and experiences streamwise vorticity. If unsteadiness is present, then any analytical analysis that is not time-dependent may have difficulty attaining agreement with test results.

There are several classical analytical methods available in the literature for estimating labyrinth seal leakage. However, each of these methods is based on certain simplifying assumptions which limit the areas of applicability. Several of the more recent theoretical methods will yield reasonable estimates of leakage, but the area of applicability of each method is restricted to a narrow range of geometries and overall pressure. None of the available methods account for more than four or five variables. No general solution is available for calculating labyrinth seal leakage flows, nor has an analytical method been developed that examines the seal interior flow field to provide aerodynamic details and guidance to improve the efficiency of the labyrinth seal.

The origin of the labyrinth seal can be traced to C.A. Parsons (Ref. 1) who apparently introduced the concept of a steam turbine and reported the event in 1892 (Ref. 2). The design concept was to provide a tortuous path between high and low pressure regions by using a series of non-contacting restrictions and chambers. The characteristic functions of the restrictions were to convert the pressure head into kinetic energy which would then be dissipated as completely as possible in the intervening chambers. The effectiveness of this concept is shown by its continued use in the current most modern gas turbine designs.

Although the labyrinth seal is relatively simple in design, the numerous geometric and aerodynamic parameters associated with determining the overall performance are numerous and complex as noted earlier. However, theoretical formulations to describe the flow field through the labyrinth seal have been attempted apparently starting with E. Becker in 1907 (Ref. 3). Closely following Becker was a paper by H.M. Martin (Ref. 4). It is interesting to note that these two papers establish the classical labyrinth seal theories which can be organized into two families:

(1) Treat the seal knives as a series of individual throttles (Martin approach, Ref. 4).

(2) Treat the seal as a friction device (Becker approach, Ref. 3).

Generally speaking, existing labyrinth seal flow calculation theories make assumptions that place the theories in one of two classifications

(1) Small ΔP is assumed across each restriction.

(2) Last restriction choked.

Stodola's (Ref. 5) and Martin's (Ref. 4) formulas assume small ΔP across each restriction, i.e., all kinetic energy is recovered as internal heat in the seal cavities. These formulas also assume the discharge coefficient is 1.0 for each restriction. These two often-quoted formulas, as well as others that are similar, assume that the gas experiences an ideal isothermal expansion across each seal knife followed by dispersion of the kinetic energy and reheating before entering the next seal knife. The many theoretical studies in this classification which have appeared in the literature are of little value in the prediction of leakage rates through the commonly used straight labyrinth seal because the assumptions on which they are based approach the conditions which are approximated only in step seals. The authors of these theoretical studies seek to modify the theory with empirical correction factors to make the calculation fit test data.

Theoretical analyses to date have neglected or approximated the carryover (sometimes referred to as velocity of approach) of kinetic energy from knife to knife. This carryover factor varies substantially with geometry and pressure ratio. Also, the discharge coefficient must be evaluated for each particular knife (or stage) geometry and will vary depending on several factors including:

- Knife tip thickness
- Clearance
- Reynolds number
- Number of Knives

In addition to the foregoing parameters, the carryover factor and discharge coefficient may be effected by surface roughness, land porosity, honeycomb and striated lands, and knife rotation.

Trutnovsky (Ref. 6), like Becker (Ref. 3), treated the seal leakage as flow in a rough pipe. However, his solution of the basic equations describing the flow is complicated and in general difficult to use. Zabriskie and Sternlicht (Ref. 7), offer an approach that is an extension and simplification of the method used by Trutnovsky. However, numerous investigators have challenged this general approach as not being correct relative to the physical considerations of the problem.

Most theoretical approaches make a simplifying assumption regarding the intercavity vortex and eddies and give no help on how to improve these cavities to reduce leakage. It is known that the shape and size of the cavity between seal knives affects the strength of the vortex and eddies which convert the kinetic energy issuing from each knife into internal energy.

It is apparent from the foregoing discussion that existing theoretical methods, which necessarily employ empirically derived modifiers for calculating labyrinth seal flows, have significant shortcomings. A generalized theoretical approach with proven accuracy and reliability is not available.

This situation leaves the design engineer with the dubious task of selecting a method for his needs from numerous methods with varying degrees of accuracy and range of application. Furthermore, the seal design specialist does not have the analytical tools to examine the details of the labyrinth seal interior flow field and determine geometry changes that would increase seal cavity turbulence resulting in improved sealing efficiency.

The analysis tools required by the mechanical design engineer and the seal research specialist are distinctly different. The design engineer requires a simplified "design" calculation model that will determine the overall performance of a labyrinth seal when selected geometry is specified. The design engineer also has a need for a calculation model that will provide dimensional criteria for an optimum seal configuration for a given application when an absolute minimum of information is supplied, i.e., clearance, axial envelope, rotational speed, and pressure ratio. The design model input format should be simple and the computer run time should be minimum for the model to be practical as a production program. Incorporating available test data and generating seal performance

data not currently available to update and expand existing theoretical models that rely heavily on empirical correlations offers the most effective approach for the development of an advanced "design" model.

The seal research specialist requires an "analysis" calculation model that provides the aerodynamic details of the seal interior flow field in order to determine and evaluate the effects of the numerous geometric and aerodynamic parameters incorporated in the design of conventional straight-through and stepped seals. This capability will enable the seal specialist to identify and analytically evaluate design improvements to obtain higher efficiency labyrinth seals as well as to improve the accuracy of conventional seal design leakage calculations.

Recent developments in the phenomenological models of internal turbulent flows shows that the methodology has progressed to the point that the complex turbulent flow field within the labyrinth seal interior may be calculated via direct analysis using Navier-Stokes computer codes presently available, modified for the geometry of a labyrinth seal. The successful application of a compressible time dependent Navier-Stokes solution would provide a major breakthrough in seal analysis technology.

The value of a Navier-Stokes solution method for the labyrinth seal leakage calculation is that it can potentially analyze most of the geometric and aerodynamic effects individually and in matrix combinations. There may be some effects that cannot be completely modeled. In these cases, test data may be used to support and expand the Navier-Stokes solution method.

Labyrinth seal design improvements have been limited because the tools to analyze the effects of geometric changes or unique configurations do not exist except in a very fundamental or simplified analysis form. The availability of a Navier-Stokes solution would provide a capability to study and analyze many complex geometric shapes and configurations that can only be evaluated presently through expensive and time consuming tests. Although the Navier-Stokes solution may be limited in calculating the exact level of performance for exotic seal configurations, it will guide the engineer, through performance trends, to a more efficient design. The final design should be tested to verify performance characteristics of the seal.

In regard to Navier-Stokes solutions, several items need to be considered. It is clear that a viable analysis which simulates the seal flow field must allow for flow ranging from the low subsonic regime to the transonic regime, must include possible shock waves, must allow for dominating viscous effects and must allow for very large regions of recirculation. These considerations clearly dictate a Navier-Stokes approach to the problem.

In most instances the Navier-Stokes equations are so intractable that only numerical solutions can be obtained. Numerical techniques for solving the Navier-Stokes equations are discussed by Roache (Ref. 8) and more particularly for the compressible Navier-Stokes equations by Peyret and Viviand (Ref. 9). Peyret and Viviand singled out three techniques, the explicit scheme of MacCormack (Ref. 10), the scheme due to Widhoff and Victoria, (Ref. 11) also explicit, and the implicit scheme of Briley and McDonald (Ref. 12). The technique of MacCormack (Ref. 10) has been very effectively applied for instance by Shang, Hankey and Law (Ref. 13) in a shock wave-boundary layer interaction problem. However, the need to compute large regions of relatively low speed recirculating fluid interspersed with local high speed throats in the labyrinth seal problem could make the stability bounds of the MacCormack scheme very restrictive.

As a result in the labyrinth seal problem, unacceptably long computer run times could result from the required locally refined spatial meshes with the stability restricted scheme. The technique of Briley and McDonald (Ref. 12) on the other hand, is not restricted by the stability bounds of the MacCormack scheme and the Widhoff and Victoria scheme and, thus, is better suited for the labyrinth seal problem than either of the other two candidate algorithms. For these reasons the Briley-McDonald (Ref. 12) technique was used in the present effort to predict the detailed flow field in the labyrinth seal investigation.

2.0 ANALYSIS

2.1 Governing Equations

The governing equations utilized in this study are the ensemble averaged time dependent Navier-Stokes equations. These equations are the mathematical statement of the physical conservation laws of mass, momentum and energy for one phase fluid dynamic systems. Using vector notation, these transport equations can be respectively written as

$$\frac{\partial \rho}{\partial t} = -\nabla \cdot (\rho \vec{V}) \tag{1}$$

$$\frac{\partial}{\partial t}(\rho \vec{V}) = -\nabla \cdot (\rho \vec{V}\vec{V}) + \nabla \cdot \tau - \nabla P \tag{2}$$

and

$$\frac{\partial}{\partial t}\left[\rho(\hat{U} + \frac{1}{2}\vec{V}\cdot\vec{V})\right] = -\nabla \cdot \left[\rho(\hat{U} + \frac{1}{2}\vec{V}\cdot\vec{V})\vec{V}\right] - \nabla \cdot \vec{q} + \nabla \cdot (\tau \cdot \vec{V}) - \nabla \cdot (P\vec{V}) \tag{3}$$

where ρ is the fluid density, $\vec{V}$ is the Eulerian velocity vector and $\hat{U}$ is the specific internal energy. The thermodynamic pressure, P, is related to the temperature, T, and density, ρ, by the perfect gas equation of state

$$P = \rho \frac{R}{M} T \tag{4}$$

where R is the universal gas constant and M is the mixture molecular weight. The stress tensor, τ, is related to the velocity vector, $\vec{V}$, by the relationship

$$\tau = \mu(\nabla\vec{V} + \nabla\vec{V}^T - {}^2/_3 \nabla \cdot \vec{V}) \tag{5}$$

where μ is the viscosity while the heat transfer, $\vec{q}$, is related to the temperature, T, by the Fourier relationship

$$\vec{q} = -\kappa \nabla T \tag{6}$$

where κ is the thermal conductivity. Eq. (3), the energy equation, represents the balance between the time rate of charge of the internal plus kinetic energy ($\hat{U}+1/2\vec{V}\cdot\vec{V}$), the convection of that energy, the heat transfer and the stress and pressure work. Defining the static enthalpy by

$$h \equiv \hat{U} + \frac{P}{\rho} \tag{7}$$

the energy equation can be rewritten as

$$\frac{\partial}{\partial t}\left[\rho(h+\frac{1}{2}\vec{V}\cdot\vec{V})\right] - \frac{\partial P}{\partial t} = -\nabla\cdot\left[\rho(h+\frac{1}{2}\vec{V}\cdot\vec{V})\right] - \nabla\cdot\vec{q} + \nabla\cdot(\tau\cdot\vec{V}) \tag{8}$$

Using the stagnation enthalpy defined by the relationship

$$h_o \equiv h + \frac{1}{2}\vec{V}\cdot\vec{V} \tag{9}$$

yields the more compact form, viz.,

$$\frac{\partial}{\partial t}(\rho h) - \frac{\partial P}{\partial t} = -\nabla\cdot(\rho h_o \vec{V}) - \nabla\cdot\vec{q} + \nabla\cdot(\tau\cdot\vec{V}) \tag{10}$$

By dotting the velocity vector, $\vec{V}$, with the momentum equation, Eq. (2) and using the vector identities

$$\vec{V}\cdot\frac{\partial}{\partial t}(\rho\vec{V}) = \frac{\partial}{\partial t}(\rho\frac{\vec{V}\cdot\vec{V}}{2}) + \frac{\vec{V}\cdot\vec{V}}{2}\frac{\partial\rho}{\partial t} \tag{11}$$

and

$$\vec{V}\cdot\nabla(\rho\vec{V}\vec{V}) = \nabla\cdot\left[(\rho\frac{\vec{V}\cdot\vec{V}}{2})\vec{V}\right] + \frac{\vec{V}\cdot\vec{V}}{2}\nabla\cdot(\rho\vec{V}) \tag{12}$$

and applying the continuity equation, Eq. (1), one can obtain the so-called mechanical energy equation

$$\frac{\partial}{\partial t}\left(\rho \frac{\vec{V}\cdot\vec{V}}{2}\right) = -\nabla\cdot\left[\left(\rho \frac{\vec{V}\cdot\vec{V}}{2}\right)\vec{V}\right] - \vec{V}\cdot\nabla P + \vec{V}\cdot(\nabla\cdot\tau) \tag{13}$$

Subtracting the mechanical energy equation, Eq. (13), from the energy equation, Eq. (8), and applying the vector identity

$$\nabla\cdot(\tau\cdot\vec{V}) = \vec{V}\cdot(\nabla\cdot\tau) + \tau : \nabla\vec{V} \tag{14}$$

and using the definition of energy dissipation, Φ, as

$$\Phi \equiv \tau : \nabla\vec{V} \tag{15}$$

one obtains an alternate form of the energy equation expressed in terms of the time rate of charge of the static enthalpy

$$\frac{\partial}{\partial t}(\rho h) - \frac{\partial P}{\partial t} = -\nabla\cdot(\rho h\vec{V}) - \nabla\cdot\vec{q} + \vec{V}\cdot\nabla P + \Phi \tag{16}$$

The static enthalpy, h, can be related to the temperature, T, by the relationship

$$h = \int_{T_r}^{T} C_p(T)\, dT \tag{17}$$

where c_p is the specific heat at constant pressure. If a calorically ideal gas is assumed, (c_p is a constant).

$$h = C_p T \tag{18}$$

Eq. (16) can be further simplified and written in terms of temperature.

The system of coupled nonlinear partial differential equations represented by Eq. (1), (2), and (16) are the basis of the governing equations used in this study. The equations are valid for both laminar and turbulent flow. However, for turbulent flow, all variables are ensemble averaged (Ref. 14) and the viscosity and thermal conductivity, k, must be considered as effective values. Thus, the viscosity must be considered as the sum of the laminar and turbulent viscosities (the turbulent viscosity comes from the Boussinesq approximation to the Reynolds stress terms).

$$\mu = \mu_\ell + \mu_T \tag{19}$$

The viscosity is related to the thermal conductivity and the specific heat by the concept of a Prandtl number (which is presumed to be known)

$$k_\ell = \frac{C_p \mu_\ell}{Pr_\ell} \tag{20}$$

$$k_T = \frac{C_p \mu_T}{Pr_T} \tag{21}$$

and

$$k = k_\ell + k_T \tag{22}$$

In this study, two methods were used to represent the turbulent viscosity, μ_t. The first uses the algebraic mixing length of Prandtl where

$$\mu_T = \rho \ell_m^2 \sqrt{D:D} \tag{23}$$

where D:D is the second variant of the mean flow rate of deformation tensor, i.e.,

$$D:D = \frac{\Phi}{\mu} + \frac{2}{3}(\nabla \cdot \vec{V})^2 \tag{24}$$

and ℓ_m is the mixing length which will be discussed at a later time.

The second method utilized in this study is to assume the Prandtl-Kolmogorov relationship (Ref. 15) for turbulent viscosity, the so-called k-ε model

$$\mu_T = C_\mu \frac{\rho K^2}{\epsilon} \tag{25}$$

where c_μ is a 'constant' (to be discussed at a later time) k is the turbulence kinetic energy defined by

$$k = \sqrt{\frac{\overline{u'^2} + \overline{v'^2} + \overline{w'^2}}{2}} \tag{26}$$

and ε is the dissipation of turbulence kinetic energy. Partial differential equations govern the distribution of k and ε in the flow. For a discussion of these equations, the reader is referred to Refs. 16 and 17. The resultant equations are

$$\frac{\partial \rho K}{\partial t} = -\nabla\cdot(\rho \vec{V} K) + \nabla\cdot\left(\frac{\mu_T}{\sigma_K}\nabla K\right) + (\mu_T\, D:D - \rho\epsilon) \tag{27}$$

and

$$\frac{\partial \rho \epsilon}{\partial t} = -\nabla\cdot(\rho \epsilon K) + \nabla\cdot\left(\frac{\mu_T}{\sigma_\epsilon}\nabla \epsilon\right) + \frac{\epsilon}{K}(C_1 \mu_T D:D - C_2 \rho\epsilon) \tag{28}$$

Thus, when a k-ε turbulence model is used, two additional coupled nonlinear partial differential equations are added to the original governing partial differential equations.

In summary, the governing system of equations used in this study include the partial differential equations, Eqs. (1), (2), and (16) plus (27) and (28) if a k-ε turbulence model is used. The constitutive relationships are represented by Eqs. (4)-(7), (15), (17) or Eqs.(18), (19)-(22), and (23) if a mixing length model is used, or Eq. (25) if a k-ε turbulence model is used.

2.2 Coordinate Systems

Application of the governing system of partial differential equations to a given problem is not in general straight forward and several decisions must be made before these equations can be put in a form suitable for solution by numerical techniques. First, a coordinate system must be chosen. For the cases of interest in this study, a body or boundary conforming coordinate system is normally used. Except for the simplest cases, a noncartesian coordinate system must be employed. In many cases a nonorthogonal coordinate system must be used, e.g., the case of a seal with a tapered knife blade. Use of a noncartesian coordinate system requires the choice of both the components of velocity vector, $\vec{V}$, and the choice of the directions in which the vector momentum equation is to be expressed. For instance, the velocity components and the directions in which the momentum equations are written can be aligned with the coordinate directions (Ref. 18), or if one desires, the velocity components and momentum equation directions could be aligned with the cartesian or cylindrical polar coordinate directions (Refs. 19-21). Combinations of the above are also possible, although to the author's knowledge, have not been used to date.

In this study two basic types of geometric configurations are considered: (1) planar configurations and (2) axisymmetric configurations. The planar configurations are utilized primarily to simulate experimental setups where the data is taken in a two-dimensional planar environment. The axisymmetric configurations are used primarily to simulate engine component performance in a rotating or nonrotating (but still axisymmetric) environment. When a rotating system is analyzed, the flow is three-dimensional, however, there is symmetry with respect to the rotating direction, i.e., $\partial/\partial\theta=0$. Thus the governing partial differential equations can be expressed in terms of two coordinate directions, but three velocity components are required to define the velocity vector and three momenta equations must be solved.

The remainder of this section will describe the derivation of the governing system of partial differential equations to be used for planar nonorthogonal configurations. The derivation for axisymmetric configurations is similar and the details are discussed in Ref. 19.

Although in this study the governing equations were only solved in two dimensions and axisymmetric flow, the technique is applicable to two and three space dimensions. For generality here the three-dimensional derivation is presented.

The technique utilized in this study is similar to that reported in Refs. 19-21. The dependent variables are chosen as the three cartesian velocity components, u_1, u_2 and u_3, the density, ρ, and the static enthalpy, h,. The momentum equation is also expressed in terms of the three cartesian directions $\bar{x}_1$, $\bar{x}_2$ and $\bar{x}_3$. These governing partial differential equations in cartesian coodinates can be expressed in the form

$$\frac{\partial W}{\partial t} = \frac{\partial F_i}{\partial x_i} + S \tag{29}$$

where

$$W = \begin{bmatrix} \rho u_1 \\ \rho u_2 \\ \rho u_3 \\ \rho \\ \rho h \end{bmatrix} \tag{30}$$

and

$$F_1 = \begin{bmatrix} \rho u_1^2 + P + \tau_{\bar{x}_1\bar{x}_1} \\ \rho u_1 u_2 + \tau_{\bar{x}_2\bar{x}_1} \\ \rho u_1 u_3 + \tau_{\bar{x}_3\bar{x}_1} \\ \rho u_1 \\ \rho u_1 h + q_{\bar{x}_1} \end{bmatrix} \tag{31}$$

$$F_2 = \begin{bmatrix} \rho u_2 u_1 + \tau_{\bar{x}_1\bar{x}_2} \\ \rho u_2^2 + P + \tau_{\bar{x}_2\bar{x}_2} \\ \rho u_2 u_3 + \tau_{\bar{x}_3\bar{x}_2} \\ \rho u_2 \\ \rho u_2 h + q_{\bar{x}_2} \end{bmatrix} \tag{32}$$

$$F_3 = \begin{bmatrix} \rho u_3 u_1 + \tau_{\bar{x}_1 \bar{x}_3} \\ \rho u_3 u_2 + \tau_{\bar{x}_2 \bar{x}_3} \\ \rho u_3 + P + \tau_{\bar{x}_3 \bar{x}_3} \\ \rho u_3 \\ \rho u_3 h + q_{\bar{x}_3} \end{bmatrix} \tag{33}$$

and

$$S = \begin{bmatrix} 0 \\ 0 \\ 0 \\ 0 \\ \mu(D:D + \frac{2}{3} \nabla \cdot \vec{V} \\ + \vec{V} \cdot \nabla P) \end{bmatrix} \tag{34}$$

where in tensor notation, the normal and shear stress components and the heat transfer are respectively

$$\tau_{\bar{x}_i \bar{x}_i} = \mu \left(2 \frac{\partial u_i}{\partial \bar{x}_i} - \frac{2}{3} \nabla \cdot \vec{V}\right) \tag{35}$$

$$\tau_{\bar{x}_i \bar{x}_j} = \tau_{\bar{x}_j \bar{x}_i} = \mu \left(\frac{\partial u_i}{\partial \bar{x}_j} + \frac{\partial u_j}{\partial \bar{x}_i}\right) \tag{36}$$

$$D:D = \frac{1}{2}\left(\frac{\partial u_i}{\partial \bar{x}_j} + \frac{\partial u_j}{\partial \bar{x}_i}\right)^2 \tag{37}$$

$$\nabla \cdot \vec{V} = \frac{\partial u_i}{\partial \bar{x}_i} \tag{38}$$

and

$$q_{\bar{x}_i} = -\kappa \frac{\partial T}{\partial \bar{x}_i} \tag{39}$$

Transforming Eq. (30) to a general coordinate system in which the general coordinates, y^j, are related to the cartesian coordinates $\bar{x}_1$, $\bar{x}_2$ and $\bar{x}_3$ by the relationship

$$y^j = y^j(\bar{x}_1, \bar{x}_2, \bar{x}_3) \tag{40}$$

and use of the chain rule yields

$$\frac{\partial W}{\partial t} = \frac{\partial F_i}{\partial y^j} \frac{\partial y^j}{\partial x_i} + S \tag{41}$$

Defining the Jacobian determinant of the inverse transformation, J, by

$$J = \left| \frac{\partial(\bar{x}_1, \bar{x}_2, \bar{x}_3)}{\partial(y^1, y^2, y^3)} \right| = \begin{vmatrix} \frac{\partial \bar{x}_1}{\partial y^1} & \frac{\partial \bar{x}_1}{\partial y^2} & \frac{\partial \bar{x}_1}{\partial y^3} \\ \frac{\partial \bar{x}_2}{\partial y^1} & \frac{\partial \bar{x}_2}{\partial y^2} & \frac{\partial \bar{x}_2}{\partial y^3} \\ \frac{\partial \bar{x}_3}{\partial y^1} & \frac{\partial \bar{x}_3}{\partial y^2} & \frac{\partial \bar{x}_3}{\partial y^3} \end{vmatrix} \tag{42}$$

and multiplying Eq. (41) by the Jacobian yields

$$J \frac{\partial W}{\partial t} = J \frac{\partial y^j}{\partial \bar{x}_i} \frac{\partial F_i}{\partial y^j} \tag{43}$$

This form is sometimes referred to as the weak conservative form. By assuming that the Jacobian is not a function of time, t, one can rearrange Eq. (44) in the form

$$\frac{\partial}{\partial t}(JW) = \frac{\partial}{\partial y^j}\left(J \frac{\partial y^j}{\partial \bar{x}_i} F_i\right) - F_i \frac{\partial}{\partial y^j}\left(J \frac{\partial y^j}{\partial \bar{x}_i}\right) \tag{44}$$

However, it can be shown that (Appendix A)

$$\frac{\partial}{\partial y^j}\left(J \frac{\partial y^j}{\partial \bar{x}_i}\right) = 0 \tag{45}$$

The derivation of Eq. (44) in fact is general in that if the transformation of Eq. (43) had a moving coordinate system, the Jacobian could be taken inside the time derivative, and thus the transformed equation can be written in the form

$$\frac{\partial}{\partial t}(JW) = \frac{\partial}{\partial y^j}\left(J \frac{\partial y^j}{\partial \bar{x}_i} F_i\right) \tag{46}$$

This form of the transformed governing partial differential equations is sometimes referred to as the strong conservative form, and this is the form of the governing equations solved in this study. The primary advantage of using the cartesian velocity components and solving the scalar momenta equations associated with the cartesian directions is that the number of terms of the governing differential equations is kept to a minimum for nonorthogonal systems. If there is no specific reason why the cartesian velocity components and directions for the momenta equations are unsuitable for a given application, this is the most efficient means of solving the governing equations. For this study and many other applications this technique does not appear to have any disadvantages vis a vis other methods, and hence that procedure was chosen here.

In three dimensions each convective and pressure term from the cartesian equations in general becomes three terms in the transformed system. Each stress and heat transfer term becomes nine terms in the transformed system. For two-dimensional flow, the corresponding numbers are, two and four. To define the stress and heat transfer terms in the transformed coordinate system requires applying the transformation to Eqs. (35-39). This yields in tensor notation,

$$\tau_{\bar{x}_i \bar{x}_l} = \mu\left(2 \frac{\partial y^j}{\partial x_l} \frac{\partial u_l}{\partial y^j} - \frac{2}{3} \nabla \cdot \vec{V}\right) \tag{47}$$

$$\tau_{\bar{x}_i \bar{x}_j} = \tau_{\bar{x}_j \bar{x}_i} = \mu \left(\frac{\partial y^k}{\partial \bar{x}_i} \frac{\partial u_l}{\partial y^k} + \frac{\partial y^k}{\partial \bar{x}_i} \frac{\partial u_l}{\partial y^k} \right) \tag{48}$$

and

$$\nabla \cdot \vec{V} = \frac{\partial y^j}{\partial \bar{x}_i} \frac{\partial u_l}{\partial y^j} \tag{49}$$

and

$$q_{\bar{x}_i} = -\kappa \frac{\partial y^j}{\partial \bar{x}_i} \frac{\partial T}{\partial y^j} \tag{50}$$

2.3 Initial and Boundary Conditions

Steady solution of the system of governing partial differential equations represented by Eq. (46) is obtained by time marching this system of equations until the steady state is reached. Before the solution procedure is described two important aspects must be discussed: (1) the initial conditions and (2) the boundary conditions. Any procedure which utilizes either a time marching method to obtain a steady state (or transient) solution or a Newton-Raphson iteration procedure requires some initial guess of the flow variables (in this case all the dependent variables and other necessary variables such as pressure, temperature, viscosity, etc.). In some of the simpler cases, a reasonable approximation to a converged solution can either be guessed or obtained through physical reasoning. However, since the range of geometries considered under this effort were so diverse, it was felt that no reasonable general initial guess procedure could be developed. The approach taken here was to assure that the flow was initially stagnant (all velocity components were zero) by assuming that the pressure and temperature were a constant and set equal to the stagnation conditions of the source flow. The downstream or back pressure is then lowered to some desired level over a period of time, and the flow is drawn through the seal until a steady state is achieved.

This technique has the advantage of being easy to implement in any geometric configuration. In addition, the lowering of the back pressure can be considered to be similar to an experimental apparatus where the source tank is pumped up and the back pressure gradually lowered by opening a downstream valve.

To obtain a solution of the governing system of partial differential equations represented by Eq. (46), it is necessary to define boundary conditions on each bounding surface of the computational domain. For the purposes of this investigation boundary conditions can be classified as occurring on three different types of bounding surfaces: (1) walls or solid surfaces, (2) inlets and (3) exits. The boundary conditions utilized on each different type of surface will now be discussed in turn. Analysis of the characteristics of the boundary layer equations shows that (in three dimensions) four conditions must be specified on walls. For this study, the no-slip conditions are used for the tangential (to the wall) velocity components, i.e.,

$$u_{T_1} = 0 \tag{51}$$

and

$$u_{T_2} = 0 \tag{52}$$

where the subscripts T_1 and T_2 refer to the two tangential velocity components. (For two-dimensional flow only one tangential velocity component is used). For the normal velocity component either the normal velocity component or the normal mass flux is specified, i.e.,

$$u_N = u_W \tag{53}$$

or

$$\rho u_N = \dot{m}_W \tag{54}$$

where the subscript w refers to the specified wall value. The fourth condition used, the thermal condition, either specifies the wall as being adiabatic or specifies the wall temperature. These conditions can be written respectively as

$$\vec{n}_w \cdot \nabla T = 0 \tag{55}$$

or

$$T = T_w \tag{56}$$

where in this case $\vec{n}_w$ represents the unit vector normal to the wall. In addition, a fifth condition (in two-dimensions a fourth) not required by the characteristic analysis, is used for convenience to close the set of equations. The need for this fifth condition could be removed by the use of one-sided difference approximations or by applying one of the governing equations at the wall. In this study, the second method was used and the boundary layer approximation to the normal momentum equation was applied at the wall. This can be expressed as

$$\vec{n}_w \cdot \nabla P = 0 \tag{57}$$

Studies have indicated that there is little difference between using this equation or using the full normal momentum equation. The condition of Eq.(57) approximates the normal momentum equation to order Re^{-1} for viscous flow at a no-slip surface. The symmetry equations are meant to be applied on a plane or axis of symmetry. The normal component of velocity is set equal to zero on the axis of symmetry, i.e.,

$$\vec{n}_s \cdot \vec{V} = 0 \tag{58}$$

where $\vec{n}_s$ is the unit vector normal to the axis or plane of symmetry. In addition the normal derivatives of the remaining two tangential components of velocity are set to zero. Two other conditions must be set on the axis

or plane of symmetry. Usually the symmetry conditions on pressure and temperature are used, viz.,

$$\vec{n}_s \cdot \nabla P = 0 \tag{59}$$

and

$$\vec{n}_s \cdot \nabla T = 0 \tag{60}$$

On inlets the characteristic analysis shows that four conditions must be set (for three-dimensional flow). The procedure used in this study is to divide the flow on the inlet into two regions: (1) a central core where the flow is essentially inviscid and (2) the attached boundary layers where the normal pressure gradient is zero. This technique, which can be called the 'two-layer model', sets a constant stagnation pressure in the central core region of the inlet boundary. In the attached boundary layer(s), the static pressure is set at the central core edge value, and the form of the streamwise velocity profile is set. It is to be emphasized that the magnitude of the streamwise velocity is not specifically set. Rather interaction of the core flow and the rest of the flow with the inlet boundary layers sets the magnitude of the boundary layer inlet streamwise velocity profile. In this study two forms of boundary layer profiles were used: (1) for laminar flow the von-Karman-Polhausen (Ref. 22) profile was used, and (2) for turbulent flow the Maise-McDonald (Ref. 23) profile was used. In addition to the 'two layer model' boundary condition, two additional velocity conditions must be specified. In this study the flow angle between the streamwise velocity component and the transverse component was specified (usually as zero) and if the apparatus was rotating a swirl velocity profile was specified. The fourth boundary condition was the thermal condition that the stagnation enthalpy on the inlet boundary remains constant. In addition, a fifth condition, not required by the characteristic analysis, is used to numerically close the set of equations. In this case the weak condition that second derivative of pressure normal to the inlet plane equals zero was used. The advantage of this condition is that it allows pressure waves to exit the computational domain rather than reflect off boundaries.

A characteristic analysis of the governing equations on an exit plane shows that for subsonic flow only one condition must be set. In this study the condition is met by setting the back pressure to some desired value. Thus, since the upstream (inlet) stagnation pressure is set in the inlet boundary core region, the mass flux is determined by these two variables and the loss mechanism that occurs in the physical domain. As before to numerically close the set of equations, four more exit conditions must be set. In this case weak conditions are set, viz., the second derivative of the three velocity components and the temperature are set to zero, the so-called parabolic assumptions.

If the two-equation (k-ε) turbulence model is used, two additional partial differential equations must be solved, and hence initial and boundary conditions must be specified for these equations. The procedure used in this study is to obtain a converged solution with a mixing length model, then use the assumption of an 'equilibrium turbulence model' as an initial guess for the k and ε fields, and obtain a converged solution with a k-ε turbulence model. The 'equilibrium turbulence model' assumes that the production and dissipation of turbulence kinetic energy are balanced and that the turbulent viscosity, μ_T, can be calculated from the mixing length model, i.e., Eq. (27). Thus by setting the source term of Eq. (27) to zero and by using Eqs. (23) and (25), 'equilibrium' values of k and ε can be obtained, viz.,

$$k = \frac{\ell_m^2 D:D}{\sqrt{C_\mu}} \tag{61}$$

and

$$\epsilon = \frac{C_\mu^{3/4} k^{3/2}}{\ell_m} \tag{62}$$

In this study the Jones-Launder (Ref. 16) formulation for C_μ is used

$$C_\mu = 0.09 e^{-\frac{2.5}{1 + 0.02 Re_T}} \tag{63}$$

where Re_T is the turbulence Reynolds number defined by

$$Re_T = \frac{\mu_T}{C_\mu \mu_l} \tag{64}$$

Therefore

$$C_\mu = 0.09\, e^{-\frac{2.5}{1 + 0.02 \frac{\mu_T}{C_\mu \mu_l}}} \tag{65}$$

Eq. (65) is a transcendental equation in C_μ (as an initial guess μ_T is calculated from the mixing length model and the laminar viscosity μ_l is known) which is solved by a straightforward 'Newton-Raphson' iteration technique. Once this is done the value of C_μ can be substituted into Eqs. (61) and (62) and initial guesses of the k and ε fields obtained. Boundary conditions for the k and ε equations are as follows: (1) on inlets the values of k and ε are frozen at their equilibrium values from the converged mixing length solution, (2) on walls the values of k and ε are set to zero, (3) on axis or plane of symmetry the normal derivatives of k and ε are set to zero, and (4) on the exit plane the second derivatives of k and ε are set to zero.

2.4 Numerical Procedure

The numerical procedure used to solve the governing equations is a consistently split linearized block implicit (LBI) scheme originally developed by Briley and McDonald (Ref. 12). A conceptually similar scheme has been developed for two-dimensional MHD problems by Lindemuth and Killeen (Ref. 24). More recently Beam and Warming (Ref. 25) have derived this and other related schemes by the method of approximate factorization. The procedure is discussed in detail in Refs. 12 and 26. The method can be briefly outlined as follows: the governing equations are replaced by an implicit time difference approximation. Terms involving nonlinearities at the implicit time level are linearized by Taylor expansion in time about the solution at the known time level, and spatial finite difference approximations are introduced. The result is a system

of multidimensional coupled (but linear) difference equations for the dependent variables at the unknown or implicit time level. To solve these difference equations, the Douglas-Gunn (Ref. 27) procedure for generating alternating-direction implicit (ADI) schemes as perturbations of fundamental implicit difference schemes is introduced in its natural extension to systems of partial differential equations. This technique leads to systems of coupled linear difference equations having narrow block-banded matrix structures which can be solved efficiently by standard block-elimination methods.

The method centers around the use of a formal linearization technique adapted for the integration of initial-value problems. The linearization technique, which requires an implicit solution procedure, permits the solution of coupled nonlinear equations in one space dimension (to the requisite degree of accuracy) by a one-step noniterative scheme. Since no iteration is required to compute the solution for a single time step, and since only moderate effort is required for solution of the implicit difference equations, the method is computationally efficient. This efficiency is retained for multidimensional problems by using what might be termed block ADI techniques. The method is also economical in terms of computer storage, in its present form requiring only two time-levels of storage for each dependent variable. Furthermore, the block ADI technique reduces multidimensional problems to sequences of calculations which are one dimensional in the sense that easily-solved narrow block-banded matrices associated with one-dimensional rows of grid points are produced. A more detailed discussion of the solution procedure as discussed by Briley, Buggeln and McDonald (Ref. 28) is given in the Appendix B.

2.5 Artificial Dissipation

One major problem to be overcome in calculating high Reynolds number flows using the Navier-Stokes equations is the appearance of spatial oscillations associated with the so-called central difference problem. When spatial derivatives are represented by central differences, high Reynolds number flows can exhibit a saw tooth type oscillation unless some mechanism is added to the equations to suppress their appearance. This dissipation mechanism can be added implicitly to the equations via the

spatial difference molecule (e.g. one-sided differencing) or explicitly through addition of a specific term. The present authors favor this latter approach for two reasons. First, if a specific artificial dissipation term is added to the equations, it is clear precisely what approximation is being made. Secondly, if a specific term is added to suppress oscillations, the amount of artificial dissipation added to the equations can be easily controlled in magnitude and location so as to add the minimum amount necessary to suppress spatial oscillations. Studies can also be easily performed to evaluate the effect of the explicitly added dissipation on the solution.

Various methods of adding artificial dissipation were investigated in Ref. 12, and these were evaluated in the context of a one-dimensional model problem. The model problem used was one-dimensional flow with heat transfer. Flow was subsonic at the upstream boundary, accelerated via heat sources until a Mach number of unity was reached and then accelerated to supersonic velocity by heat sinks. The exit back pressure was raised to cause a shock to appear in the supersonic region. This basic one-dimensional problem contained many relevant features including strong accelerations and the appearance of a normal shock wave. Therefore, it served as a good test case for various forms of artificial dissipation which could be used in the presence of shock waves.

The results of the Ref. 29 investigation led to the conclusion that for the model problem a second order artificial dissipation approach was the best of those considered. This approach adds a term of the form $\nu_{art}\ \partial^2\phi/\partial Z^2$ or $\partial/\partial Z\ \{\nu_{art}\ \partial\phi/\partial Z\}$ to each governing equation where $\phi = \rho, u, v, w$ for the continuity, x-momentum, y-momentum and z-momentum equations respectively and ν_{art} is determined by

$$\frac{|U_Z|\Delta Z}{\nu+(\nu_{art})_Z} \leq \frac{1}{\sigma_Z} \tag{66}$$

The ΔZ in Eq. (66) is the distance between grid points in a given coordinate direction, U_Z is the velocity in this direction, σ_Z is the

artificial dissipation parameter for this direction and ν is the effective kinematic viscosity. The equation determines ν_{art} with ν_{art} taken as the smallest non-negative value which will satisfy the expression. It should be noted that in two space dimensions each equation contains two artificial dissipation terms, one in each coordinate direction. For example, the streamwise momentum equation expressed in two-dimensional Cartesian coordinates would contain the artificial dissipation terms

$$(\nu_{art})_x \frac{\partial^2 W}{\partial X^2} + (\nu_{art})_z \frac{\partial^2 W}{\partial Z^2}. \tag{67}$$

3.0 RESULTS

The primary objective of the computational effort is to demonstrate the capability of the previously described numerical technique to accurately calculate the flow in realistically configured labyrinth seals at typical operating conditions. It is hoped that the achievement of this objective will provide insight into the details of the flow structure not easily obtainable by experimental methods, and that this demonstration will lead to the use of this analytical tool in the design of future labyrinth seals. In order to achieve the above objective, a series of calculations were performed. These calculations can logically be divided into four categories: (1) calculations designed to show the ability of the numerical procedure to accurately predict the leakage of various labyrinth seal designs at typical operating conditions, (2) calculations to obtain a performance curve for two seal configurations, (3) calculations of the flow for two seal configurations which can be compared with experimental data obtained at Allison Gas Turbine Operations (Ref. 30) for the same seal configurations and at the same operating conditions, and (4) a demonstration calculation of the ability of the numerical procedure to calculate the flow in a sample configuration while the seal assembly is rotating.

Before going into the details of the calculations, it is desirable to define the labyrinth seal nomenclature that is appropriate to the configurations considered in this study. The geometric capability of the computer program developed under this study allows for the analysis of a wide variety of both conventional straight-through and stepped seal configurations. Nomenclature that is common to both types of seals is shown in Fig. (2). CL is the clearance between the seal knife tip(s) and the stator or land. KT represents the knife blade thickness at the tip. KB is the knife blade taper angle, and KΘ is the knife blade slant angle relative to the rotor surface. KH represents the knife blade height and KP is the distance between successive knife blades. For stepped seal configurations DTC is used to represent the minimum horizontal distance-to-contact between the knife blade and the stator, and SH is the step height. In addition for stepped seal configurations the leakage flow direction is referred to as either from the large-to-small seal diameter (LTSD) or from the small-to-large seal diameter (STLD).

The flow reference conditions were determined in a similar manner for all cases considered. The inlet stagnation pressure, P_o, and stagnation temperature, T_o, were specified as was the ratio of upstream to downstream pressure, P_o/P_D. In addition an estimate of the leakage rate (mass flow), W, through the seal was obtained either from the results of the Allison experimental program or the Allison design model. Given the upstream pressure and temperature, the upstream density, ρ_o, can be calculated from the perfect gas law while the upstream viscosity, μ, can be calculated from Sutherland's viscosity law, Ref. 31. The average inlet velocity, V, can be calculated from the relationship (for the cases considered the inlet Mach numbers were on the order of 0.01, hence the stagnation and the static conditions are virtually identical)

$$V = \frac{W}{\rho_o A} \tag{68}$$

where A is the known inlet area. All cases considered in this study had a spanwise distance, of 6.28 in. = .160 m. The above now yields enough information so that reference (or upstream) Reynolds and Mach numbers can be calculated. Using the above upstream variables as reference quantities, the governing equations can be nondimensionalized. When a case is converged for a given ratio of upstream to downstream pressure ratio (sometimes referred to as the seal expansion ratio $r = P_o/P_D$), the leakage rate through the seal can then be recalculated and compared to the initial estimate. For instance if the calculated nondimensional average upstream velocity V is 0.5, the computed leakage rate would be 50% of the estimated rate. The calculated reference Reynolds and Mach numbers would correspondingly have to be reduced by 50%. The initial conditions for all cases considered was to assume that the flow was initially at rest at the stagnation conditions. The back pressure was then gradually lowered until the desired value of P_D was obtained. The solution was then time marched until a steady state solution was obtained. The output of each calculation consists of the fields of the independent and dependent variables, i.e., the Cartesian or cylindrical polar coordinates and the velocity components, density, enthalpy and, if appropriate, the turbulence kinetic energy and the turbulence dissipation. In addition any of the derived variables such as pressure, temperature, viscosity, stream function, total temperature and pressure, etc. can be calculated and displayed.

3.1 Calculation of Leakage Rates

The majority of the calculations performed under this effort were done in the first category of calculations and were designed to demonstrate the ability of the computational procedure to predict the leakage rate for a large number of straight-through and stepped seal configurations at various flow conditions. A total of 18 cases were run, 13 straight-through seal configurations and 5 stepped seal configurations. Tables 1 and 2 and Figs. 3 and 4 give a brief synopsis of the configurations considered, the flow conditions and the modelling assumptions under which the calculations were performed. Several of the calculations were made before the energy equation option was operational in the computer code. For these calculations the energy equation was approximated by assuming that the stagnation enthalpy, h_o, was constant. For flow in the Mach number range considered in this study (essentially incompressible on the inlet plane to a peak in the flow field of between 0.7 and 1.6 depending on the flow conditions and the geometry of the seal), this assumption, which neglects heat conduction and stress work, is a reasonable approximation to the physics. If, however, the walls are nonadiabatic, i.e., either highly cooled or heated, the assumption of zero heat transfer is invalid. For the cases considered under this study, the walls were neither heated nor cooled. Hence the adiabatic assumption was valid. In addition the earlier calculations presumed that the inlet flow was fully developed, and, hence, in these calculations a one-seventh (1/7) power law (Ref. 22) was used for the inlet streamwise velocity profile. For later calculations, a boundary layer equal to 50% of the clearance was assumed on both the inlet section of the rotor and the land. Within the boundary layers, the method of Naise and McDonald (Ref. 23) was used to obtain the turbulent streamwise velocity profile. The mixing length turbulence model utilized was a hybrid model consisting of a Williamson's model (Ref. 32) in the regions away from solid walls and a van Driest damped model (Ref. 33) in the regions near walls. In practice, both mixing length values were calculated at each grid point and the locally minimum value chosen. This gives a smooth variation of mixing length throughout the flow field. In the later calculations, the flows were calculated with both the mixing length and the previously discussed k-ε turbulence model.

The number of grid points utilized for each calculation is presented in Tables 1 and 2. The basic philosophy was to concentrate the grid points in the regions where the largest physical gradients of the dependent variables were expected. These areas were: (1) in the region between the tip of the knife blades and the land, (2) in the wall boundary layers, and (3) in the vicinity of rapid expansion or compression. The total streamwise extent of the physical domain chosen for the computations was 300 clearances in length. The inlet plane was chosen at a distance of 50 clearances upstream of the front face root of the first knife leaving as much as 250 clearances (depending on the seal configuration) from the last knife to the exit plane. The relatively large extent of the domain downstream of the last knife was required by the existence of a large streamwise recirculation zone downstream of the last knife for each case investigated. This large domain was needed to ensure that the recirculation zone would remain inside the region chosen for the computation. A typical distribution of grid points is shown in the vicinity of the seal assembly (see Fig. 5). In the regions both upstream and downstream of the knives, the streamwise grid spacing was considerably larger since in these regions the streamwise gradients were relatively small.

Both Tables 1 and 2 compare the calculated leakage rates, W_{calc}, with the Allison correlation leakage rates, W_{corr}. The Allison correlation leakage rates are a composite of the calculated leakage rates as determined by the Allison design model and experimentally measured leakage rates. The Allison design model (Ref. 30) is based on a multiple regression analysis of a large bank of experimental data. The design model can predict the leakage rates for a wide variety of seal geometries at various flow conditions. The data used as the basis for this model are taken from experiments performed on full-scale labyrinth seals since this model is intended to be used to design contemporary gas turbine engine seals. The calculations performed under this effort, however, were made for large-scale (nominally 10X scale for the straight-through seals and 5X scale for the stepped seals) labyrinth seals as were the leakage rate measurements performed under the experimental portion of this effort. When an experiment had been performed on the particular labyrinth seal at the specified flow conditions, the Allison correlation leakage rate was taken to be the experimentally determined value. This is noted on Tables 1 and 2 by the Allison designated test number. However for several of the

cases calculated, no experimental leakage rates were available. To determine correlation leakage rates for these cases, the following procedure was used. First the cases were divided into straight through and stepped seal configurations, Tables 1 and 2, respectively. For the straight through seals, the Allison design model was used to predict the leakage rates for the cases for which experimental data existed, i.e. cases 5, 6, 7 and 7A. For these cases it was found that the Allison design model underpredicted the leakage rates by an average of 12%. It is felt that this underprediction is due to the Reynolds number effect of the smaller full-scale seals used in the design model. Hence, to account for this effect for the cases where experimental data were not available, the Allison design model was used to determine preliminary values which were then scaled by the factor of 1.12 to account for the large-scale seals used in the calculation.

Of the four stepped seal cases considered in this study, experimental data existed for two cases, cases 12 and 13. These values were used as the Allison correlation leakage rates, W_{calc}, for these cases. For case 11 (a 10X-scale model), experimental results existed for a 5X-scale seal at the same flow conditions. This result was compared with the Allison design model prediction for the full-scale seal. The ratio of leakage rates, 1.09, was applied to the 10X-scale Allison design model leakage rate to obtain the final correlation value. For case 14, the experimental leakage rate for case 12 (the three knife stepped seal with rectangular knives, STLD) was compared with the design model full-scale leakage rate for the case 12 seal. The ratio of these two leakage rates, 0.96, was then used to correct the design model leakage rate for case 14. The assumption was that the ratio between the experimental leakage and the design model for the tapered knives is the same as that for rectangular knives. The results for the stepped seal cases are contained in Table 2.

Examination of the results for the straight-through seal cases Table 1 shows generally good agreement between the calculated leakage rates and Allison correlation leakage rates. To better understand the implications of the results presented in Table 1, it is perhaps desirable to examine the cases individually and/or in logical groupings. Cases for which experimenal data are available, excepting case 8, the three-knife straight-through seal with tapered knives, show excellent agreement. The average discrepancy is 3%. The calculated leakage rate

for case 8 is from 15 to 25 percent lower than that measured depending on whether a mixing length or a k-ε turbulence model was utilized in the calculation. For this case the k-ε turbulence model gives larger values of turbulent viscosity than the mixing length model and, hence, thicker boundary layers and less leakage. On the other hand the predicted and measured leakage rates for case 7, the three knife straight-through seal with tapered knives at a pressure ratio of 4.98, shows excellent agreement, the calculated value predicting only 1.5 percent more than the measured value. The flow for this case was choked as the peak Mach number was 1.398. Examination of the flow for the other straight-through case where the flow was choked and experimental data existed, case 5, indicates a general ability to accurately calculate leakage rates for choked cases; the discrepancy between the calculated and measured leakage rates for this case is approximately 0.9 percent.

For case 1, the single knife straight-through seal with a rectangular knife at a pressure ratio of 3.98, no experimentally measured value of leakage rate was available. The correlation value predicts approximately 30 percent more leakage than the calculated value. This might be due to the use of only 21 grid points in the transverse direction which could possibly lead to an underprediction of mass flux (this was the first case run under this effort).

The three-knife straight-through seal with rectangular knives run at a pressure ratio of 2.0, case 2, shows a reasonable agreement between the calculated and the correlation leakage rates (no experimental data were available for this case). The calculated value of leakage was 1.7 percent lower than the correlation.

For the cases of the single knife and triple knife straight-through seals with slanted knives at a pressure ratio of 2.0, (cases 3 and 4) the agreement between the calculated leakage rates and the correlation values are reasonable with an overprediction of leakage rates of 12 and 7 percent for cases 3 and 4 respectively. From a computational viewpoint, these cases are extremely difficult because of the geometric requirements that the width of the base of the knife blade is large compared to the width of the tip of the knife blade, i.e., a ratio on the order of 100:1. This not only causes difficulty in generating a grid structure, but inherently yields a coordinate system that is highly skewed (as opposed to orthogonal) relative to the other cases considered in this study. Because the flow running up the leading edge surface of the knife

is oriented at an angle greater than 90° to the incoming flow, this results in extremely large gradients in the vicinity of the leading edge of the tip of the knife, i.e., in the entrance region of the gap between the first knife and the land. The large gradients require the use of a large number of grid points in the vicinity of the leading edge in order to resolve the large gradients. The existence of the large gradients in this region leads to strong dissipation and hence the excellent performance of this seal.

In the case of the worn single knife straight-through seal, the calculated leakage rate underpredicts the measured rate by 5.8 percent and 1.2 percent for the mixing length and a k-ε turbulence modelsrespectively. In this case the k-ε turbulence model in general predicts slightly lower values of turbulent viscosity and hence a slightly higher leakage rate. In both cases the discrepancy between the measured and calculated rates are low.

The calculation of the flow in the three knife straight-through seal with tapered knives at a pressure ratio of 2.0, case 8, was run in three modes: (1) a mixing length model with a fully developed 1/7 power law turbulent inlet profile with a 51 x 71 computational grid, (2) a mixing length model with a turbulent inlet profile on the inlet land and rotor equal to 50% of a clearance height with a 61 x 101 grid and (3) a k-ε turbulence model with the same inlet profile and grid structure as in (2). For the first two modes, the calculated leakage rate was approximately 15 percent less than the measured value, while for the k-ε turbulence model the calculated leakage rate was approximately 25 percent lower. In light of the excellent agreement for the three knife straight-through seal with rectangular knives and the single knife straight through seal with a tapered knife, where the physical processes should be similar to the three knife straight-through seal with tapered knives, the amount of the discrepancy was unexpected. Possible reasons for the discrepancy could be the existence of leaks in the experimental apparatus, three-dimensional effects in the apparatus, the sudden expansion downstream of the last knife blade (which did not exist in the calculation) or numerical truncation error in the calculation. Without either repeating the experiment and/or the calculation, it is difficult to draw any firm conclusions for case 8. In addition, it is interesting to note that pressure taps were placed at key locations in the experimental apparatus (see Fig. 6), and that the agreement between the pressure calculation and experiment were excellent.

For the three knife straight-through seal with tapered knives and with a rough land (the roughness was produced by attaching a 30 grit sand paper to the land) at a pressure ratio also of 2.0 (case 9), the agreement between the calculated and measured leakage rate is reasonable. The calculated leakage value is 1.4 percent lower than the measured value. The wall roughness was simulated by using the method of van Driest (Ref. 33) where a slip velocity is assumed on the rough wall. Computationally this has the effect of making the boundary layer thinner and hence more mass can pass through the device. The initial condition for this case was taken as the converged solution for case 8B. The no-slip condition on the land was then replaced by the van Driest model, and a converged solution obtained. It is interesting to note that the effect of the roughness was to increase the peak Mach number from 0.776 to 0.946.

Finally the last case considered was the three knife straight-through seal with tapered knives and with injection at a pressure of 2.0 (case 10). The injection rate was chosen as nominally 10 percent of the total leakage rate. The injection port was positioned in the land midway between the first and second knives. Again the initial condition was taken as the converged result of case 8b. The injection had the same effect as land roughness on the overall leakage rate. The effect of the injection (from a computational viewpoint) is that the amount of leakage is increased over the noninjection case. (Note that no correlation value of leakage rate is available for this case). One possible explanation is that the injected fluid is not exposed to the large losses associated with the leading edge of the first knife. The injection has only the minimal local effect of forcing the flow emerging from between the first knife and land slightly further into the cavity region between the first and second knives. Thus the tentative conclusion is that for this injection case is the effect is negative, i.e., the leakage rate is increased. Perhaps the more desirable location for injection would be in the vicinity of the leading edge of the first knife to further increase the losses in this critical region.

The results for the stepped seal configurations are presented in Table 2. All cases were run in the flow direction of small-to-large seal diameters (STLD mode). Experimental data existed for cases 12 and 13. Cases 11 and 14 had the predicted correlation leakage rates previously

discussed. For the stepped seal configurations, only case 11 was run under choked conditions. For this case the pressure ratio was 2.5 (all other stepped configurations were run at a pressure ratio of 2.0), and the peak calculated Mach number was 1.229. The calculated leakage rate was approximately 12 percent larger than the correlated value. A similar trend was also noted for case 12, the three knife stepped seal with rectangular knives, where the predicted leakage rate was 25 percent higher than the experimentally determined rate. Possible reasons for this discrepancy would be as was previously discussed for the three knife straight-through seal with tapered knives. Again it is of interest to note that the correlation between the measured and calculated static pressures at key points in the seal is excellent (see Fig. 7). This result is similar to that observed for the case of the three knife straight through seal with tapered knives. The other stepped seal configuration for which experimental data existed was case 13, the single knife stepped seal with a slanted knife configuration. In this case, the predicted leakage rate was 8 percent higher than the measured value. The three knife stepped seal with tapered knives configuration (case 14) was calculated with both a mixing length and a k-ε turbulence model. The calculated results were not significantly different. The mixing length model predicting a leakage rate about 10 percent higher than the correlated value, and the k-ε turbulence model predicting a leakage rate about 11 percent higher.

In general the capability of the numerical procedure to accurately predict the leakage rates for a wide variety of seal configurations under various flow conditions appears to be jusified. In the worst case the prediction differed from the Allison correlation value by 30 percent. In the vast majority of cases a more typical variation would be 5-10 percent, and in many cases the predicted and measured values differed by only a few percent. Since this was the first effort in applying this numerical procedure to labyrinth seals, it is to be expected that future results would be even more encouraging. A primary advantage of the calculation procedure is that details of the flow are calculated at every point in the flow, hence the manner in which the flow develops, the basic flow patterns, etc. can be discerned immediately. Typical CPU calculation times for these cases were on the order of 1.5 hours on a CDC 7600 at the Ballistic Research Laboratory, i.e., about $500 per case at the overnight rate. In

addition, recent efficiencies incorporated into the computer program used in the above calculations, viz., in the vectorization on the CRAY computers, have resulted and will result in even lower cost per case rates in the future.

Plots of streamlines, velocity vectors and Mach number contours are shown for representative cases calculated in the leakage rate study (Figs. 8 to 13). When the earlier cases were run, the capability to calculate streamlines was not operational. However, basic streamline patterns can be inferred from the velocity vector plots. The plots represent the flow only in the region of the knives. For all cases investigated, a large clockwise streamwise recirculation was generated downstream of the last knife for flow from left to right. Usually this was accompanied by a small counterclockwise recirculation zone at the junction of the downstream base of the last knife at the rotor. In some cases small clockwise recirculation zones were calculated in the gap between the leading edge of the first knife and the land. When no recirculation zone was calculated in this region, the flow was significantly decelerated due to the strong adverse pressure gradient in this region. In all cases a recirculation pattern existed in the cavity regions. In some cases a small counterclockwise recirculation zone would exist at the trailing edge of the knives due to the separation of the flow. At the junction of the upstream face of the first knife and the rotor cylinder, a small clockwise recirculation zone would usually exist. In addition, in the case of stepped seals, the flow would separate off the convex corner of the land step forming a counterclockwise recirculation pattern. In general, the controling location of the flow for the cases investigated appeared to be the entrance region between the tip of the first knife and the land. In this region the streamwise flow would accelerate and large (on the order of the streamwise velocity) transverse flows would be generated. At the inlet regions of any downstream knives, the accelerations (and hence losses) would be much less as the flow did not significantly turn into the cavity regions. Thus, the flow enters the clearance gaps of the subsequent knives with relatively small tansverse velocities and, hence, the loss is not nearly as great as at the first knife. For the cases where the flow is choked, an expansion pattern was predicted in the region of the exit of the last knife. This can be seen in the Mach number contour plots where the

gradient in Mach number is large, i.e., the Mach number contours are close together.

3.2 Generation of Performance Curves

The purpose of the second classification of calculation was to demonstrate that the computer code could be used to generate designers' curves or performance plots for specific seal geometries. Specifically, it is desired to construct curves of the flow parameter, ϕ,

$$\phi = \frac{W\sqrt{T_0}}{P_0 A} \tag{69}$$

(where again W is the leakage rate, T_0 is the upstream stagnation temperature, P_0 is the upstream stagnation pressure and A is the clearance area over one of the knives) versus the expansion ratio, P_0/P_D, for a specific seal geometry. In this study two seal geometries were considered: (1) a three knife straight through seal with tapered knives, Fig. 3f, and (2) a three knife stepped seal with tapered knives, Fig. 4c. Both of these geometries were considered in the previously described leakage calculations. The main idea here is to generate the curves for cases for which experimental data exist and for which the Allison design model can be used to generate similar curves. Demonstration of the ability of the numerical procedure to produce reasonable performance plots for these two designs would be part of the overall validation process for the code. In addition, it would lend credence to the use of the numerical procedure to generate performance curves for either advanced seal configurations for which data did not exist or for investigating variants of existing seal configurations such as the effects of injection, the effects of various rotational speeds, the effects of wear on various seal designs, etc. These curves could then be used by a designer of labyrinth seal systems to investigate various candidate configurations without the need for setting up experimental rigs. Using this as a method of eliminating undesirable configurations, the designer would then be able to experimentally investigate the performance of the remaining candidate configurations. Considerable savings could be realized by the use of such a process and, in addition, a better seal could be produced.

The technique utilized in this study to obtain the performance plots was started from a converged solution at a pressure ratio of 2.0. For the two seal configurations considered in this study the converged solutions from the previously described leakage investigation (cases 8B and 14A) were used as the initial conditions, i.e., the pressure ratio of 2.0 cases. The back pressures for these two cases were further lowered to a second desired pressure and a converged solution obtained for these cases. This process was continued at other back pressures. For this study converged solutions were obtained for pressure ratios of 2.0, 2.5, 3.5 and 5.0. Initially for both seal configurations the flow was unchoked. However, as the back pressure was lowered the flow choked. For both cases considered, a mixing length turbulence model was utilized.

Overall the use of the computational procedure to produce a performance curve for the two seal configurations seems to be well justified. The two curves produced, although not yielding quantitatively the same results as the design model, gave curves that were qualitatively similar to the measured data. In addition, the prediction of the choke points appear to be in reasonable agreement with the data. It is to be expected, although this has not been demonstrated, that similar curves could be generated for the other configurations considered in the leakage rate study. In addition, the performance curves could also be generated for alternate designs such as smaller or larger clearance, knife tip thicknesses, slant angle, etc. A major advantage would be the ability to generate performance plots for configurations not presently in the Allison or other design models.

Performance curves were generated for two seal configurations: (1) the three knife straight-through seal with tapered knives and (2) the three knife stepped seal with tapered knives. These seal configurations are the same as those analyzed for leakage rates under cases 8 and 24, i.e., Fig. 3f and Fig. 3e, respectively. Results for these two configurations are presented in Figs. 14 and 15. For both cases the calculated values of the flow parameters are compared with the experimental data, the Allison full-scale design model and the Allison design model corrected for the effect of Reynolds number (previously discussed). For the three knife stepped seal with tapered knives no experimental data were available, so in that case the experimental data for the three knife

stepped seal with rectangular knives was used. It is expected that the tapering of the knives would have a small effect on the performance of the seal.

The results for the three knife straight-through seal with tapered knives presented in Fig. 14 show that the calculated values of flow parameter are lower than the measured values of flow parameter by approximately 15 per cent at all pressure ratios. This is consistent with the results shown in the leakage study. Possible explanations for the difference between the measured and calculated flow parameter could be the following: (1) leaks in the experimental apparatus which would yield a larger mass-flux, (2) hot wire measurement/calibration errors, (3) under-resolution of the boundary layers in the calculation which would lead to thicker boundary layers and hence less computational mass flux and, (4) errors associated with the turbulence model used in the calculation. In addition, it is also possible that the three-dimensional experimental apparatus might have had significant three-dimensional effects, and thus a discrepancy would exist when comparing the results with a two-dimensional calculation. The shape of the curves is similar and the predicted choke point (somewhere between a pressure ratio of 2.5 and 3.5) is consistent with the experimentally observed choke pressure ratio of 2.72. The full-scale design model values of flow parameter are approximately 5 percent higher than the calculated values while the design model values corrected for the apparent effect of Reynolds number are approximately 15 percent higher than the calculated values.

The results for the three knife stepped seal with tapered knives is presented in Fig. 15. In this case the predicted values of the flow parameter are approximately 10 percent higher than the measured values. The shape of the calculated performance curve is of the same form as the measured values. The calculated choke value of the pressure ratio is approximately 3.5-4.0 which is consistent with the measured value of 3.84. At the higher values of pressure ratio there is some scatter in the data. In addition from Fig. 15 it can be seen that the full-scale Allison design model uniformly overpredicts the flow parameter for all pressure ratios.

3.3 Comparison of Calculated and Experimental Results

To further validate the ability of the computational procedure to accurately calculate the flow in labyrinth seals, a comparison between available experimental data and computed results was made. Two labyrinth seal configurations were considered in this effort: (1) the three knife straight through seal with tapered knives (see Fig. 3f) and (2) the three knife stepped seal with tapered knives (see Fig. 4c). For both of the configurations extensive hot wire measurements were made as part of the experimental portion of this contractual effort. Details of the experimental work, performed by the Allison Gas Turbine Division, GMC, are reported in Ref. 25. In addition details of the experimental techniques, data reduction, etc. can be found in the above-mentioned reference. Both seal configurations considered were tested at pressure ratios of 2.0, and these are the cases that will be considered in this report. Schematics of the two seals are shown in Figs. 16 and 17. Probe locations are noted by the stations A, B, etc.

For the straight-through seal configuration probes were made in the centers of the first and third knife tip clearance gaps, i.e., stations B and I. Probes were also made at 0.20 inches upstream and downstream of the edges of the knife tips, i.e., at stations A, C, E, G, H, and J . Additionally, a probe was made at the half point of the first cavity, i.e., station D . Measurements in the clearance gaps consist of the streamwise velocity component while measurements fore and aft of the knife tips and in the first cavity consist of both streamwise and transverse velocity components.

For the three knife stepped seal with tapered knives, probes were made in the centers of each knife tip in the clearance gaps, i.e., stations B, F, and I of Fig. 17. The measured results for this seal consist of the streamwise velocity component only.

The calculations used for the comparison were previously described in the section on the calculation of leakage rates, specifically cases 8C and 14B. Both of the computed cases utilized a k-ε turbulence model to account for the effects of turbulence. The governing equations consisted of the two momentum equations, the continuity equation and the energy equation. Boundary conditions were as previously described. Cases 8C

and 14B utilized the mixing length solutions of cases 8B and 14A respectively as initial conditions. The two turbulence equations, the turbulence kinetic energy equation, Eq. (27), and the dissipation of turbulence kinetic energy equations, Eq. (28), were then solved to convergence with the fluid dynamic variables, u, w, ρ and h frozen to obtain initial values of k and ε. Then the fluid dynamic and the k and ε equations were simultaneously solved until a steady state solution was obtained.

The results for the three knife straight-through seal with tapered knives are presented in Figs. 18 through 23. For the flow across the centerline of the clearance gap at the tip of the first knife (Fig. 18), the calculated flow is uniformly of lower velocity. Qualitatively the shape of the streamwise velocity profile is similar with both measured and calculated profiles showing a tendency of the flow to separate on the tip of the knife. This can be seen by the shape of the streamwise velocity profile on the knife tip having a significantly smaller gradient (skin friction) than on the land. The measured velocity profile shows a thinner boundary layer on both the knife tip and the land than the predicted boundary layer profile. The measured profile shows no discernable boundary layer on the land. The difference in the magnitude of the calculated and measured streamwise velocity is consistent with the results of the leakage study where the calculated leakage rate was lower than the measured value (as was previously discussed). The results for the streamwise velocity profile in the clearance gap at the third knife tip (Fig. 19) again shows uniformly lower calculated values than those measured. In this case the measured profile shows a monotonically increasing streamwise velocity as the distance from the knife tip is increased. The calculated velocity profile shows a slightly skewed profile around the centerline in the middle of the gap with the tip boundary layer being somewhat thicker than the land boundary layer. Again the measured results show no discernable boundary layer on the land.

The results in the region 0.20 inches upstream of the leading edge of the first knife are presented in Fig. 20 and the tabulated data are presented in Table 3. Qualitatively the experimental data agree with the calculated flow angles. (If the calibration of the hot-wire is valid, flow angles and velocity magnitudes should be accurate to a few percent).

The velocity magnitudes calculated are uniformly lower than those measured which is again consistent with the calculated leakage rate being lower than the measured values.

The results in the cavity regions between the knives are presented in Figs 21 and 22. Fig. 21 shows the calculated and measured velocity vectors in the first cavity and Fig 22 shows the calculated and measured velocity vectors in the second cavity. The corresponding tabular values are presented in Table 3. In the cavity between the first and second knives the calculated and measured flow angles are quite similar, viz., the flow angles very nearly match. This indicates that the sizes and locations of the recirculation zone are similar. Generally the measured values of the velocity in the cavity are higher than the calculated values. However, in the region above the recirculation zone the calculated magnitude of the velocity is higher at stations C and D and lower at station E.

In the cavity between the second and third knives the results are similar to those in the first cavity. The flow angles predicted by the calculation are a good approximation of the measured values, see Table 3. Again the measured speeds in the recirculation zone are higher than those calculated. The behavior of the speeds above the recirculation zone is the same as in the first cavity, i.e., at station G the calculated speeds are higher than measured and at station H the calculated speeds are lower than the measured speeds.

At the last station where speeds and flow angles were measured, station J , measurements show a considerably different flow structure than that calculated (see Fig. 23 and Table 3). The calculated flow angles do not in general agree with the measured values. The calculated speeds behind the knife are of approximately the same magnitude as those measured. However the calculated speed at the upper most data point is over three times the measured value. The calculation predicts a larger recirculation zone downstream of last knife than the measured data seem to predict. Although it is difficult to determine from the limited amount of data available in this region, the measured recirculation zone appears to be much thinner than the predicted one.

The results for STLD flow through the three knife stepped seal with tapered knives are presented in Figs. 24 through 26. Qualitatively the computed and measured values of the streamwise velocity profiles in the

clearance gaps above the first and second knife tips are similar. In the first knife tip clearance gap (Fig. 24) the peak velocities are of approximately the same value, while in the second knife tip clearance gap the calculated peak velocity is 16 percent lower than the measured value.

At the first knife tip no discernible land boundary layer is observed in the measurements. In the case of the stepped seal (which is contrary to the case of the straight-through seal) the calculated flow has a somewhat lesser tendency to separate over the leading edge of the first knife than does the measured flow.

For the second knife (Fig. 25) the calculated boundary layer profile over the knife tip is very similar to the measured one.

For the third knife tip clearance gap (Fig. 26) the measured flow is qualitatively similar to that measured for the previously described straight-through seal. A monotonically increasing streamwise velocity profile with increasing normal distance from the knife tip is observed in both cases. Again no discernible measured boundary layer is seen on the land. Although qualitatively the calculated and measured profiles are dissimilar, the peak speeds for the two profiles are within a few percent of each other. As with the three knife straight-through seal with tapered knives, the measured data would seem to indicate a smaller recirculation zone downstream of the last stepped seal knife and hence a more rapid expansion than that predicted by the calculation.

In general the comparisons between the measured and the calculated flows are encouraging. Since this is the first effort to both predict the flow in such environments and to perform detailed measurements on these types of labyrinth seals, the results are better than might have been anticipated. More experience in both the experimental and analytical efforts should lead to considerable improvements in both areas. An important point to be mentioned at this juncture is that no attempt was made to 'fine tune' the calculations to get better comparisons with the experimental data. The analysis models were in fact run before the test data were available. The measured data comparison was performed with model calculations that were not influenced by the experimental program.

The type of 'tuning' which could be examined would concern improving the numerical accuracy and modifying the inflow profiles to more accurately reflect the conditions (apparently) occurring in the experimental seals.

3.4 Rotating Labyrinth Seal Calculation

The first three categories of calculations performed in this study were concerned with "two-dimensional" labyrinth seal configurations having a rectangular clearance gap. All experimental cases were run with a spanwise dimension of 6.28 inches to simulate the static test rig. The flow through the clearance gaps would essentially be two-dimensional at the experimental aspect ratios, i.e., the endwall effects were neglected. Most practical applications of labyrinth seals are for rotating equipment in which case an axially symmetric set of coordinates must be used to describe the seal geometry. In order to demonstrate this capability a sample case was run with rotation.

The three knife straight seal with tapered knives was chosen with the knife side rotating for demonstration at a pressure ratio of 2.0. As in the nonrotating case the flow was initially assumed to be stagnant and the back pressure lowered. The flow was then drawn through the seal and the basic nonrotating flow pattern established. Then the rotor was turned until the desired rotational speed was obtained and the converged solution with rotation was obtained. The equations solved are the transformed cylindrical polar Navier-Stokes equations. The transformation is required because of the tapered knives which yield a nonorthogonal coordinate system. Three separate momentum equations, the continuity equation and an energy equation are solved. Because of the rotation of the rotor, a rotational momentum equation must be solved even though all rotational derivatives are zero. The physical dimensions for the seal configuration chosen are shown in Fig. 3g. In addition the radius of the inner cylindrical surface of the rotor was arbitrarily chosen as 0.254 meters (or 100 clearances) and the rotational speed was chosen as 6,000 revolutions per minute, 628 radians per sec.

A sample streamline plot in the vicinity of the first knife for the rotating seal case is shown in Fig. 27. Qualitatively the streamline patterns are the same as for the nonrotating case. The steady state value of the flow parameter for the rotating case was 0.315 lbm $^{\circ}R^{1/2}$/lbf-sec vs 0.331 lbm $^{\circ}R^{1/2}$lbf-sec for the nonrotating case. Thus the calculated overall effect of the cylindrical symmetry and the rotational effects is to decrease the value of the flow parameter

(and hence comparable leakage rate) for this seal configuration by about 5 percent over the nonrotating case.

Another effect predicted by the calculation procedure was the rather large amount of swirl velocity that exists far downstream of the last knife. Since the height of the knives are 11/12 of the total distance from the rotor cylinder to the land, the knives impart large amounts of swirl into the upper portion of the flow domain (the knife tip speeds are 12.6 times the mean inlet velocity and 71 percent of the peak streamwise velocity downstream of the last knife tip). In the immediate vicinity fo the trailing edge of the last knife, the swirl is rather rapidly dissipated by the large viscous effects (at one clearance downstream the swirl velocity has decreased to 45 percent of the peak tip velocity). However downstream of this region the losses are much smaller. At 100 clearances downstream the swirl velocity drops by 18 percent. Thereafter the decreases in the swirl level become essentially zero. This is probably due to the small viscous forces in the core of the flow far downstream and the lack of a circumferential pressure gradient. On the other hand in the region upstream of the first knife, the extent of the penetration of the swirl into the flow is minimal. The swirl imparted into the flow by the rotor is small upstream of the first knife. As the first knife is approached some of the swirl is convected away from the rotor surface by the increasing transverse velocity (caused by the turning of the streamwise velocity to flow over the knife).

The general observation for the rotation case is that the code appears to be able to successfully calculate seal flows in the presence of rotation. In future work this should probably be an area where considerable effort should be expended both experimentally and computationally as this is the actual environment in which real seals exist.

4.0 CONCLUSIONS

The results of this first effort to calculate the flow in labyrinth seals by the numerical solution of the Navier-Stokes equations is very encouraging. It has been demonstrated that the flow in a wide variety of realistic labyrinth seal geometries can be calculated under various flow conditions. The flow in both straight-through and stepped seal geometries has been successfully calculated. Both orthogonal and nonorthogonal coordinate systems have been used, and the flow has been calculated for both a planar and axisymmetric system. Pressure ratios as large as five to one have been calculated with no apparent problem. Seals with multiple knives have been considered, and the flow was successfully predicted. A variety of boundary conditions have been successfully utilized in these calculations, and a general starting procedure has been developed that can be used with any seal geometry and for any pressure ratio. The numerical procedure has proven to be robust, i.e., all calculations that were attempted produced converged solutions. Both mixing length and two-equation turbulence models were successfully used for the calculations. Numerical difficulties often associated with the two-equation (k-ε) turbulence model were eliminated and converged solutions obtained for cases that had not previously converged with the use of the k-ε turbulence model. Calculation of the flow for an axisymmetric rotating labyrinth seal presented no problem either with the physics or in numerically converging the case.

Comparison of the calculated results with experimental results was in general very encouraging, especially when it is remembered that this is the first effort for these classes of geometries. The computer code has demonstrated an ability to accurately calculate the leakage rates for a wide variety of geometries and flow conditions. The two notable exceptions are the three knife straight-through seal with tapered knives and three knife stepped seal with rectangular knives at pressure ratios of 2.0. The comparison of the hot-wire data with the calculated results for the three knife straight-through seal with tapered knives shows qualitatively similar results. The three knife stepped seal with tapered knives shows good qualitative agreement between experiment and calculation. The performance curves predicted by the calculation procedure generated

curves similar to experimental data and to those predicted by the Allison design model. A major advantage of the calculation procedure would be its ability to calculate these performance curves for labyrinth seals for which there is no data base.

The calculations performed under this effort required a reasonable amount of computer time. Further, it is expected that in the near future with a vectorized program typical calculations could be run for on the order of less than $200 per data point. It is hoped that the computer code will be integrated into the design process in the near future. Because of the very general nature of the computer code, i.e., it has the ability to accept any reasonable coordinate system and to perform calculations in that system, it would be desirable to utilize the code to perform calculations for advanced seal concepts. Finally, it would be desirable to perform calculations for actual full-scale labyrinth seals in the rotating mode as this is the environment that is actually experienced in sealing applications.

REFERENCES

1. The Labyrinth Packing, Engineer, Vol. 165, No. 4280, Jan. 21, 1938.

2. Parsons, C.A.: Electrical Lighting at Cambridge, Engineer, Nov. 4, 1892.

3. Becker, E.: Stromungsvorgange in Ringformigen Spalten, V.D.I., Vol. 51, 1907.

4. Martin, H.M.: Labyrinth Packings, Engineer, Jan. 10, 1908.

5. Stodola, A.: Steam nd Gas Turbines, sixth edition, Vol. 1, 1927.

6. Trutnovsky, K.: Beruhrungsfreie Dichtungen, V.D.I., Verlag, Berlin, 1943 (Library of Congress call No. TJ529T78).

7. Zabriskie, W., and Sternlicht, B.: Labyrinth Seal Analysis, Journal of Basic Engineering, Trans. ASME, Series D, Vol. 81, No. 3, Sept. 1959.

8. Roache, P.J.: Computtional Fluid Dynamics, Hermosa Publishers, New Mexico, 1972.

9. Peyret, R. and Viviand, H.: Computation of Viscous Compressible Flows Based on the Navier-Stokes Equations, AGARD-AG-212, 1975.

10. MacCormack, R.W.: The Effect of Viscosity in Hypervelocity Impact Cratering, AIAA Paper No. 69-354, 1969.

11. Widhopf, G. and Victoria, K.: On the Solution of the Unsteady Navier-Stokes Equations Including Multicomponent Finite Rate Chemistry, Comput. Fluids, Vol. 1, 1973, pp. 159-184.

12. Briley, W.R. and McDonald, H.: Solution of the Multidimensional Compressible Navier-Stokes Equations by a Generalized Implicit Method, Journal of Computational Physics, Vol. 24, 1977, pp. 372-397, 1977.

13. Shang, J.S. and Hankey, W.L., Jr.: Numerical Solution of Shock Wave-Turbulent Boundary-Layer Interaction, AIAA Journal, Vol. 14, No. 10, October 1976, p. 1451.

14. Favre, A.J., The Equations of Compressible Turbulent Gases. Annual Summary Report No. 1, Institute de Mechanique Statistique de la Turbulence, January 1965.

15. Kolmogorov, A.N.: Equations of Turbulent Motion of an Incompressible Turbulent Fluid, IZC Adak. Naut. SSSR Ser. Phys. VI, No. 1-2, 56, 1942.

16. Launder, B.E. and Spalding, D.B.: The Numerical Computation of Turbulent Flows. Computer Methods in Applied Mechanics and Engineering, Vol. 3, 1974.

17. Jones, W.P. and Launder, B.E.: The Prediction of Laminarization with a Two-Equation Model of Turbulence. Int. J. Heat Mass Transfer, Vol. 15, 1972.

18. Buggeln, R.C., Briley, W.R. and McDonald, H.: Solution of the Navier-Stokes Equations for Three-Dimensional Turbulent Flow with Viscous Sublayer Resolution, AIAA Paper No. 81-1023, 1981.

19. Gibeling, H.J. and McDonald, H.: Development of a Two-Dimensional Implicit Interior Ballistics Code. Contract Report ARBRL-CR-00451, March 1981.

20. Thomas, P.D. and Lombard, C.K.: The Geometric Conservation Law - A Link Between Finite-Difference and Finite-Volume Methods of Flow Computation on Moving Grids. AIAA Paper No. 78-1208, 1978.

21. Liu, N.-S., Shamroth, S.J. and McDonald, H.: Numerical Solution of Navier-Stokes Equations for Compressible Turbulent Two/Three Dimensional Flows in the Terminal Shock Region of an Inlet/Diffuser. NASA-CR-3723, August 1983.

22. Schlicting, H.: Boundary-Layer Theory, Sixth Edition, McGraw-Hill Book Company, 1968, pp. 192-193.

23. Maise, G. and McDonald, H.: Mixing Length and Kinematic Eddy Viscosity in a Compressible Boundary Layer. AIAA Journal Vol. 6, No. 1, Jan. 1968, pp. 73-80.

24. Lindemuth, I. and Killeen, J.: Alternating Direction Implicit Techniques for Two-Dimensional Magnetohydrodynamic Calculations. Journal of Computational Physics, Vol. 13, pp. 181, 1973.

25. Beam, R.M. and Warming, R.F.: An Implicit Factored Scheme for the Compressible Navier-Stokes Equations. AIAA Journal, Vol. 16, pp. 393-402, 1978.

26. Briley, W.R. and McDonald, H.: On the Structure and Use of Linearized Block Implicit Schemes. Journal of Computational Physics, Vol. 34, pp. 54-72, 1980.

27. Douglas, J. and Gunn, J.E.: A General Formulation of Alternating Direction Methods. Numerische Math., Vol. 6, pp. 428-453, 1964.

28. Briley, W.R., Buggeln, R.C. and McDonald, H.: Computation of Laminar and Turbulent Flow in 90 Degree Square Duct and Pipe Bends Using the Navier-Stokes Equations. SRA Rpt. R82-920009-F, 1982.

29. Shamroth, S.J., McDonald, H. and Briley, W.R.: A Navier-Stokes Solution for Transonic Flow Through a Cascade. SRA Rpt. 81-920007-F, 1982.

30. Tipton, D.L., Scott, T.E. and Vogel, R.E.: Labyrinth Seal Analysis, Volume III - Analytical and Experimental Development of a Design Model for Labyrinth Seals, AFWAL-TR-85-2103, Volume III, January 1986.

31. Ames Research Staff: Equations, Tables, and Charts for Compressible Flow. NACA Report 1135, pg. 19, 1953.

32. Williamson, J.W.: An Extension of Prandtl's Mixing Length Theory. Applied Mechanics and Fluids Engineering Conference, ASME, June 1969.

33. Van Driest, E.R.: On Turbulent Flow Near a Wall. Journal of the Aeronautical Sciences, November 1956.

34. Beam, R.M. and Warming, R.F.: An Implicit Finite-Difference Algorithm for Hyperbolic Systems in Conservation Law Form. J. Comp. Physics, Vol. 22, 1976, p. 87.

LIST OF SYMBOLS

Symbols

A	Area or matrix of time linearization coefficients
c_p	Specific heat at constant pressure
c_1	Constant for two equation turbulence model
c_2	Constant for two equation turbulence model
c_μ	Constant for two equation turbulence model
D	Rate of deformation tensor or elements of spatial differential operators
F	Vector of convection and diffusion terms (Eqs.(31)-(33))
H	Vector of time terms
h	Enthalpy
J	Jacobian
k	Turbulence kinetic energy
L	Matrix of linear differential operators
ℓ_m	Mixing length
$\dot{m}$	Mass flux
M	Mixture molecular weight
$\vec{n}$	Unit vector in normal direction
$\vec{n}_s$	Unit vector in symmetry direction
P	Pressure
Pr	Prandtl number
$\vec{q}$	Heat flux vector
R	Universal gas constant
Re	Reynolds number
r	Seal expansion ratio
S	Vector of source terms (Eq.(34))

Symbols

t	Time
T	Temperature
U	Velocity component
$\hat{U}$	Specific internal energy
u	Cartesian velocity component
V	Average velocity
$\vec{V}$	Velocity vector
W	Vector of flux variables (Eq.(30)) or mass flux
$\bar{x}$	Cartesian coordinate
y	General coordinate

Greak Symbols

β	Crank-Nicolson factor
Δ	Change
δ	Kronecker delta
ϵ	Dissipation of turbulence kinetic energy
θ	Rotational direction
κ	Thermal conductivity
μ	Dynamic viscosity
ν	Kinematic viscosity
ρ	Density
σ	Dissipation parameter
τ	Stress tensor
Φ	Energy dissipation
ϕ	Vector of dependent variables or flow parameter

Subscripts

art	Artificial
call	Calculated
corr	Correlated
D	Downstream
ℓ	Laminar
n	Normal
o	Stagnation
s	Symmetry
T	Turbulent
T_1	First tangential direction
T_2	Second tangential direction
w	Wall
$\bar{x}_i$	Associated with i^{th} Cartesian direction
$\bar{x}_j$	Associated with j^{th} Cartesian direction
1	First direction
2	Second direction
3	Third direction

Superscripts

n	n^{th} time step
T	Transpose
*	First intermediate time level
**	Second intermediate time level
'	Fluctuation
1	First direction
2	Second direction
3	Third direction

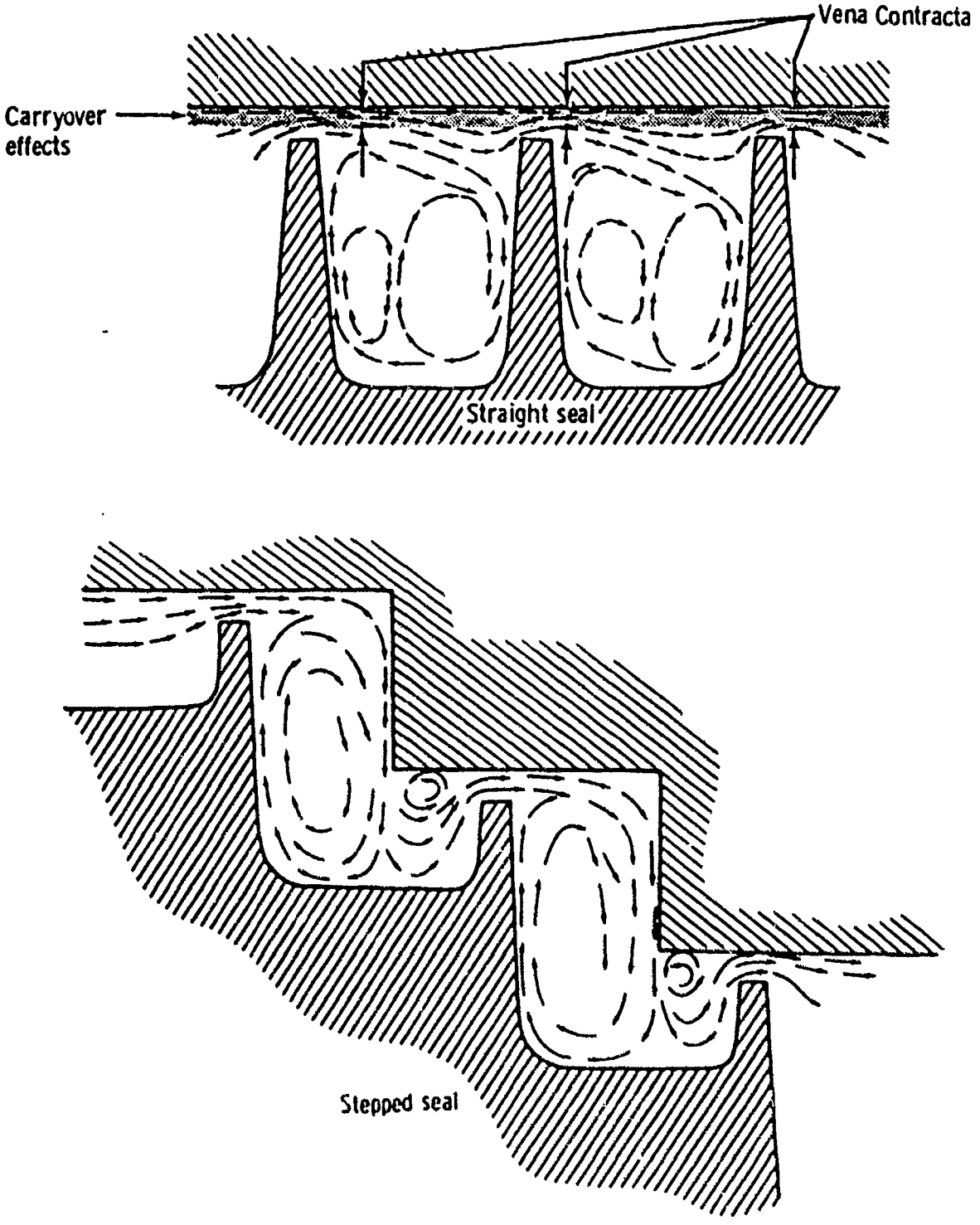

Figure 1 - Conceptual Flow Fields for Straight-Through and Stepped Labyrinth Seals.

STEPPED SEALS

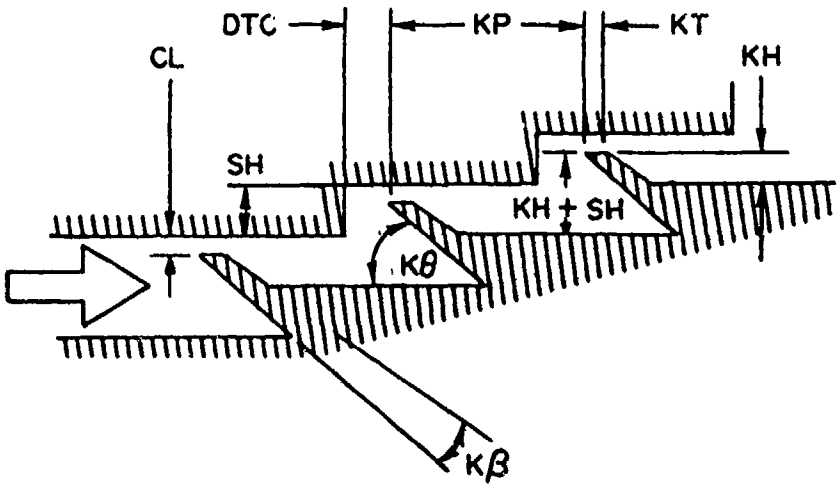

STRAIGHT SEALS

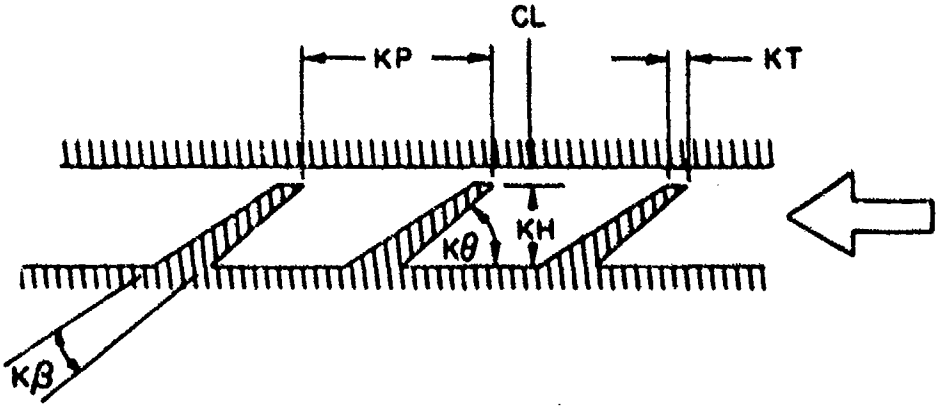

Figure 2 - Labyrinth Seal Nomenclature.

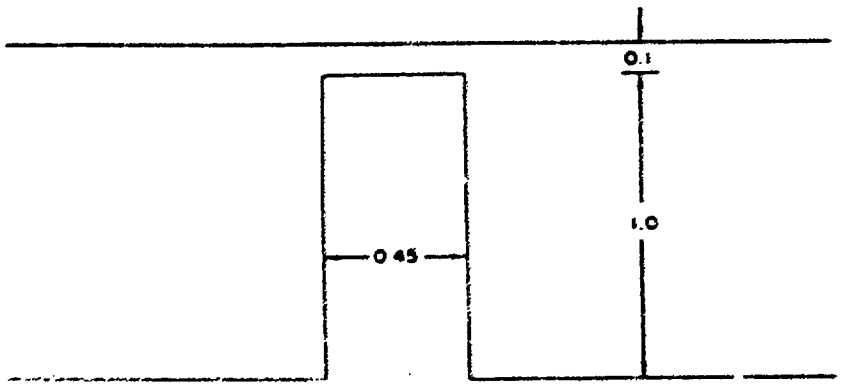

(a) Rectangular - Single Knife

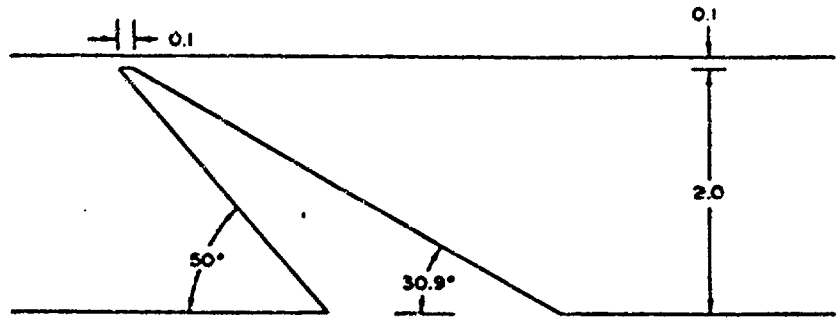

(c) Slanted - Single Knife

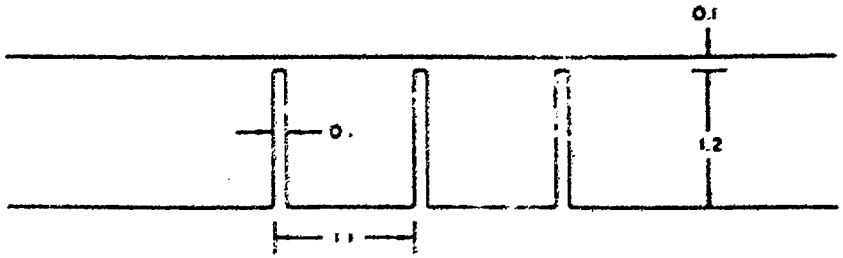

(b) Rectangular - Three Knives

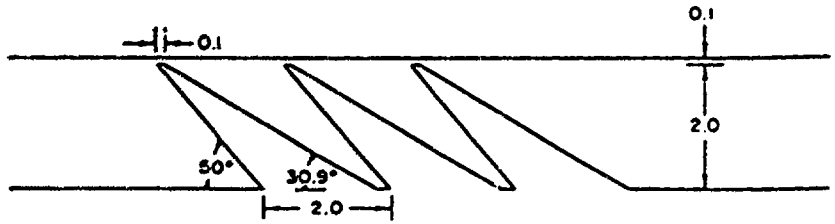

(d) Slanted - Three Knives

Figure 3 - Straight-Through Seal Configurations.

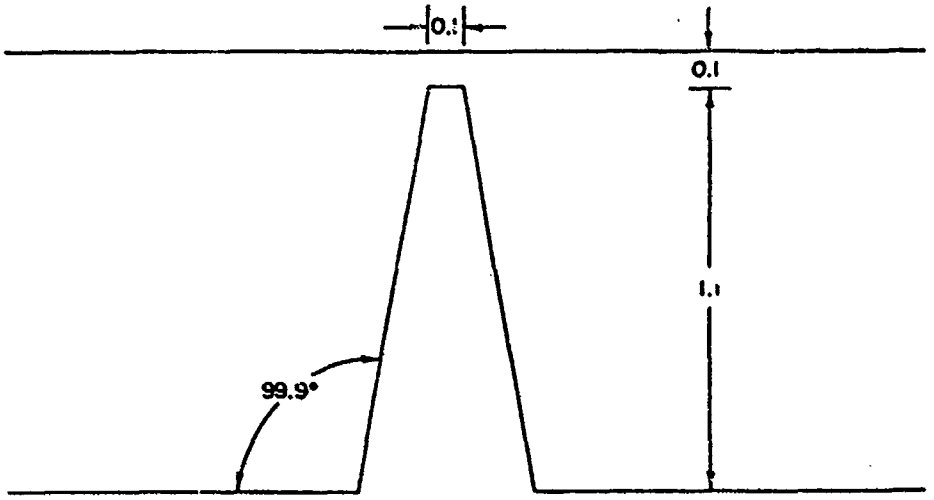

(e) Tapered - Single Knife

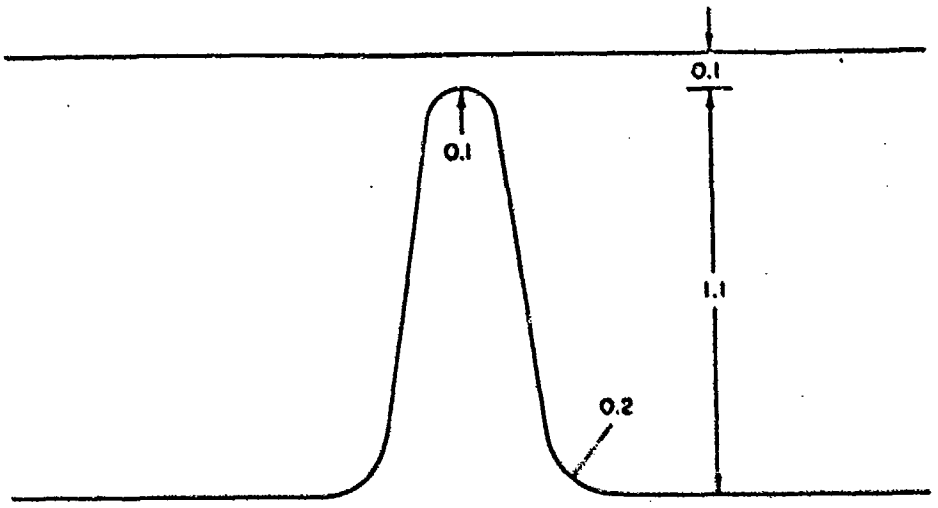

(f) Worn - Single Knife

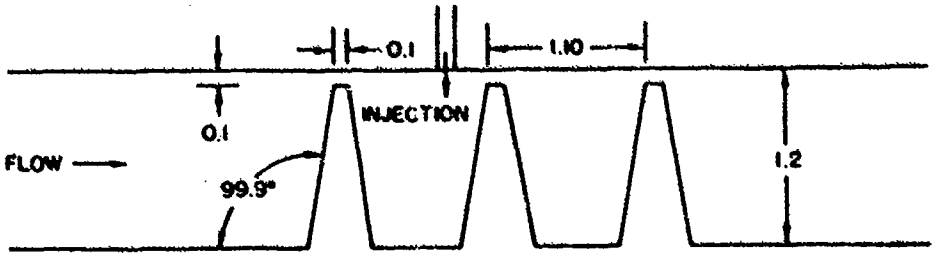

(g) Tapered - Three Knives

Figure 3 - (Continued)

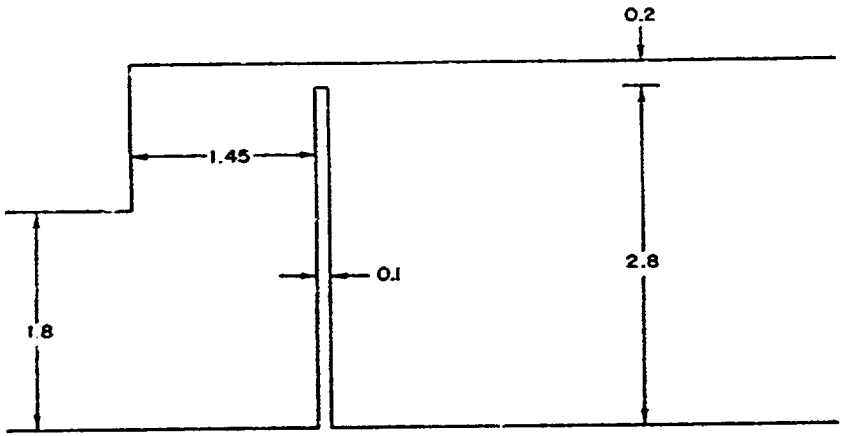

(a) Rectangular - Single Knife

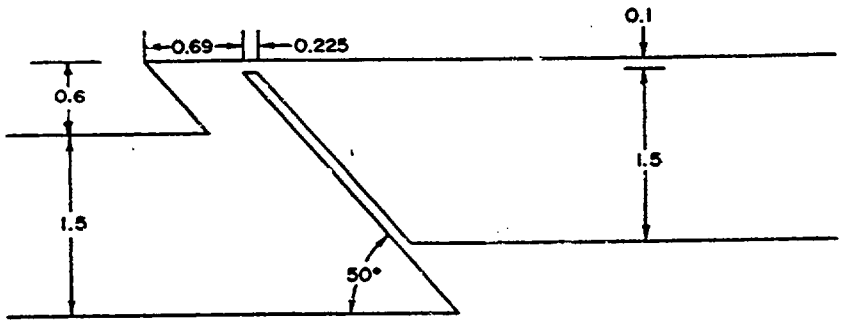

(c) Slanted - Single Knife

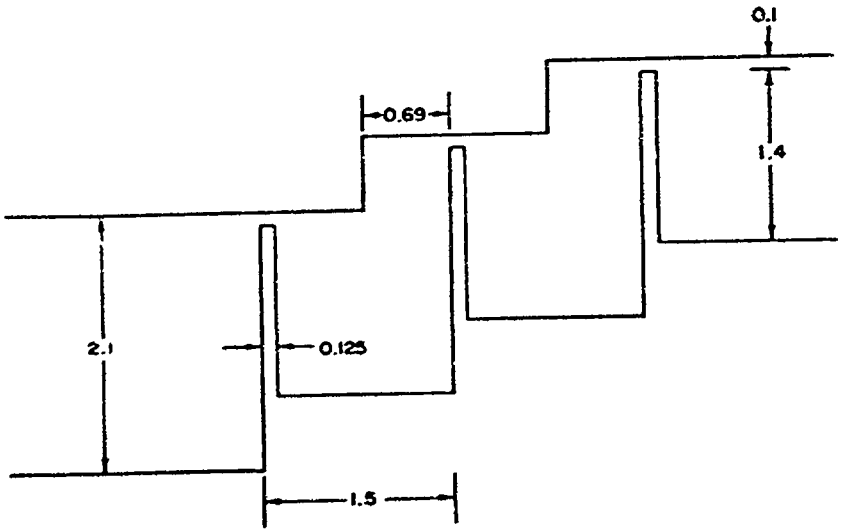

(b) Rectangular - Three Knives

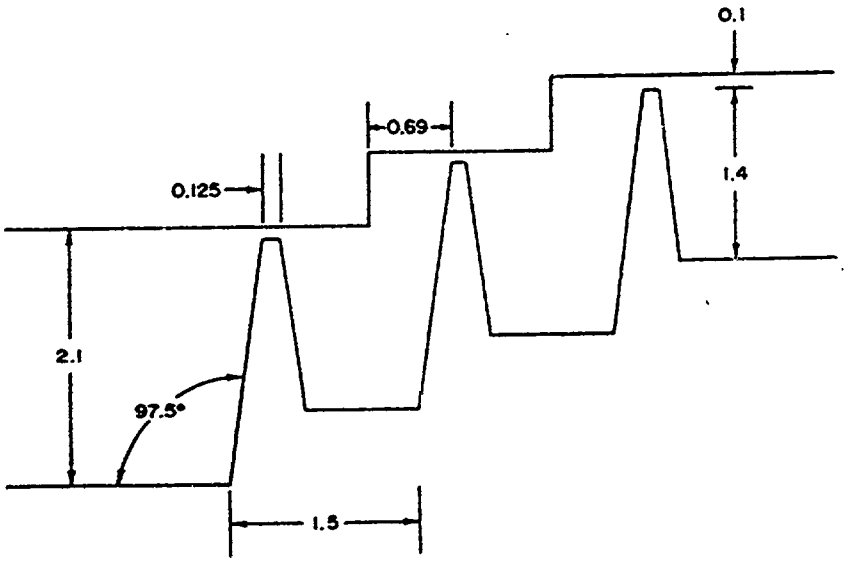

(d) Tapered - Three Knives

Figure 4 - Stepped Seal Configuration, STLD.

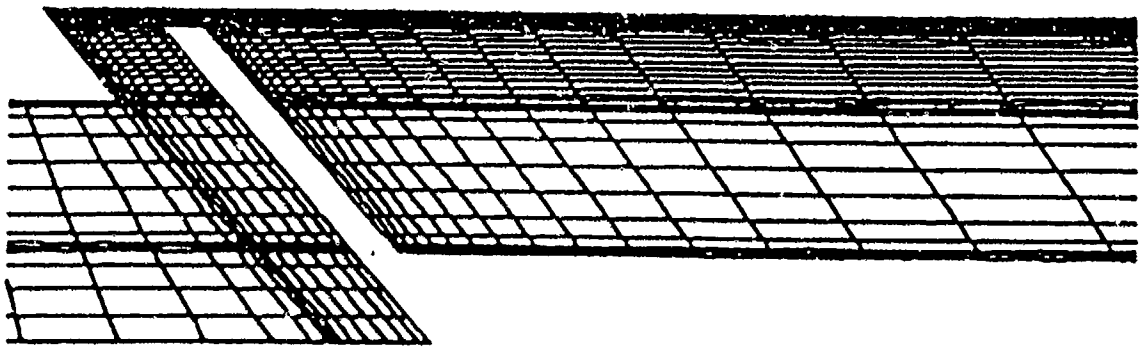

Figure 5 - Sample Grid Structure - Single Knife Stepped Seal with a Slanted Knife

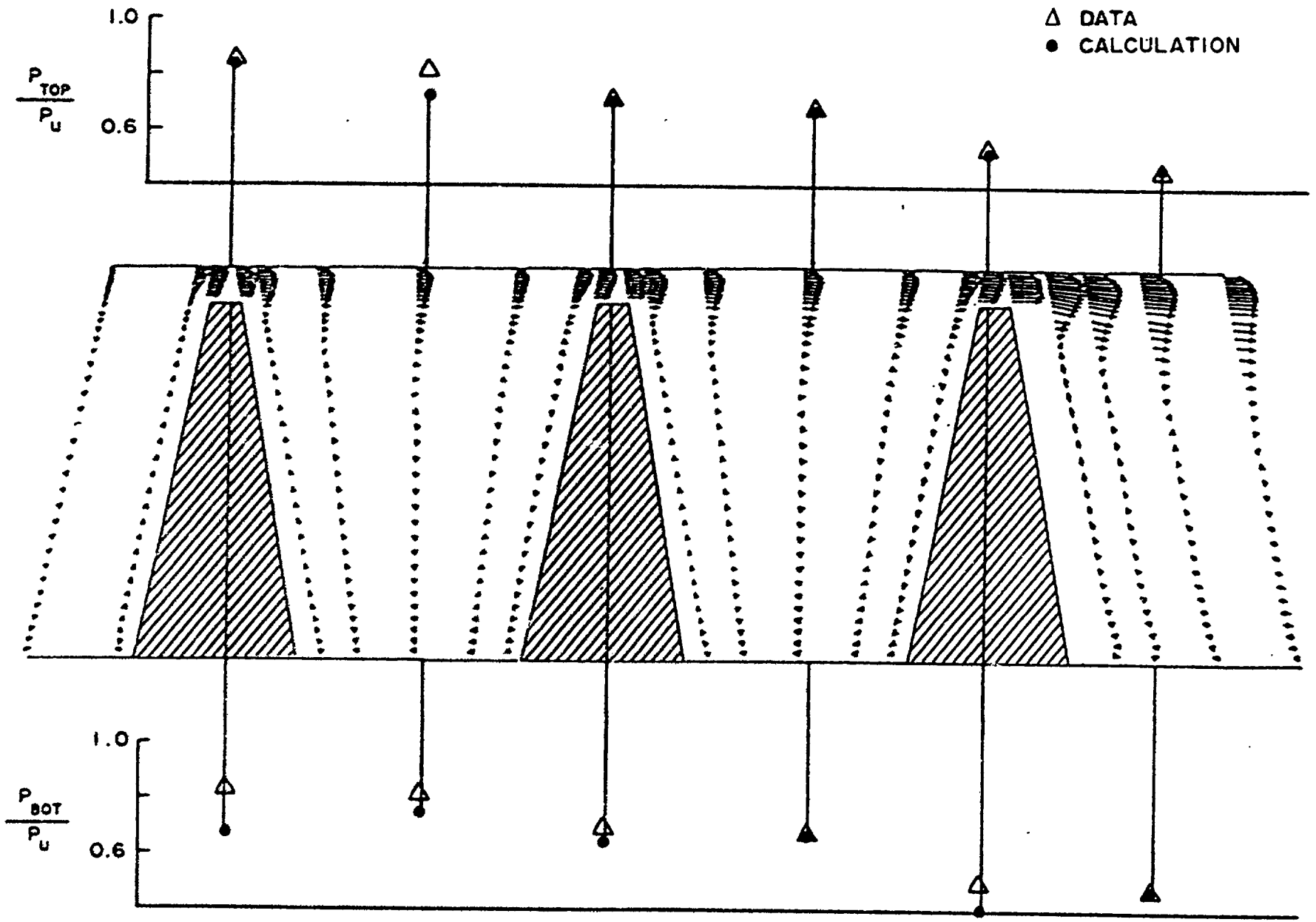

Figure 6 - Pressure Comparisons - Three Knife Straight-Through Seal with Tapered Knives.

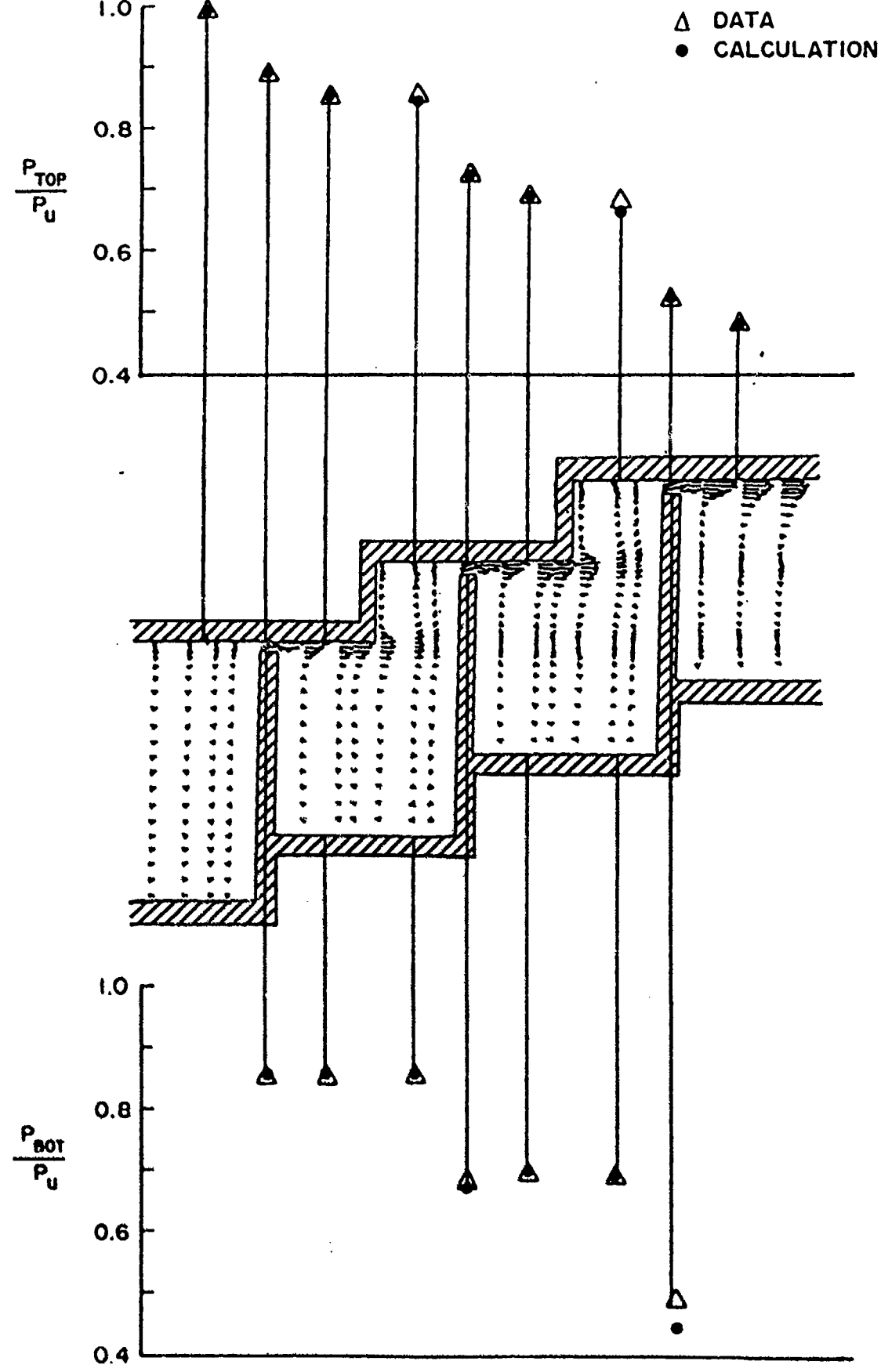

Figure 7 - Pressure Comparisons - Three Knife Stepped Seal with Tapered Knives.

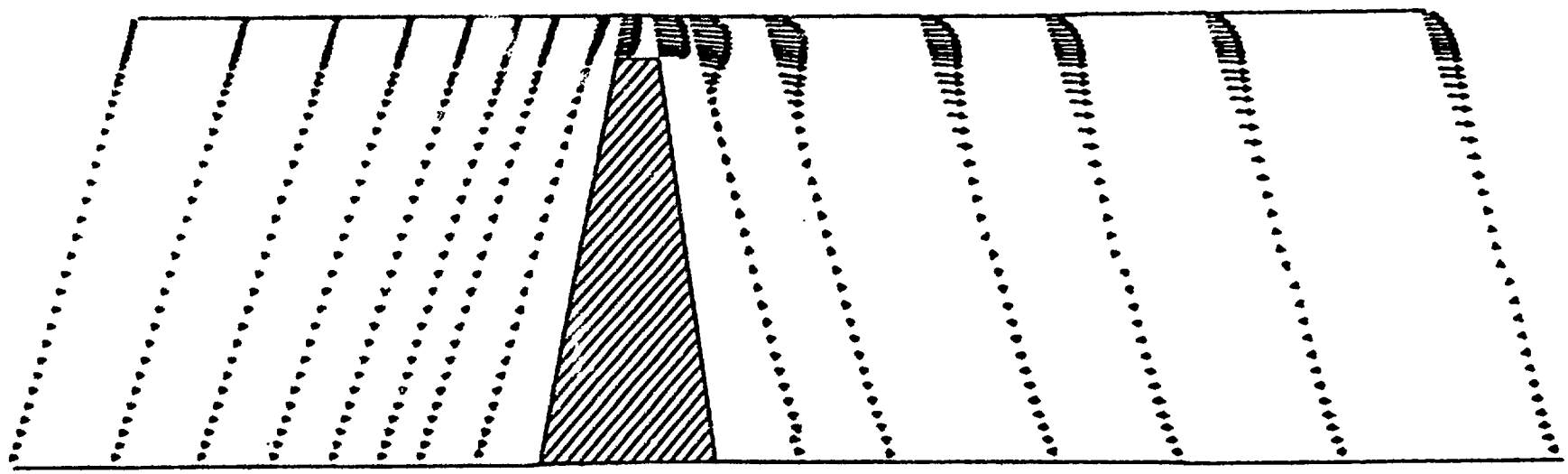

Figure 8 - Velocity Vectors - Single Knife Straight-Through Seal with a Tapered Knife.

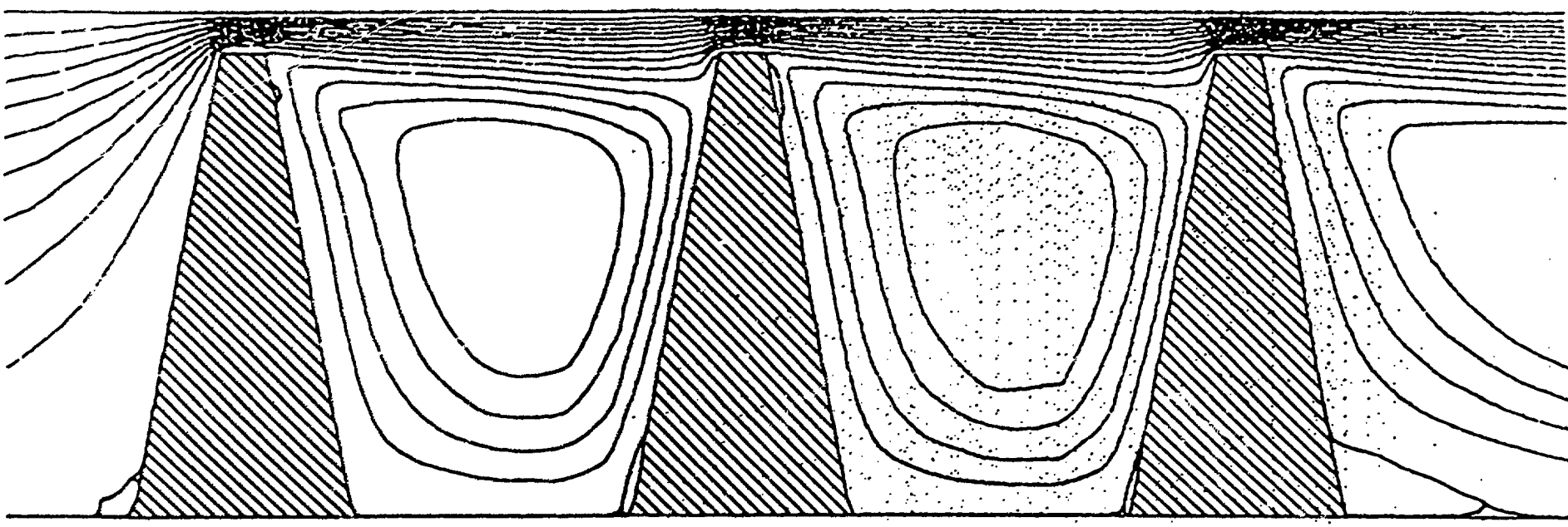

Figure 9 - Streamlines - Three Knife Straight-Through Seal with Tapered Knives.

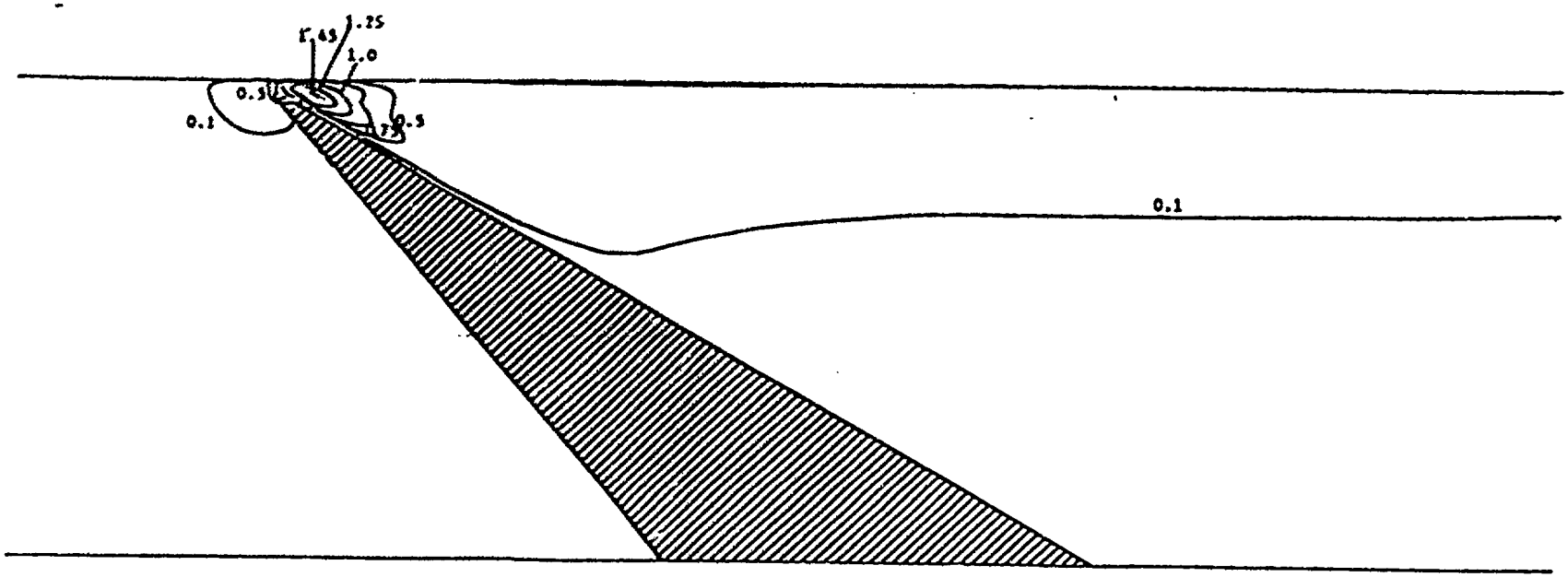

Figure 10 - Mach Number Contours - Single Knife Straight-Through Seal with a Slanted Knife.

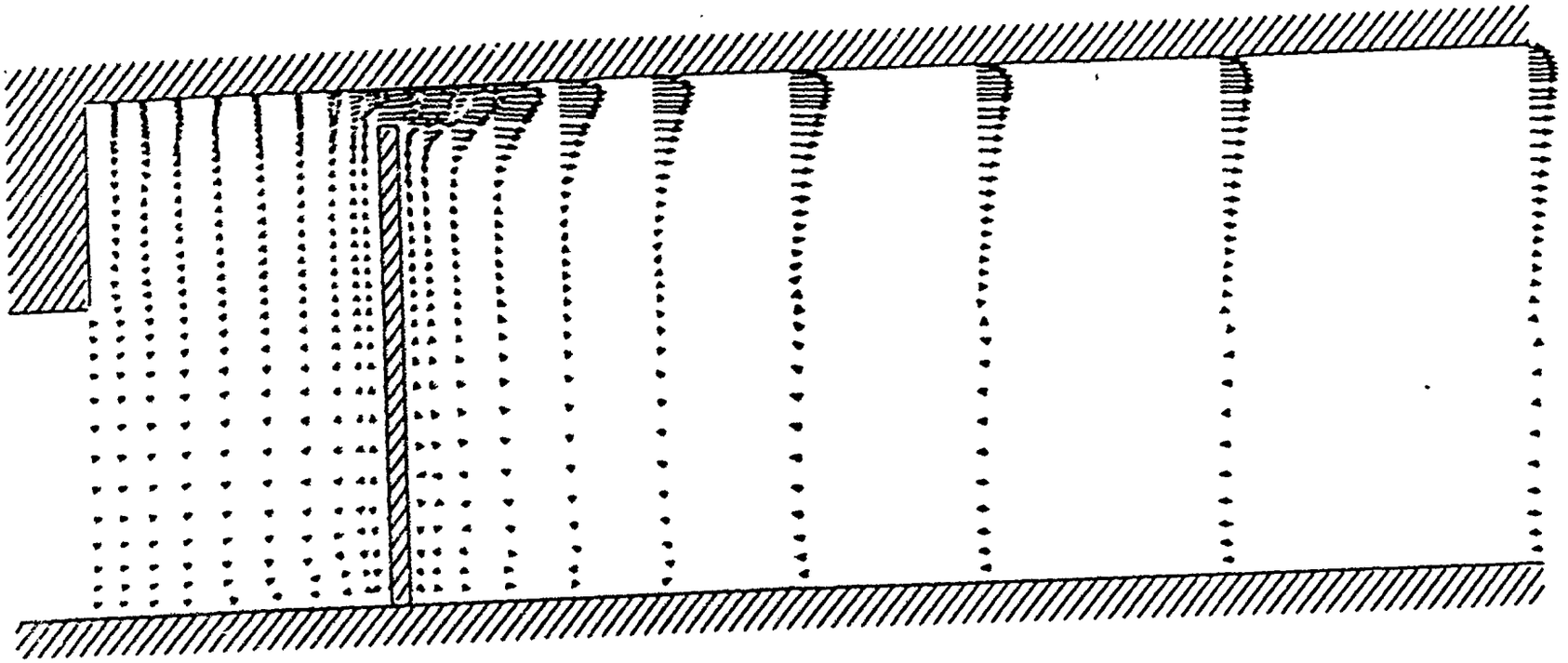

Figure 11 - Velocity Vectors - Single Knife Stepped Seal with a Rectangular Knife.

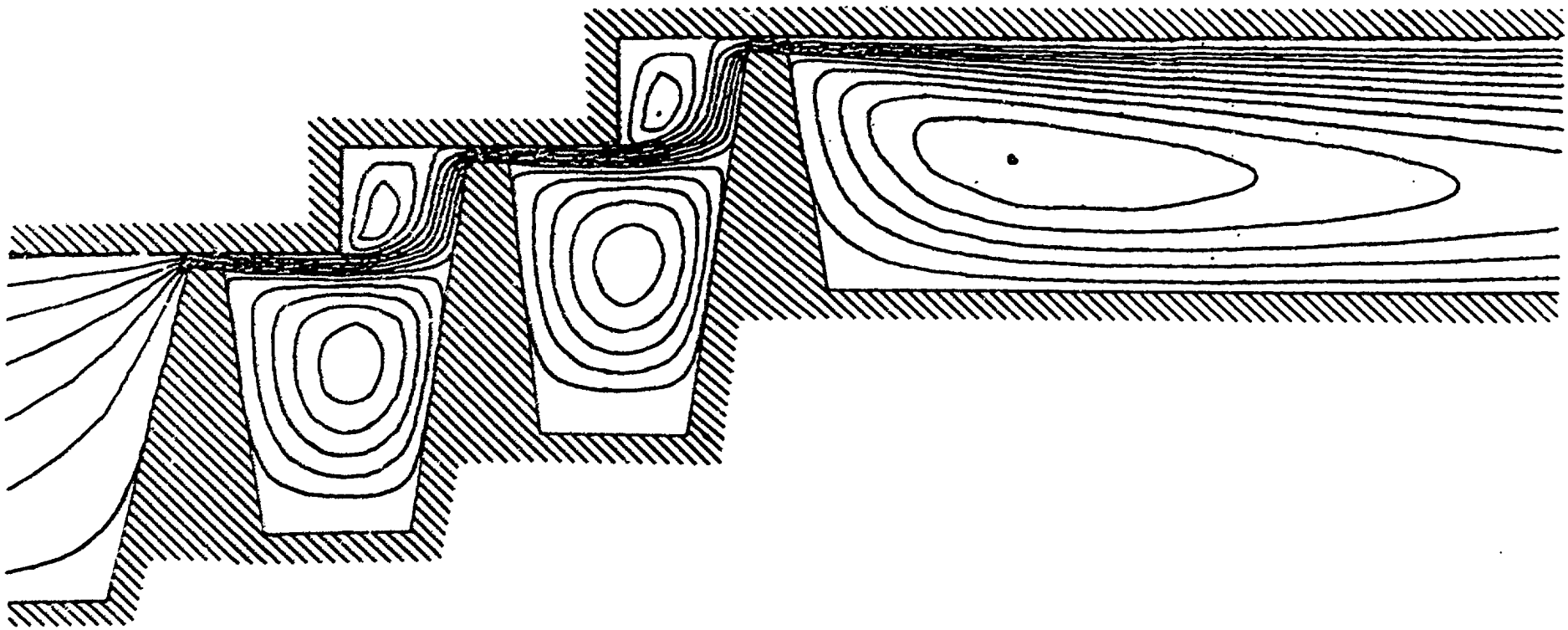

Figure 12 - Streamlines - Three Knife Stepped Seal with Tapered Knives.

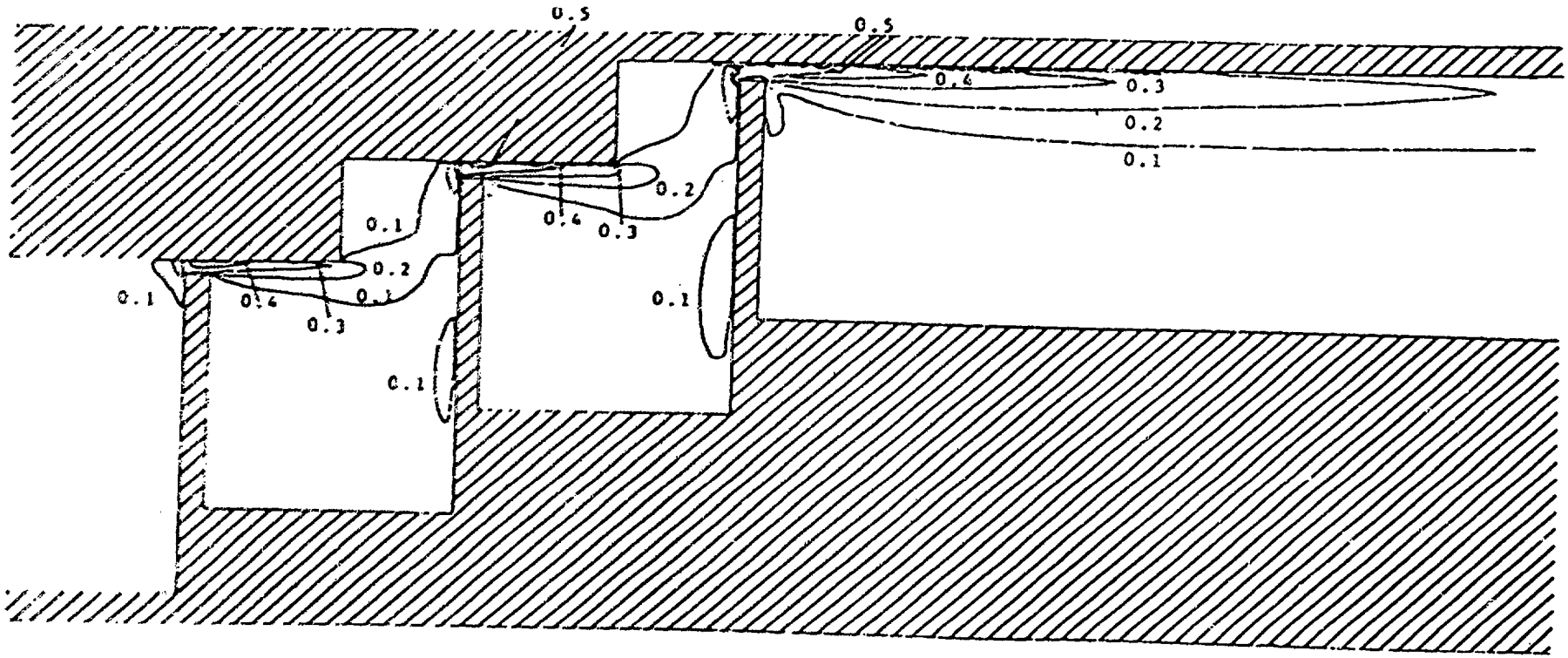

Figure 13 - Mach Number Contours - Three Knife Stepped Seal with Rectangular Knives.

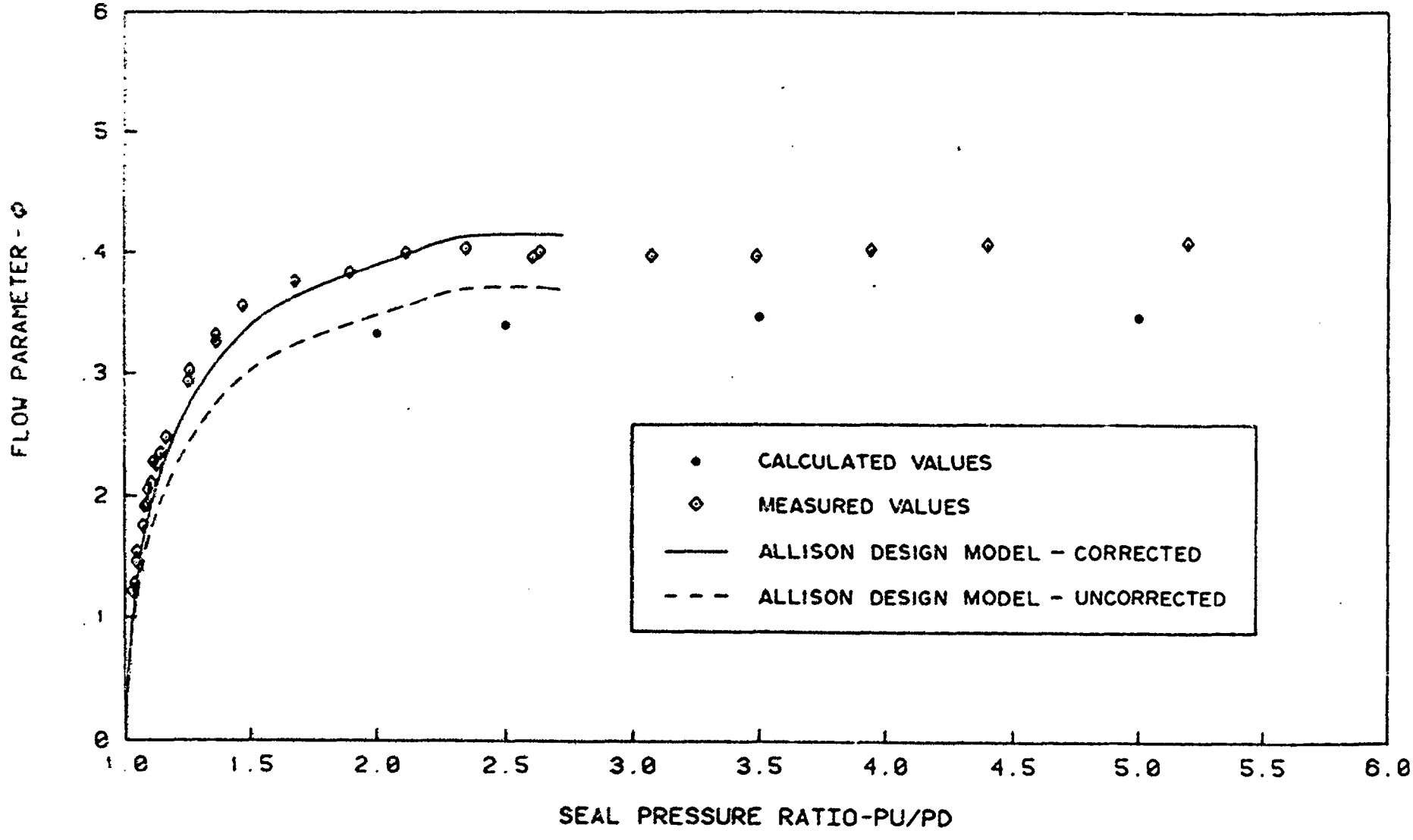

Figure 14 - Performance Plot - Three knife Straight-Through Seal With Tapered Knives.

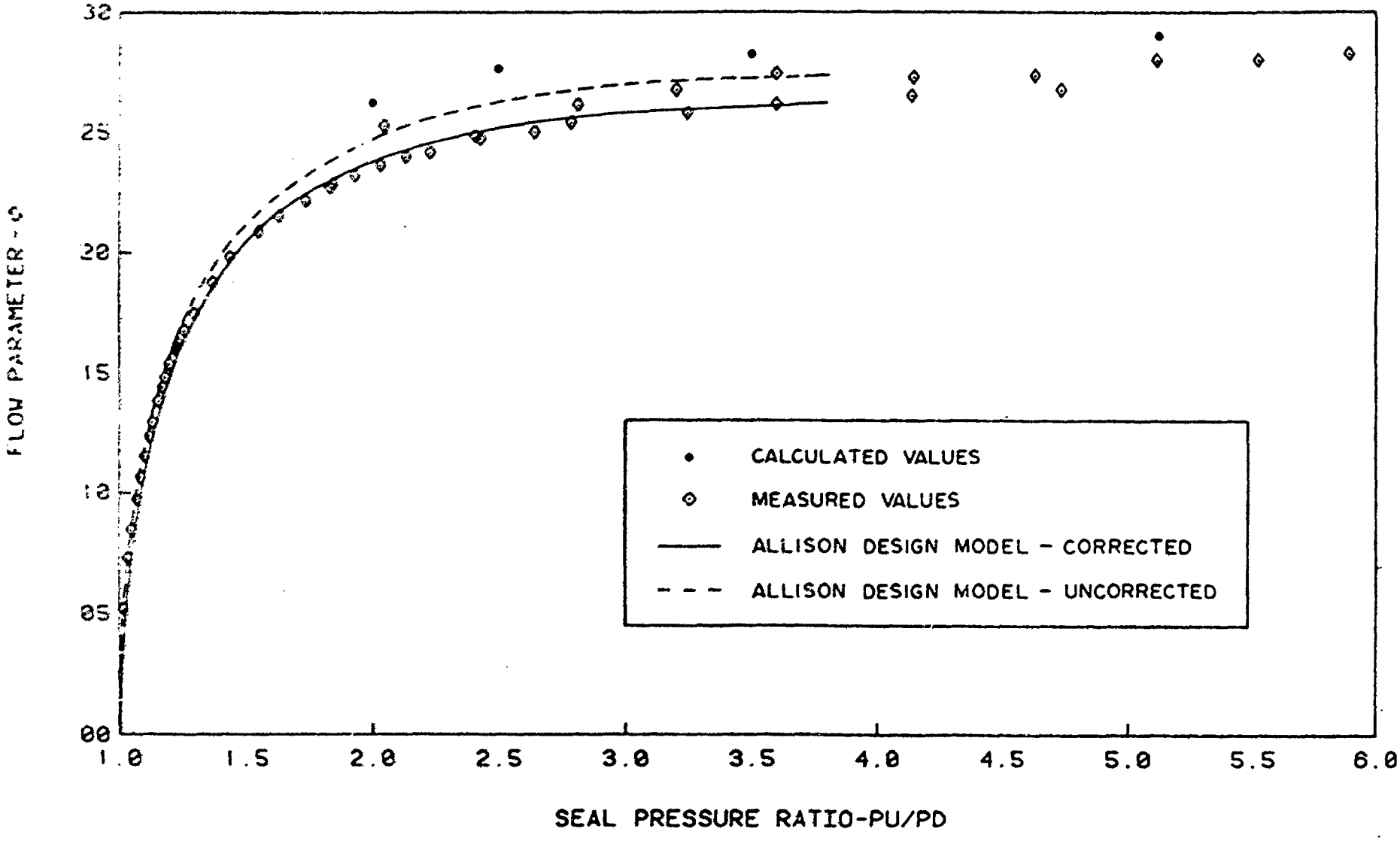

Figure 15 - Performance Plot - Three knife Stepped Seal With Tapered Knives.

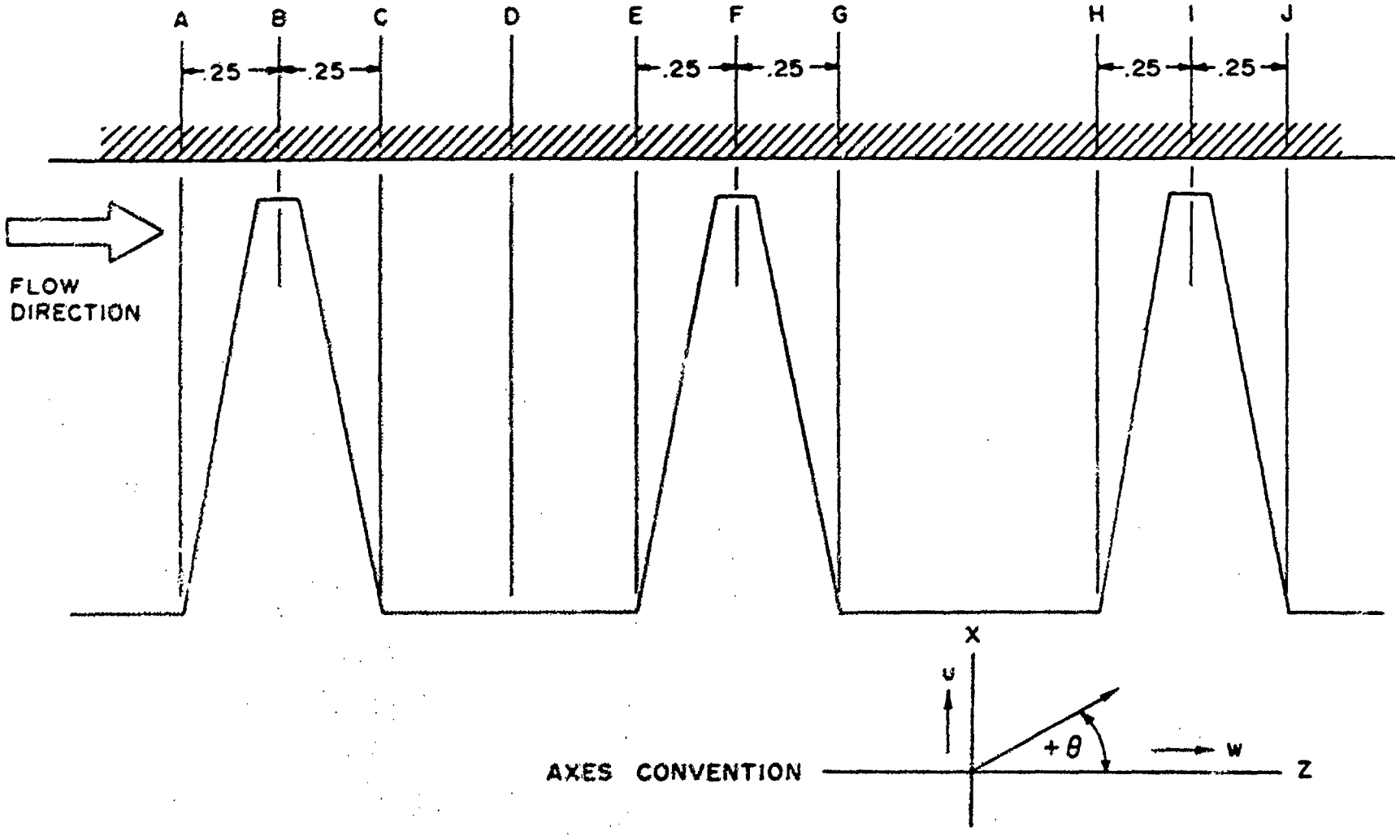

Figure 16 - Data Stations - Three Knife Straight-Through Seal with Tapered Knives.

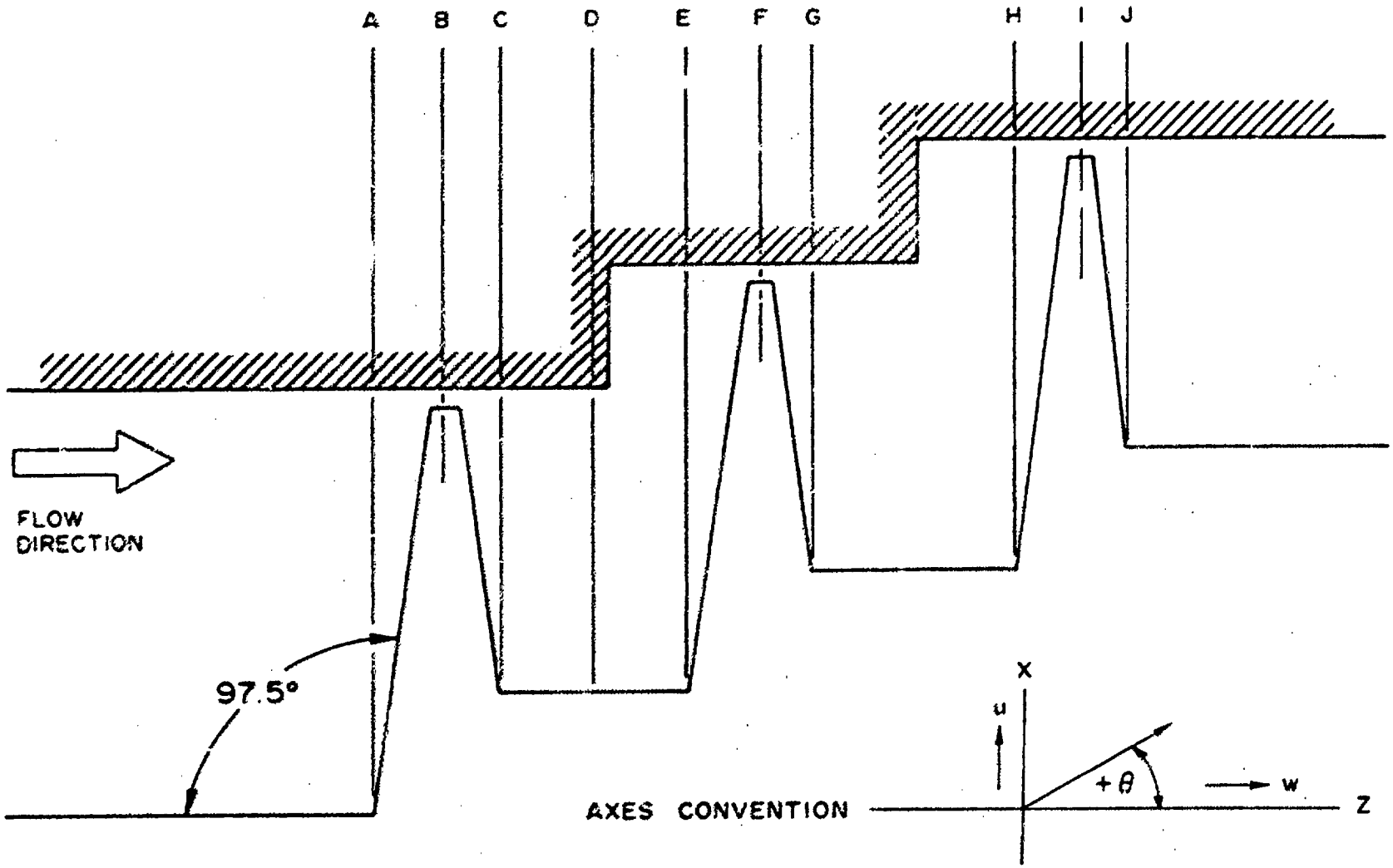

Figure 17 - Data Stations - Three Knife Stepped Seal with Tapered Knives.

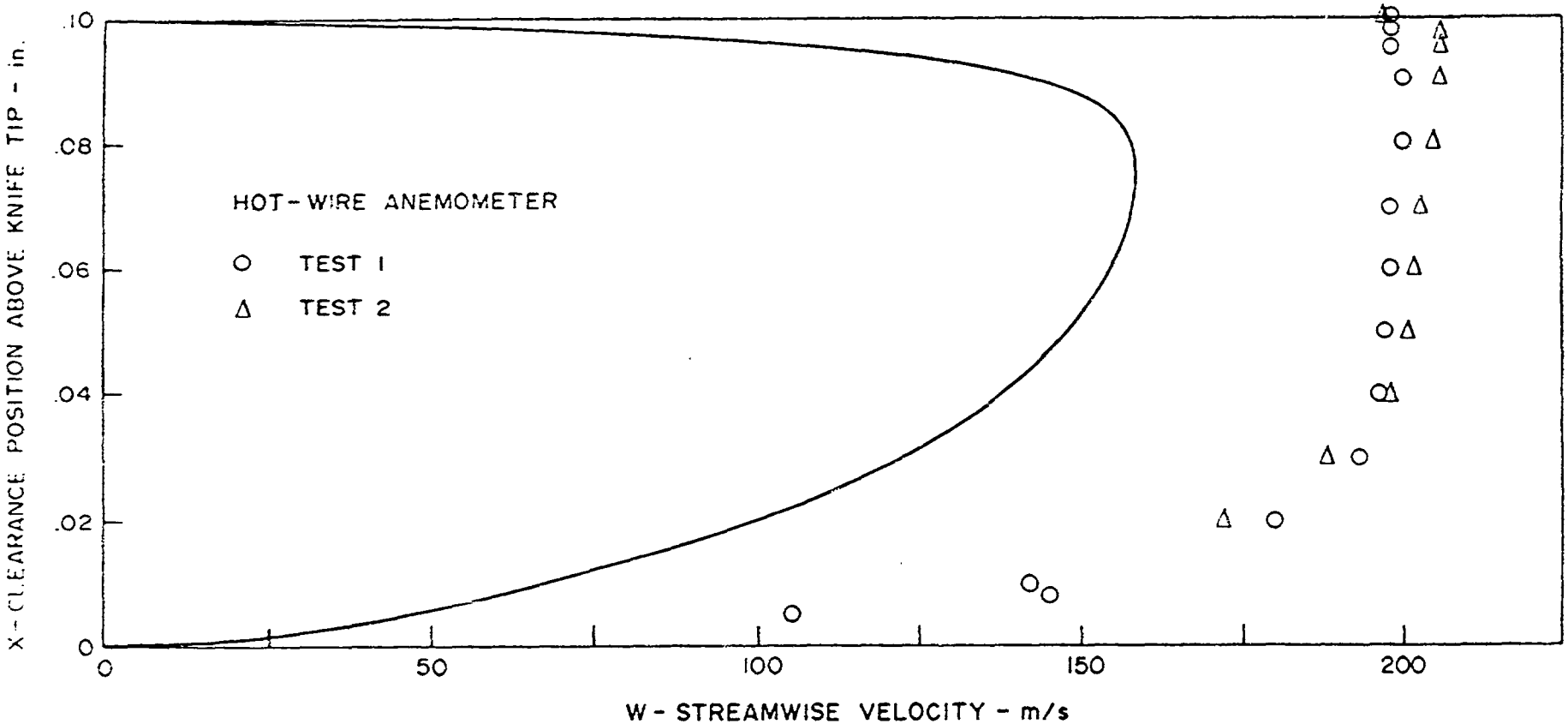

Figure 18 - Streamwise Velocity Comparison - Station B - Three Knife Straight-Through Seal with Tapered Knives.

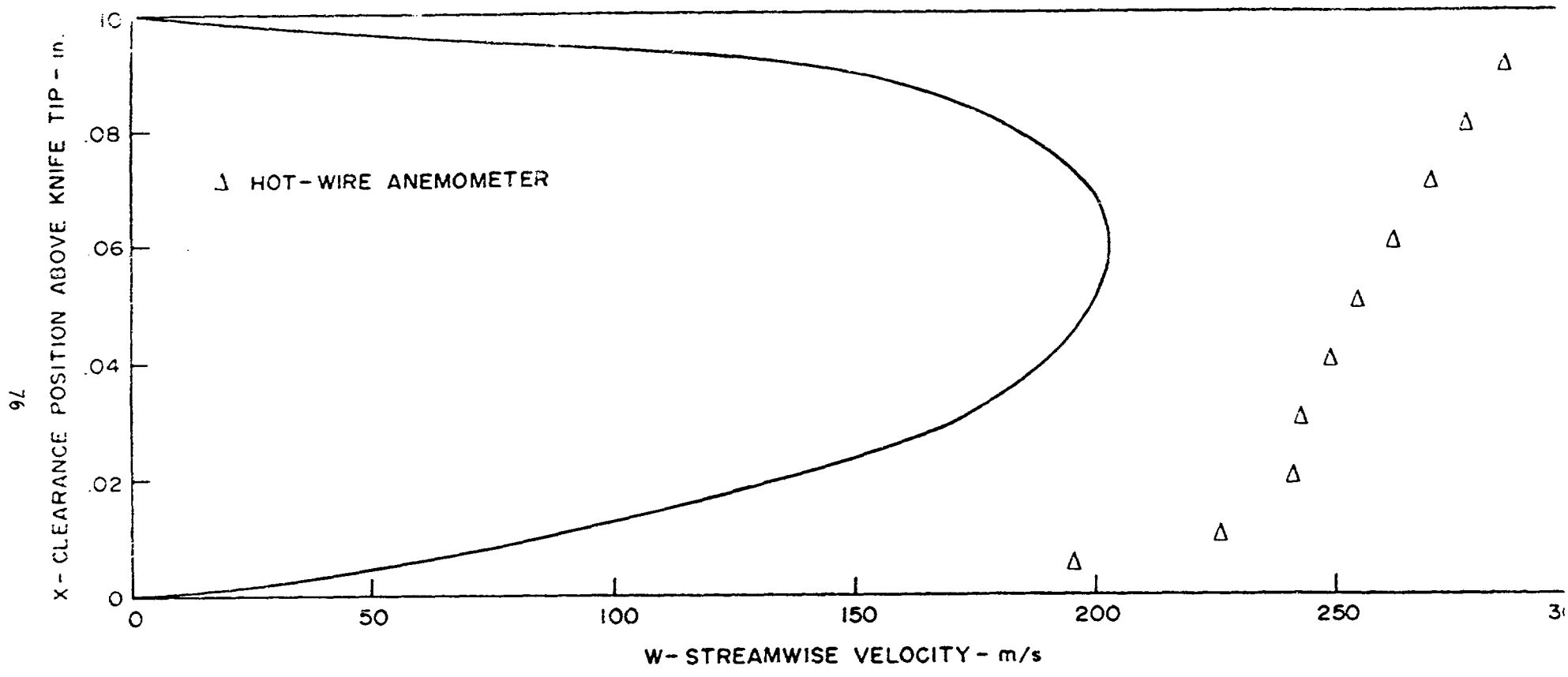

Figure 19 - Streamwise Velocity Comparison - Station I - Three Knife Straight-Through Seal with Tapered Knives.

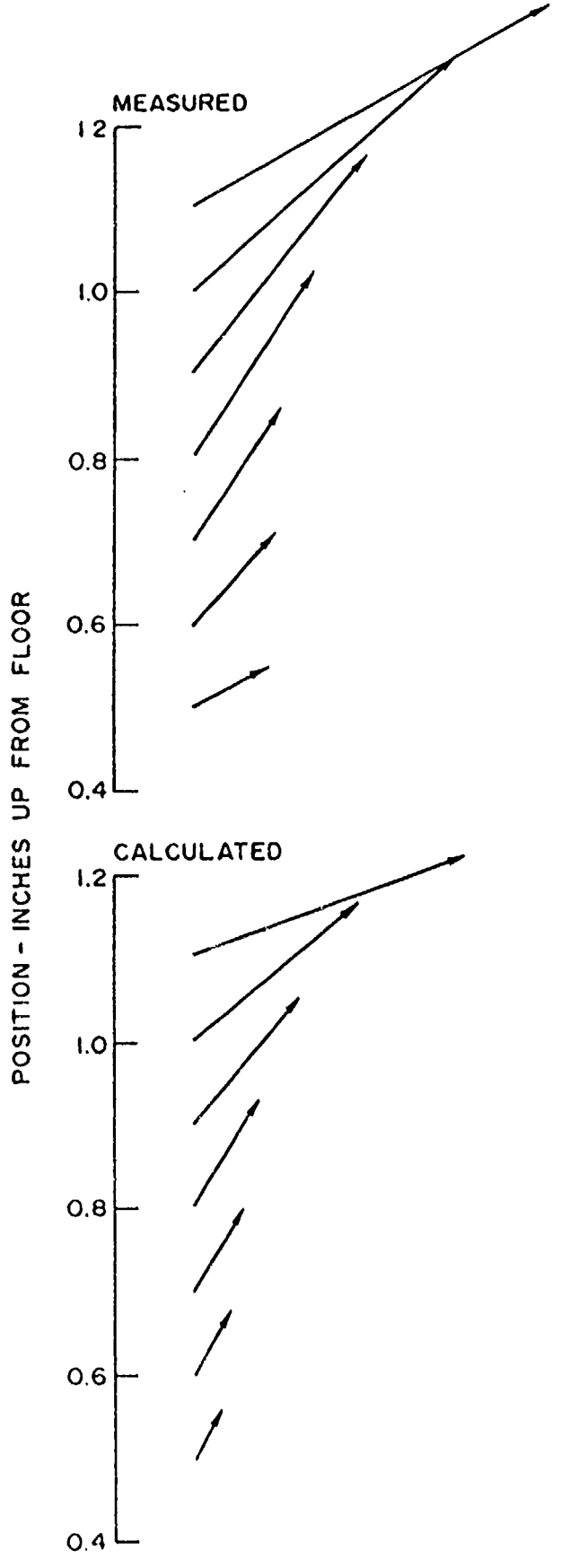

Figure 20 - Velocity Component Comparison - Station A - Three Knife Straight-Through Seal With Tapered Knives.

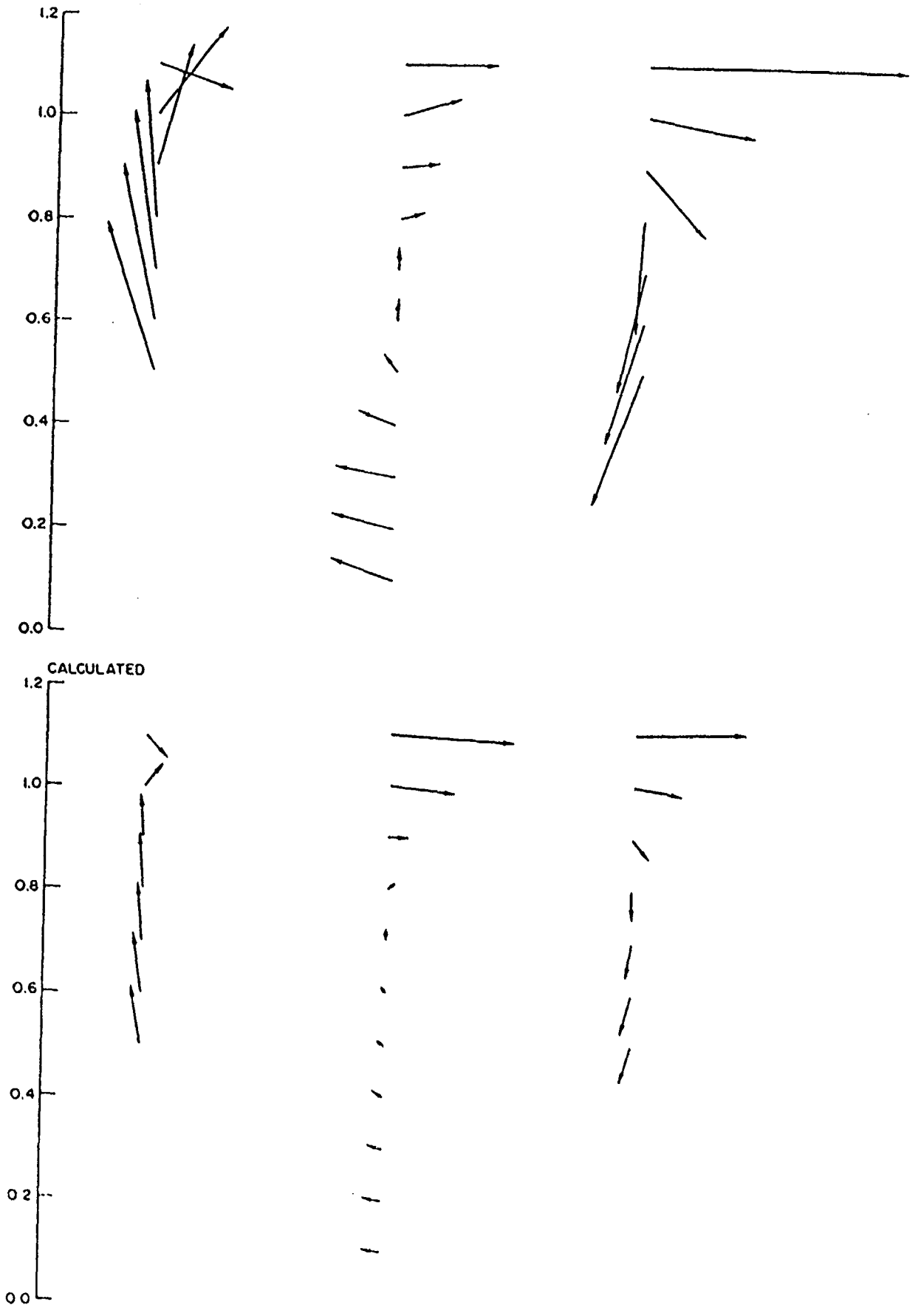

Figure 21 - Velocity Component Comparison - First Cavity (Stations C, D, and E) Three Knife Straight-Through Seal with Tapered Knives.

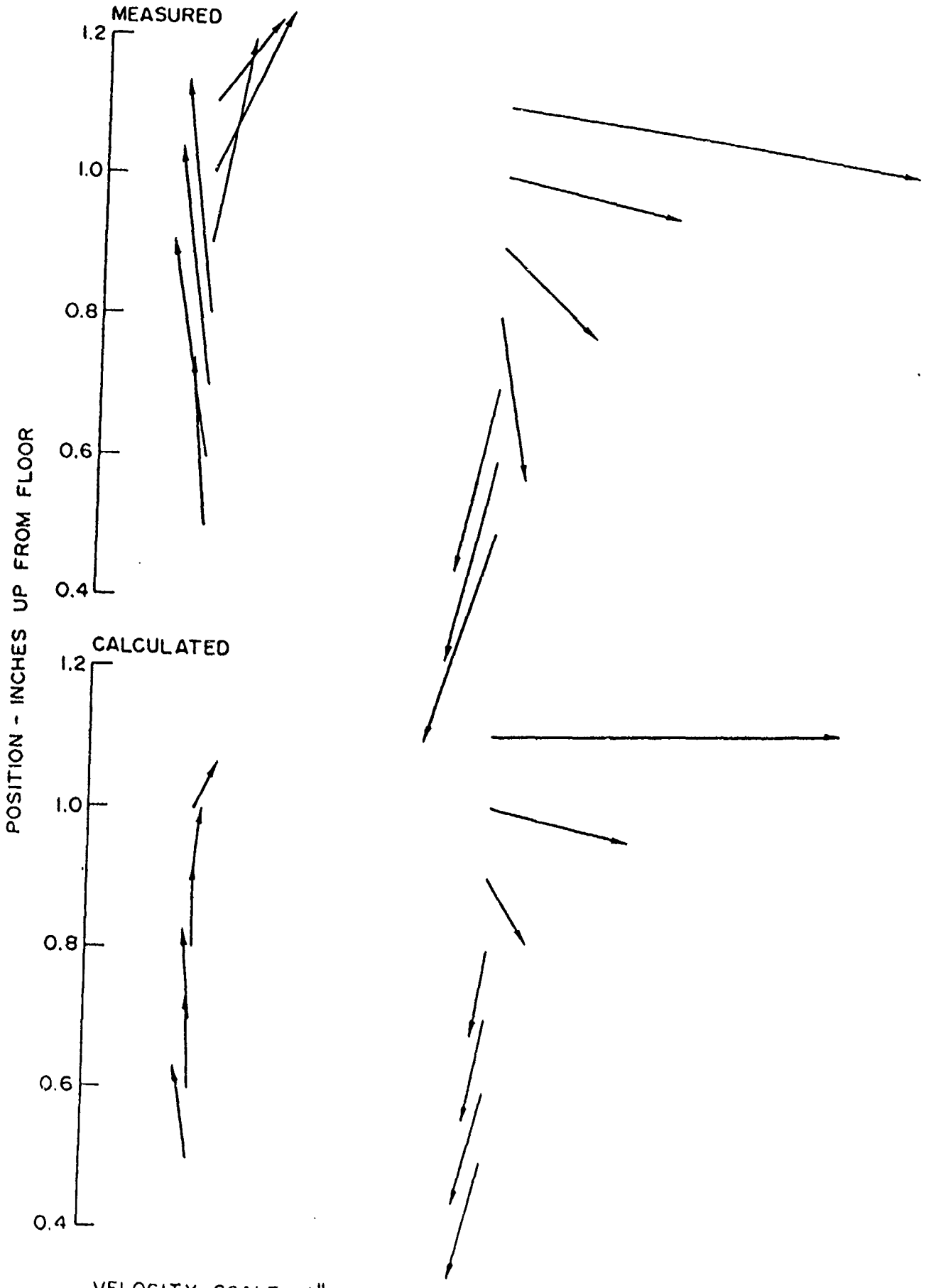

Figure 22 - Velocity Component Comparison - Second Cavity (Stations G and H) Three Knife Straight-Through Seal With Tapered Knives.

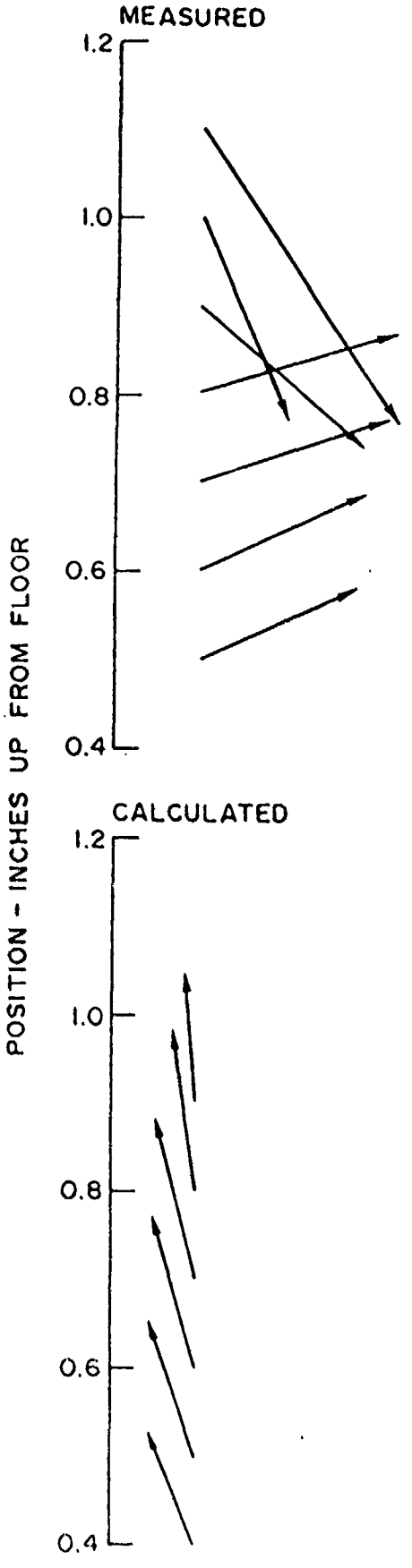

Figure 23 - Velocity Component Comparison - Station J - Three Knife Straight-Through Seal With Tapered Knives.

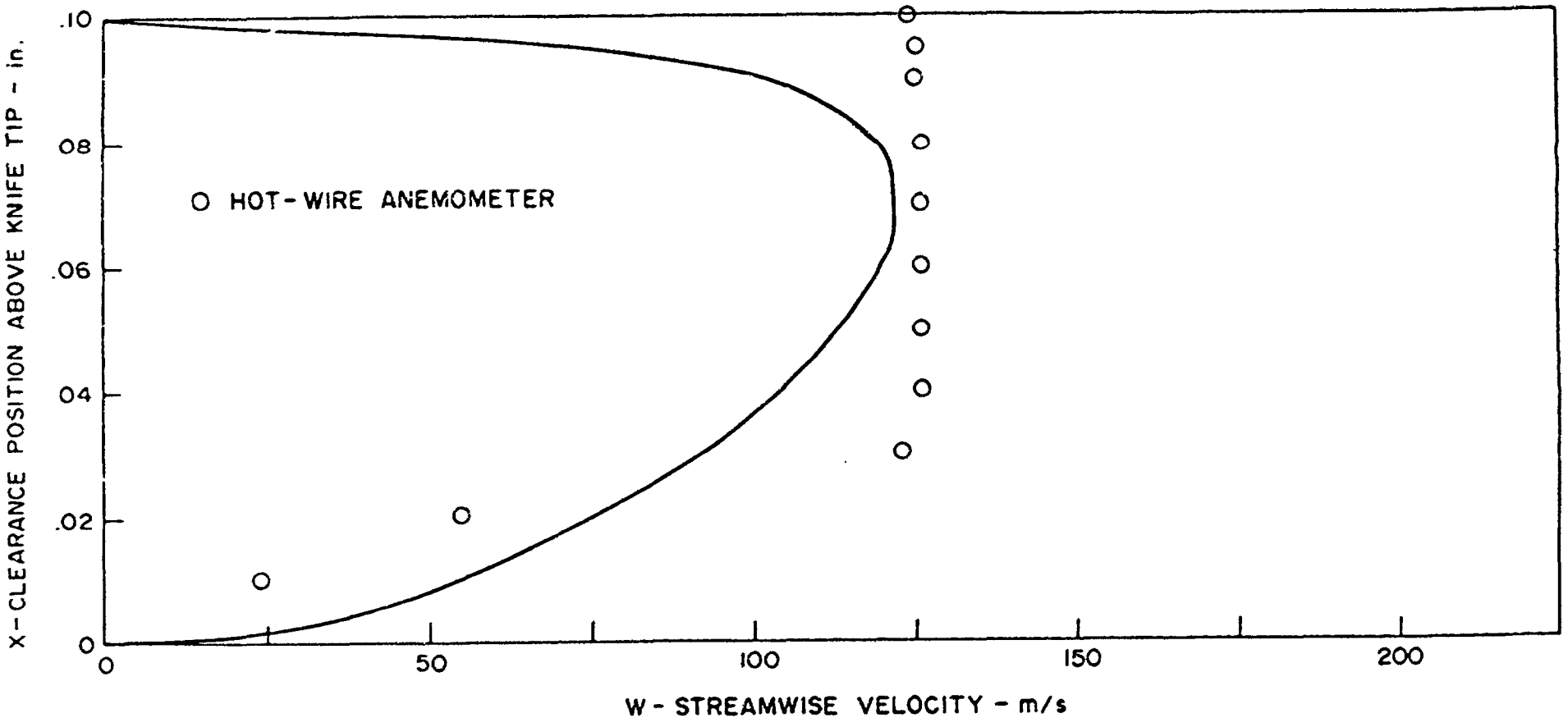

Figure 24 - Streamwise Velocity Comparison - Station B - Three Knife Stepped Seal with Tapered Knives.

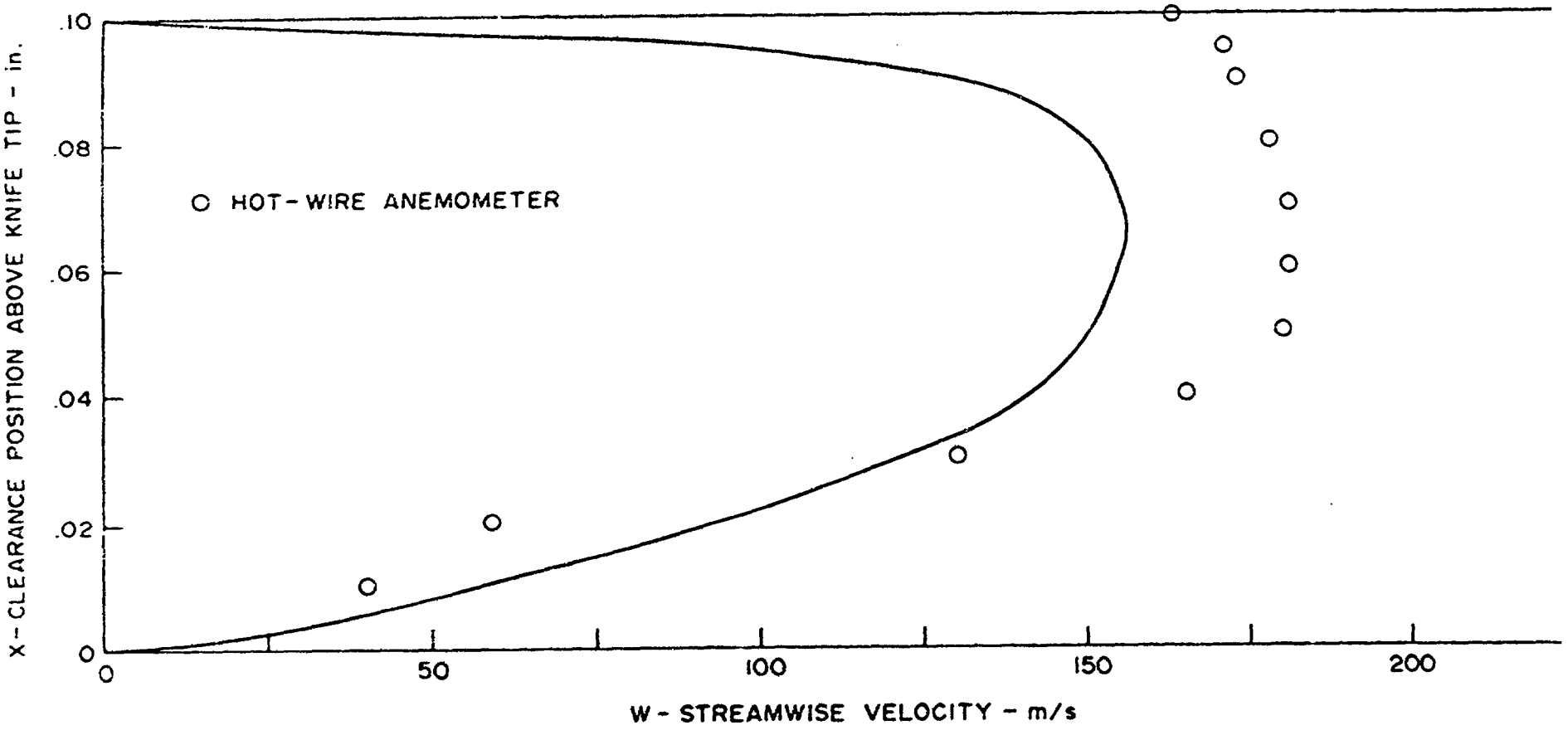

Figure 25 - Streamwise Velocity Comparison - Station F - Three Knife Stepped Seal with Tapered Knives.

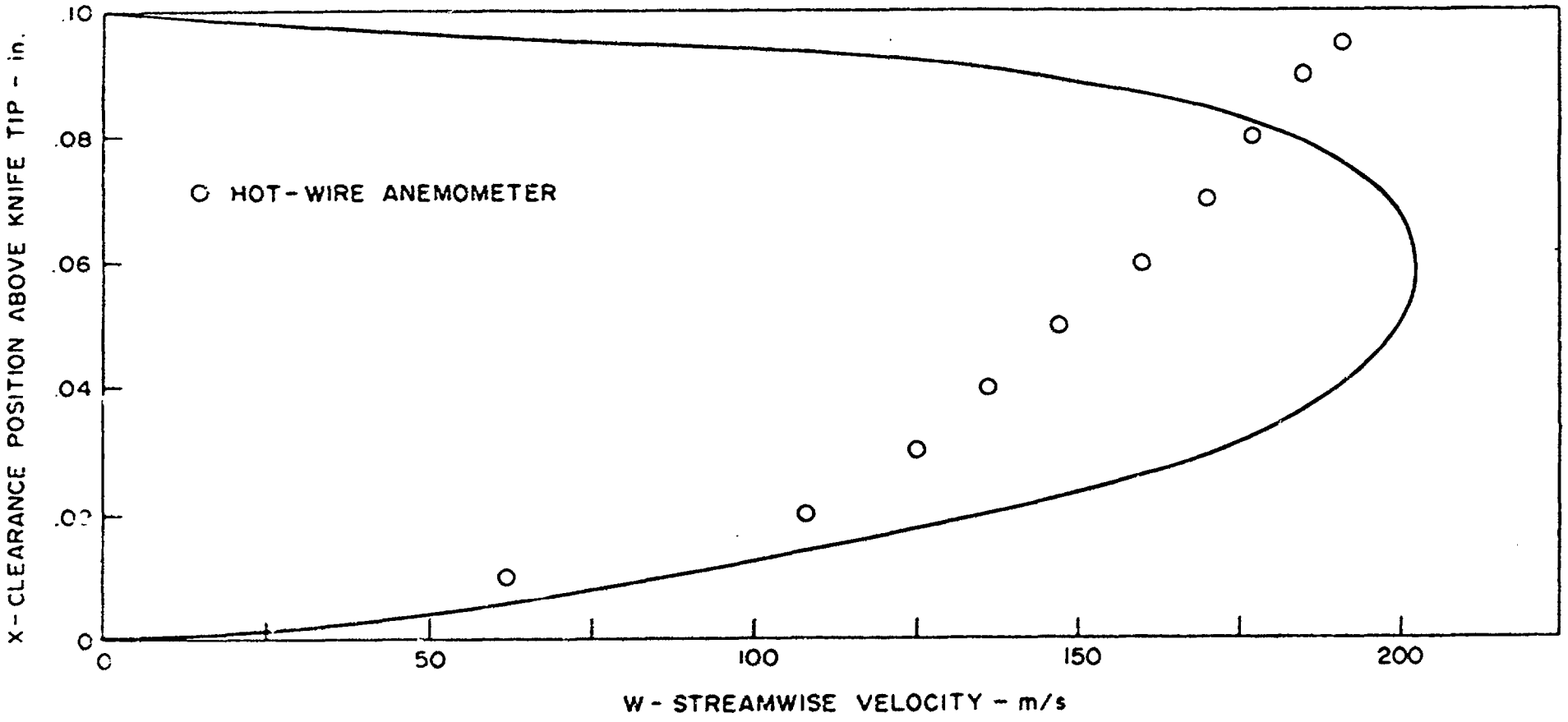

Figure 26 - Streamwise Velocity Comparison - Station I - Three Knife Stepped Seal with Tapered Knives.

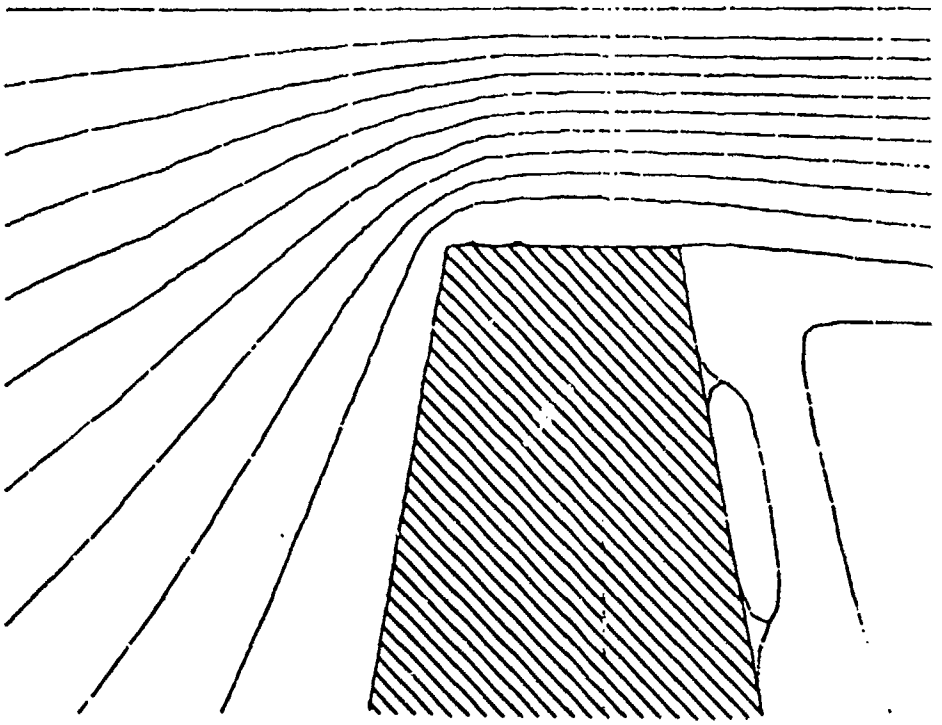

With Rotation - 6000 rpm

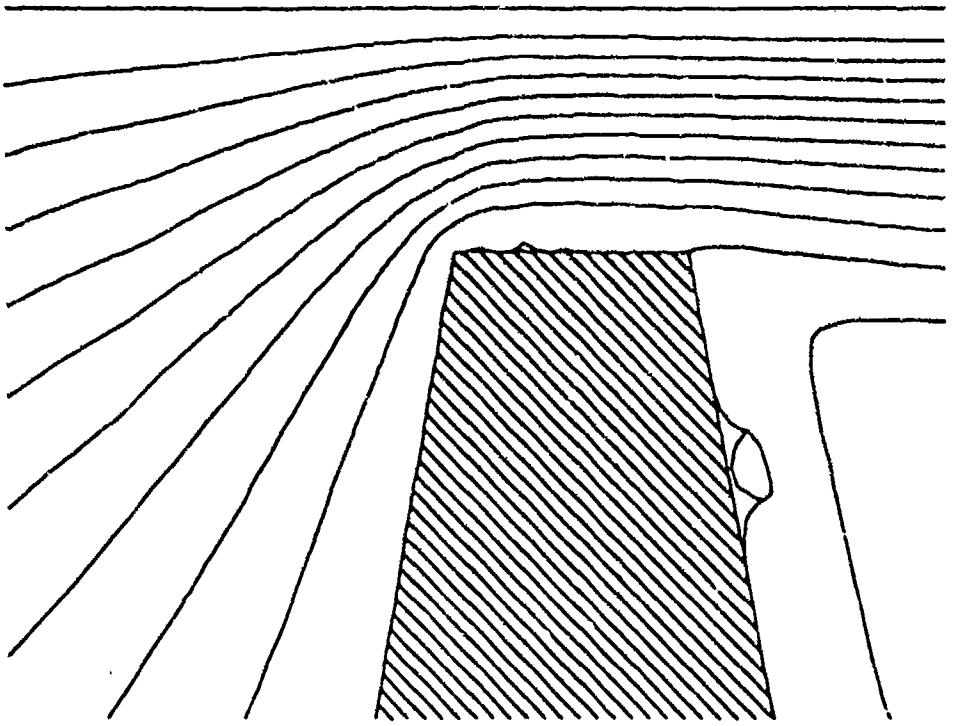

Without Rotation

Figure 27 - Streamlines - Three Knife Straight-Through Seal With Tapered Knives - First Knife.

Table 1 - Straight Through Labyrinth Seals.

CASE	CONFIGURATION	FIG. NO.	TEST	P_o/P_D	TURB MODEL	ENERGY EQN.	INLET PROFILE	GRID	w_{calc}	w_{corr}	$\frac{w_{calc}}{w_{corr}}$	PEAK MACH NO.	Re $X10^{-5}$
1	Rectangular - Single Knife	3a	N/A	3.98	ℓ_m	No	1/7	21 x 61	0.546	0.776	0.704	1.619	2.386
2	Rectangular - Three Knives	3b	N/A	2.00	ℓ_m	No	1/7	51 x 61	0.296	0.301	0.983	0.832	0.926
3	Slanted - Single Knife	3c	N/A	2.00	ℓ_m	No	1/7	51 x 61	0.364	0.325	1.120	1.472	0.999
4	Slanted - Three Knives	3d	N/A	2.00	ℓ_m	No	1/7	51 x 101	0.257	0.240	1.071	0.803	0.738
5	Tapered - Single Knife	3e	7	3.56	ℓ_m	No	1/7	51 x 61	0.663	0.662	1.002	1.580	2.036
6A	Worn - Single Knife	3f	3R	2.00	ℓ_m	Yes	Turb	31 x 101	0.391	0.415	0.942	0.945	1.276
6B	Worn - Single Knife	3f	3R	2.00	k-ε	Yes	Turb	31 x 101	0.410	0.415	0.988	1.112	1.276
7	Tapered - Three Knives	3g	24A	4.98	ℓ_m	No	1/7	51 x 61	0.800	0.788	1.015	1.398	2.423
8A	Tapered - Three Knives	3g	1	2.00	ℓ_m	No	1/7	51 x 71	0.268	0.315	0.851	0.776	0.969
8B	Tapered - Three Knives	3g	1	2.00	ℓ_m	Yes	Turb	61 x 101	0.264	0.315	0.838	0.759	0.969
8C	Tapered - Three Knives	3g	1	2.00	k-ε	Yes	Turb	61 x 101	0.235	0.315	0.746	0.714	0.969
9	Tapered - Three Knives Rough Land	3g	2R	2.00	ℓ_m	No	1/7	51 x 71	0.292	0.296	0.986	0.946	0.910
10	Tapered - Three Knives Injection	3g	N/A	2.00	ℓ_m	No	1/7	51 x 71	0.292	N/A	N/A	0.801	0.898

Table 2 - Stepped Labyrinth Seals.

CASE	CONFIGURATION	FIG. NO.	TEST	P_o/P_D	TURB MODEL	ENERGY EQN.	INLET PROFILE	GRID	w_{calc}	w_{corr}	$\frac{w_{calc}}{w_{corr}}$	PEAK MACH NO.	$Re \times 10^{-5}$
11	Rectangular - Single Knife	4a	N/A	2.50	ℓ_m	No	1/7	51 x 61	0.898	0.802	1.120	1.229	2.467
12	Rectangular - Three Knives	4b	5	2.00	ℓ_m	No	1/7	71 x 100	0.232	0.186	1.247	0.654	0.572
13	Slanted - Single Knife	4c	6	2.00	ℓ_m	No	1/7	51 x 61	0.300	0.278	1.079	0.803	0.855
14	Tapered - Three Knives	4d	N/A	2.00	ℓ_m	Yes	Turb	71 x 100	0.207	0.188	1.101	0.678	0.578
15	Tapered - Three Knives	4d	N/A	2.00	k-ε	Yes	Turb	71 x 100	0.206	0.188	1.096	0.632	0.578

Table 3 - Velocity Component Comparison - Three Knife Straight-Through Seal with Tapered Knives at P_U/P_D=2.0.

STATION A				
r	V_m	θ_m	V_c	θ_c
[illegible]	49.9	28	36.6	19
[illegible]	42.*	39	26.3	38
2.4	33.4	50	22.1	49
[illegible]	25.3	56	13.5	56
[illegible]	19.1	55	11.6	60
2.9	13.8	67	9.1	63
3.1	10.2	25	8.8	65
3.4				
[illegible]				
3.8				
[illegible]				

STATION C			
V_m	θ_m	V_c	θ_c
30.4	341	93.6	355
43.1	52	11.2	50
47.8	75	18.7	95
52.5	95	20.1	94
56.2	99	22.3	95
60.9	103	23.1	97
55.1	110	22.8	100

STATION D			
V_m	θ_m	V_c	θ_c
74.5	0	101.5	357
50.0	14	52.5	355
30.0	4	17.4	4
20.0	14	7.2	35
17.0	90	4.7	75
17.6	90	5.4	127
20.0	128	7.5	149
34.6	160	10.7	161
51.5	170	13.4	167
52.8	167	16.5	170
54.9	161	18.5	172

STATION E			
V_m	θ_m	V_c	θ_c
107.5	359	84.0	358
44.3	351	39.3	348
36.7	314	20.8	307
43.1	267	22.5	271
48.8	254	27.3	259
49.6	253	30.5	255
54.5	248	30.5	354

STATION G			
r	V_m	θ_m	V_c	θ_c
[illegible]	30.8	52	105.3	356
[illegible]	51.*	64	12.8	65
[illegible]	59.5	80	18.7	86
[illegible]	65.2	98	22.7	90
[illegible]	64.9	99	25.6	92
[illegible]	62.2	100	27.4	97
[illegible]	[illegible]	95	27.2	100

STATION H			
V_m	θ_m	V_c	θ_c
125.1	352	102.7	1
53.8	347	40.7	346
37.8	337	21.1	301
46.6	280	24.3	269
53.1	257	29.6	260
59.4	256	33.1	256
63.1	252	35.2	254

STATION J			
V_m	θ_m	V_c	θ_c
40.5	306	138.2	356
25.3	295	14.9	94
24.7	321	18.5	102
23.4	15	19.0	104
23.4	18	18.3	106
21.8	22	16.5	108
20.0	22	15.4	110

LEGEND

r(in) - Distance From Rotor

V_m(m/sec) - Measured Speed

θ_m(deg) - Measured Angle

V_c(m/sec) - Calculated Speed

θ_c(deg) - Calculated Angle

APPENDIX A - TRANSFORMATION

It is desired to show that given the general transformation

$$y^j = y^j(\bar{x}_1, \bar{x}_2, \bar{x}_3) \tag{A-1}$$

that the relationship

$$\frac{\partial}{\partial y^j}\left(J \frac{\partial y^j}{\partial \bar{x}_i}\right) = 0 \tag{A-2}$$

is valid. Where as in Section 2.2, J is the Jacobian of the transformation Eq. (A-1). Applying the chain rule to Eq. (A-1) yields the relationships

$$\frac{\partial y^j}{\partial y^i} = \delta_{ij} = \frac{\partial y^j}{\partial \bar{x}_k} \frac{\partial \bar{x}_k}{\partial y^i} \tag{A-3}$$

Writing Eq. (A-3) for each of the three k directions for one y^j yields three linear relationships for the unknowns $\partial y^j/\partial x_k$. These can be solved by applying Cramers rule to yield for j=1,2 and 3 respectively

$$J \frac{\partial y^1}{\partial \bar{x}_1} = \frac{\partial \bar{x}_2}{\partial y^2} \frac{\partial \bar{x}_3}{\partial y^3} - \frac{\partial \bar{x}_2}{\partial y^3} \frac{\partial \bar{x}_3}{\partial y^2} \tag{A-4}$$

$$J \frac{\partial y^1}{\partial \bar{x}_2} = \frac{\partial \bar{x}_3}{\partial y^2} \frac{\partial \bar{x}_1}{\partial y^3} - \frac{\partial \bar{x}_3}{\partial y^3} \frac{\partial \bar{x}_1}{\partial y^2} \tag{A-5}$$

$$J \frac{\partial y^1}{\partial \bar{x}_3} = \frac{\partial \bar{x}_1}{\partial y^2} \frac{\partial \bar{x}_2}{\partial y^3} - \frac{\partial \bar{x}_1}{\partial y^3} \frac{\partial \bar{x}_2}{\partial y^2} \tag{A-6}$$

$$J\frac{\partial y^2}{\partial \bar{x}_1} = \frac{\partial \bar{x}_2}{\partial y^3}\frac{\partial \bar{x}_3}{\partial y^1} - \frac{\partial \bar{x}_2}{\partial y^1}\frac{\partial \bar{x}_3}{\partial y^3} \tag{A-7}$$

$$J\frac{\partial y^2}{\partial \bar{x}_2} = \frac{\partial \bar{x}_3}{\partial y^3}\frac{\partial \bar{x}_1}{\partial y^1} - \frac{\partial \bar{x}_3}{\partial y^1}\frac{\partial \bar{x}_1}{\partial y^3} \tag{A-8}$$

$$J\frac{\partial y^2}{\partial \bar{x}_3} = \frac{\partial \bar{x}_1}{\partial y^3}\frac{\partial \bar{x}_2}{\partial y^1} - \frac{\partial \bar{x}_1}{\partial y^1}\frac{\partial \bar{x}_2}{\partial y^3} \tag{A-9}$$

$$J\frac{\partial y^3}{\partial \bar{x}_1} = \frac{\partial \bar{x}_2}{\partial y^1}\frac{\partial \bar{x}_3}{\partial y^2} - \frac{\partial \bar{x}_2}{\partial y^2}\frac{\partial \bar{x}_3}{\partial y^1} \tag{A-10}$$

$$J\frac{\partial y^3}{\partial \bar{x}_2} = \frac{\partial \bar{x}_3}{\partial y^1}\frac{\partial \bar{x}_1}{\partial y^2} - \frac{\partial \bar{x}_3}{\partial y^2}\frac{\partial \bar{x}_1}{\partial y^1} \tag{A-11}$$

$$J\frac{\partial y^3}{\partial \bar{x}_3} = \frac{\partial \bar{x}_1}{\partial y^1}\frac{\partial \bar{x}_2}{\partial y^2} - \frac{\partial \bar{x}_1}{\partial y^2}\frac{\partial \bar{x}_2}{\partial y^1} \tag{A-12}$$

Substitution of relationships (A-4) through (A-12) into Eq. (A-2) substantiates the validity of Eq. (A-2).

These relationships (A-4) through (A-12) and the definition of the Jacobian, J, (Eq. 42), are used to calculate the geometric groupings that occur in the governing system of coupled partial differential equations represented by Eq. (46) and the auxiliary relationships represented by Eqs. (47)-(50). These geometric groupings are calculated by finite difference techniques in an analogous manner to that used for the fluid dynamic derivatives. A finite difference grid distribution is setup in the computational domain (y^j) and grid points are associated with the cartesian location ($\bar{x}_i$). All derivatives of the form $\partial\bar{x}_i/\partial y_j$ are then approximated by their finite difference analog, i.e., central differences for interior grid points and three point one-sided approximations on boundaries Once these derivatives are calculated for all values of i and j the Jacobian J and the geometric groupings represented by Eq. (A-4) through Eq. (A-12) can be calculated.

APPENDIX B - SOLUTION PROCEDURE

Background

The solution procedure employs a consistently-split linearized block implicit (LBI) algorithm which has been discussed in detail in Refs. 12 and 26. There are two important elements of this method:

(1) the use of a noniterative formal time linearization to produce a fully-coupled linear multidimensional scheme which is written in "block implicit" form; and

(2) solution of this linearized coupled scheme using a consistent "splitting" (ADI scheme) patterned after the Douglas-Gunn (Ref. 27) treatment of scalar ADI schemes.

The method is thus referred to as a split linearized block implicit (LBI) scheme. The method has several attributes:

(1) the noniterative linearization is efficient;

(2) the fully-coupled linearized algorithm eliminates instabilities and/or extremely slow convergence rates often attributed to methods which employ ad hoc decoupling and linearization assumptions to identify nonlinear coefficients which are then treated by lag and update techniques;

(3) the splitting or ADI technique produces an efficient algorithm which is stable for large time steps and also provides a means for convergence acceleration for further efficiency in computing steady solutions;

(4) intermediate steps of the splitting are consistent with the governing equations, and this means that the "physical" boundary conditions can be used for the intermediate solutions. Other splittings which are inconsistent can have several difficulties in satisfying physical boundary conditions (Ref. 12).

(5) the convergence rate and overall efficiency of the algorithm are much less sensitive to mesh refinement and redistribution than algorithms based on explicit schemes or which employ ad hoc decoupling and linearization assumptions. This is important for accuracy and for computing turbulent flows with viscous sublayer resolution; and

(6) the method is general and is specifically designed for the complex systems of equations which govern multiscale viscous flow in complicated geometries.

This same algorithm was later considered by Beam and Warming (Ref. 25), but the ADI splitting was derived by approximate factorization instead of the Douglas-Gunn procedure. They refer to the algorithm as a "delta form" approximate factorization scheme. This scheme replaced an earlier non-delta form scheme (Ref. 34) which has inconsistent intermediate steps.

Split LBI Algorithm

Linearization and Time Differencing

The system of governing equations to be solved consists of three or four equations: continuity and two or three components of the momentum equation in three or four dependent variables: ρ, u, v, and/or w. Using notation similar to that in (Ref. 12), at a single grid point this system of equations can be written in the following form:

$$\partial H(\phi)/\partial t = D(\phi) + S(\phi) \qquad \text{(B-3)}$$

where ϕ is the column-vector of dependent variables, H and S are column-vector algebraic functions of ϕ, and D is a column vector whose elements are the spatial differential operators which generate all spatial derivatives appearing in the governing equation associated with that element.

The solution procedure is based on the following two-level implicit time-difference approximations of (B-3):

$$(H^{n+1} - H^n)/\Delta t = \beta(D^{n+1} + S^{n+1}) + (1-\beta)(D^n + S^n) \qquad \text{(B-4)}$$

where, for example, H^{n+1} denotes $H(\phi^{n+1})$ and $\Delta t = t^{n+1} - t^n$. The parameter β ($0.5 \leq \beta \leq 1$) permits a variable time-centering of the scheme, with a truncation error of order $[\Delta t^2, (\beta - 1/2)\,\Delta t]$.

A local time linearization (Taylor expansion about ϕ^n) of requisite formal accuracy is introduced, and this serves to define a <u>linear</u> differential operator L (cf. Ref. 12) such that

$$D^{n+1} = D^n + L^n(\phi^{n+1} - \phi^n) + O(\Delta t^2) \qquad \text{(B-5)}$$

Similarly,

$$H^{n+1} = H^n + (\partial H/\partial \phi)^n (\phi^{n+1} - \phi^n) + 0 (\Delta t^2) \quad \text{(B-6)}$$

$$S^{n+1} = S^n + (\partial S/\partial \phi)^n (\phi^{n+1} - \phi^n) + 0 (\Delta t^2) \quad \text{(B-7)}$$

Eqs. (B-5 through B-7) are inserted into Eq. (B-4) to obtain the following system which is linear in ϕ^{n+1}

$$(A - \beta \Delta t\, L^n) (\phi^{n+1} - \phi^n) = \Delta t (D^n + S^n) \quad \text{(B-8)}$$

and which is termed a linearized block implilcit (LBI) scheme. Here, A denotes a matrix defined by

$$A \equiv (\partial H/\partial \phi)^n - \beta \Delta t (\partial S/\partial \phi)^n \quad \text{(B-9)}$$

Eq. (B-8) has 0 (Δt) accuracy unless $H \equiv \phi$, in which case the accuracy is the same as Eq. (B-4).

Special Treatment of Diffusive Terms

The time differencing of diffusive terms is modified to accomodate cross-derivative terms and also turbulent viscosity and artificial dissipation coefficients which depend on the solution variables. Although formal linearization of the convection and pressure gradient terms and the resulting implicit coupling of variables is critical to the stability and rapid convergence of the algorithm, this does not appear to be important for the turbulent viscosity and artificial dissipation coefficients. Since the relationship between μ_e and d_j and the mean flow variables is not conveniently linearized, these diffusive coefficients are evaluated explicitly at t^n during each time step. Notationally, this is equivalent to neglecting terms proportional to $\partial\, \mu_e/\partial\phi$ or $\partial d_j/\partial\phi$ in L^n, which are formally present in the Taylor expansion (B-5), while retaining all terms proportional to μ_e or d_j in both L^n and D^n.

It has been found through extensive experience that this has little if any effect on the performance of the algorithm. This treatment also has the added benefit that the turbulence model equations can be decoupled from the system of mean flow equations by an appropriate matrix partitioning (cf. Ref. 26) and solved separately in each step of the ADI solution procedure. This reduces the block size of the block tridiagonal systems which must be solved in each step and thus reduces the computational labor.

In addition, the viscous terms in the present formulation include a number of cross-derivative terms implicitly within the ADI treatment which follows. It is not at all convenient to handle these implicit cross-derivative terms; and consequently, all cross-derivative

terms are evaluated explicitly at t^n. For a scalar model equation representing combined convection and diffusion, it has been shown by Beam and Warming that the explicit treatment of cross-derivative terms does not degrade the unconditional stability of the present algorithm. To preserve notational simplicity, it is understood that all cross-derivative terms appearing in L^n are neglected but are retained in D^n. It is important to note that neglecting terms in L^n has no effect on steady solutions of Eq. (B-8), since $\phi^{n+1} \equiv 0$ and thus Eq. (B-8) reduces to the steady form of the equations: $D^n + S^n = 0$. Aside from stability considerations, the only effect of neglecting terms in L^n is to introduce an $0\ (\Delta t)$ truncation error.

Consistent Splitting of the LBI Scheme

To obtain an efficient algorithm, the linearized system (B-8) is split using ADI techniques. To obtain the split scheme, the multidimensional operator L is rewritten as the sum of three "one-dimensional" sub-operators L_i $(i = 1, 2, 3)$ each of which contains all terms having derivatives with respect to the i-th coordinate. The split form of Eq. (B-8) can be derived either by following the procedure described by Douglas and Gunn (Ref. 27) in their generalization and unification of scalar ADI schemes (as done in Refs. 12 and 26), or by using approximate factorization. For the present system of equations, the split algorithm is given by

$$(A - \beta\Delta t L_1^n)\ (\phi^* - \phi^n) = \Delta t\ (D^n + S^n) \qquad \text{(B-10a)}$$

$$(A - \beta\Delta t L_2^n)\ (\phi^{**} - \phi^n) = A\ (\phi^* - \phi^n) \qquad \text{(B-10b)}$$

$$(A - \beta\Delta t L_3^n)\ (\phi^{n+1} - \phi^n) = A\ (\phi^{**} - \phi^n) \qquad \text{(B-10c)}$$

where ϕ^* and ϕ^{**} are consistent intermediate solutions. If spatial derivatives appearing in L_i and D are replace by three-point difference formulas, as indicated previously, then each step in Eqs. (B-10a,b and c) can be solved by a block-tridiagonal elimination.

Combining Eqs. (B-10a,b and c) gives

$$(A - \beta\Delta t L_1^n)\ A^{-1}\ (A - \beta\Delta t L_2^n)\ A^{-1}\ (A - \beta\Delta t L_3^n)\ (\phi^{n+1} - \phi^n) = \delta t\ (D^n + S^n) \qquad \text{(B-11)}$$

which approximates the unsplit scheme, Eq. (B-8) to $0\ (\Delta t^2)$. Since the intermediate steps are also consistent approximations for Eq. (B-8), physical boundary conditions can be used for ϕ^* and ϕ^{**} (Refs. 12 and 26). Finally, since the L_i are homogeneous operators, it follows from Eqs. (B-10a,b and c)

that steady solutions have the property that $\phi^{n+1} = \phi^{*} = \phi^{**} = \phi^{n}$ and satisfy

$$D^{n} + S^{n} = 0 \qquad \text{(B-12)}$$

The steady solution thus depends only on the spatial difference approximations used for Eq. (B-12), and does not depend on the solution algorithm itself.

U.S. GPO: 646-066